(Pre)targeting of Prostate Cancer

Katja van Rij

(Pre)targeting of Prostate Cancer
Thesis, Radboud University Nijmegen, Nijmegen, The Netherlands

Explanation of the cover:
The design shows a bispecific antibody, represented by the Man of Vitruvius by Leonardo da Vinci, bound to the TROP-2 epitopes on a prostate cancer cell, capturing a radiolabeled peptide, thus explaining the mechanism of pretargeting.

Design and Lay-out by: Paula Berkemeyer (PBVerbeelding.nl)
Printed by: GVO drukkers & vormgevers, Ede
ISBN/EAN: 978-90-9029592-3

The work described in this thesis was supported by a research grant of the Dutch Cancer Society (KWF grant no. KUN-2010-0480).

Printing and dissemination of this thesis was financially supported by the department of Radiology and Nuclear Medicine of the Radboud university medical center.

(Pre)targeting of Prostate Cancer

Proefschrift

ter verkrijging van de graad van doctor
aan de Radboud Universiteit Nijmegen
op gezag van de rector magnificus,
volgens besluit van het college van decanen
in het openbaar te verdedigenop vrijdag 24 juni 2016
om 10.30 uur precies

door

Catharina Maria van Rij
geboren op 8 december 1976
te Amsterdam

Promotoren

Prof. dr. O.C. Boerman
Prof. dr. W.J.G. Oyen

Manuscriptcommissie

Prof. dr. P.F.A. Mulders (voorzitter)
Prof. dr. W.R. Gerritsen
Prof. dr. N.H. Hendrikse (VUmc)

Contents

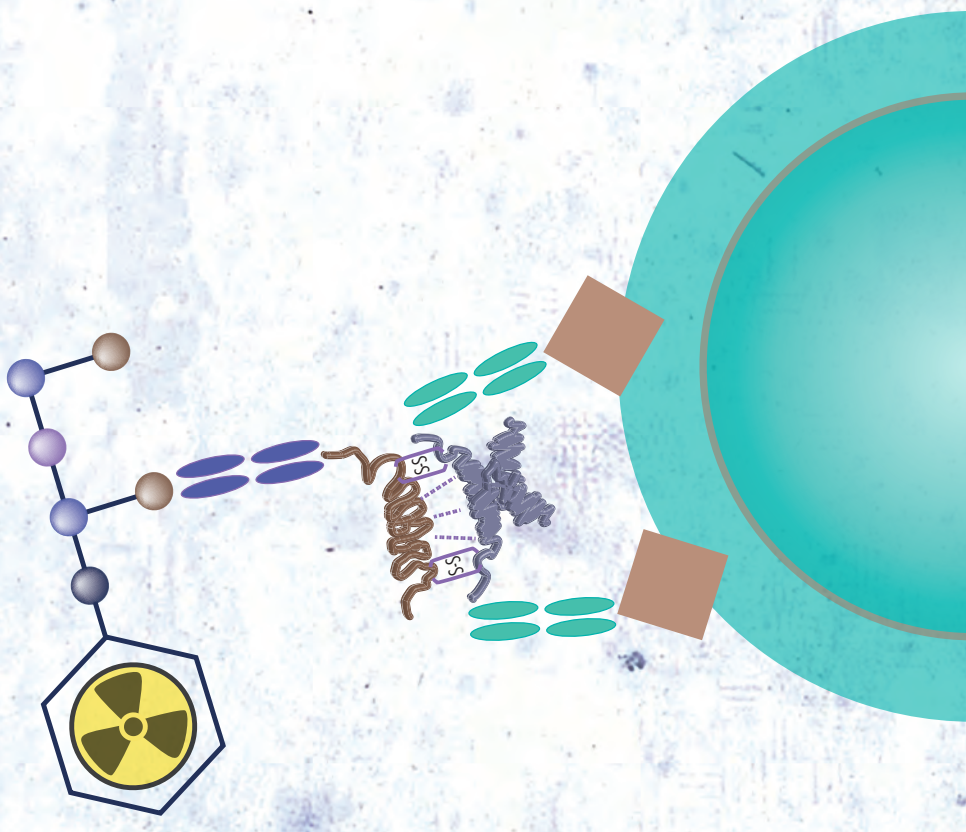

Introduction and thesis outline

1

Introduction

Prostate cancer

Prostate cancer (PC) has the highest prevalence of all cancers among men, and is responsible for 22% of all newly diagnosed cancers in the Netherlands. The risk of developing PC before the age of 80 in the western world is 10%. Although non-metastasized PC has a very good prognosis, PC still is the second leading cause of cancer-related death for men in the Western world (6%). In the last two decades, incidence of PC has risen remarkably, due to enlarged awareness of the disease, ageing of the population, the possibility to locate the tumor with ultrasound and MRI, and the introduction of the Prostate Specific Antigen (PSA) test [1]. When detected early, when the disease is still localized only in the prostate gland itself, the 5-year survival rate is nearly 99%. However, once the cancer has spread beyond the prostate gland, survival rates drop dramatically [2]. This highlights the need for sensitive diagnostic and effective therapeutic methods for PC.

Diagnosis of prostate cancer

Primary diagnosis

In several countries such as the USA, PSA levels together with digital rectal ultrasound exam are used as screening method for PC. However, PSA biomarker measurement has several drawbacks, i.e. low sensitivity and specificity, and the lack of distinction between localized and metastatic disease. In 80% of cases, patient complaints together with elevated PSA are not related to PC, but to benign prostate disease such as benign prostate hypertrophy (BPH) or prostatitis. Both age and a family history for PC are risk factors for developing this disease, although the latter has been the subject of debate lately [3]. Prostate cancer is usually diagnosed using transrectal ultrasound (TRUS) or MRI combined with biopsies. These modalities are generally able to detect and localize primary prostate cancer, but are less effective for clinical staging and therapy management. Due to the type of tissue of the prostate gland, accurate imaging by means of CT is currently not possible. An overview of current and future radionuclide imaging methods is given in chapter 2.

New developments in imaging of prostate cancer

Currently, more advanced functional multi-modality MR imaging techniques are under clinical development, such as Dynamic Contrast Enhanced MRI (DCE-MRI), that visualizes perfusion and enhances specificity of MRI, and Magnetic Resonance Spectroscopy (MRS) that uses levels of cellular metabolites like choline and citrate to

increase tumor detection rate [4]. Furthermore, MRI can be combined with intravenous injection of ultrasmall paramagnetic iron particles (USPIO) for better detection of small lymph node metastases. After intravenous administration, USPIO are retained in the lymph nodes where they are phagocytized by macrophages, which produces the hypointense signal in T2 weighted MRIs. In malignant lymph nodes, the macrophages are replaced by tumor cells, and the lymph nodes will appear hyperintense. With this technique, even small metastases in normal sized lymph nodes can be detected [5, 6]

Next to advances in MR imaging, radionuclide imaging of PC is rapidly emerging. Positron emission tomography (PET) imaging using ^{18}F-FDG is a widely used imaging modality to detect metastatic disease in several cancers, making use of trapping of ^{18}F-FDG in metabolically active cells. Unfortunately, ^{18}F-FDG PET/CT is inadequate for (re)staging of PC, as a large fraction of PC expresses only low numbers of glucose transporters such as Glut-1, which limits the ^{18}F-FDG uptake. In addition, ^{18}F-FDG is excreted mainly via the urinary system, which further limits the sensitivity and specificity of ^{18}F-FDG-PET/CT in the genitourinary region [4, 5, 7]. Several other radiotracers have been developed and tested for imaging metastatic PC, such as the radiolabeled metabolite tracers ^{11}C-choline and ^{18}F-fluorocholine. Both agents are based on choline as key precursor for cell membrane biosynthesis. For imaging of recurrent prostate tumors, lymph node metastases and bone metastases, ^{11}C-choline or ^{18}F-fluorocholine is now more and more included in everyday clinical practice [8]. Several studies have shown that choline imaging is useful in patients with short PSA-doubling times (<6 months) and high PSA serum levels (>2-10 ng/ml) as well as high-risk Gleason scores (7-10). A limitation of the use of choline-tracers in recurrent disease is their poor detection rate in patients with low PSA levels (<2.5 ng/ml). Unfortunately, clinical relevance of imaging of recurrent disease is the highest in patients with low PSA levels. At PSA values below 1 ng/ml, detection rates are less than 20%, increasing to >70% at PSA values >2.5 ng/ml [9]. Since biochemical relapse is already considered in patients with PSA levels of 0.2 ng/ml, there is an urgent need for more sensitive radiotracers [10].

In a systematic review based on 37 studies in 1244 PC patients, Bauman et al. described recommendations for the use of ^{18}F-fluorocholine for imaging of PC. While initial staging with ^{18}F-fluorocholine should be restricted to intermediate to high-risk populations with PSA levels of >10 ng/ml or Gleason scores of ≥7, restaging of recurrent and castrate-resistant disease with ^{18}F-fluorocholine is recommended in patients with PSA levels of >2 ng/ml [11]. In addition, the use of ^{18}F-fluorocholine for the definition of dominant intra-prostatic foci or limited lymph node recurrence was recommended for focal therapy escalation or focal salvage therapy. Moreover, ^{18}F-fluorocholine imaging was recommended for treatment monitoring of hormone or radiation therapy [5]. ^{11}C-acetate is another metabolite tracer, that was developed based on incorporation of acetate in membrane lipids of tumor cells due to the overexpression of fatty-acid synthase particularly in PC cells. ^{11}C-acetate has been clinically evaluated for detection of recurrent prostate cancer, showing a sensitivity of 64% and specificity of

93%, making this a less promising tracer [12].
Capromab pendetide (Prostascint®), an ^{111}In-labeled monoclonal antibody targeting the PSMA receptor has been approved by the FDA in 1996 as a diagnosing imaging agent in newly diagnosed patients with biopsy-proven PC, who are thought to be clinically localized and at high risk for pelvic lymph node metastases. In addition, ^{111}In-capromab pendetide was approved in post prostatectomy patients with a rising PSA and a negative metastatic evaluation with high clinical suspicion of occult metastatic disease. Imaging using radiolabeled capromab pendetide however is not performed regularly. Due to its non-specific uptake, possibly enhanced by biopsy-related inflammation, and the relatively poor tumor-to-background ratios, the usefulness of ^{111}In-capromab pendetide for imaging prostatic malignancies remains rather limited. An important disadvantage of capromab pendetide is the fact that it binds to an intracellular domain of PSMA. Therefore, capromab pendetide only binds to viable tumor cells following internalization or to dead cells with disrupted cellular membranes [5].
Promising developments are seen with J591, that is directed against an epitope on the extracellular domain of the PSMA receptor. This monoclonal antibody has been labeled with ^{111}In and ^{89}Zr for immunoSPECT/PET [13], as well as with ^{177}Lu for radioimmunotherapy [14].
Another group of tracers undergoing clinical investigation for PC consists of the radiolabeled bombesin-analogues targeting the gastrin releasing peptide receptor (GRPR). GRPR is overexpressed in prostate cancer in general and in 86% of PC lymph nodes and 53% of PC bone metastasis [15]. Kahkonen et al. showed a sensitivity and specificity of 81% and 88%, respectively, for detection of primary prostate cancer, and a sensitivity of 70% for detection of metastatic lymph nodes. It is deemed unsuitable for detecting bone lesions, due to its low sensitivity for detecting bone metastases [16]. There is evidence that GRPR in PC is less abundantly expressed in advanced stages of the disease, making the GRPR receptor less suitable as a target [17].
A new class of promising tracers currently under clinical development consists of radiolabeled PSMA-ligands targeting the prostate specific membrane antigen (PSMA). PSMA is an enzyme, NAALADase, expressed on the vast majority of PC. A series of radiolabeled PSMA inhibitors has been developed, such as ^{99m}Tc-MIP-1404 (Trofolastat®), ^{123}I-MIP-1072, ^{123}I-MIP-1095 [18, 19] and ^{68}Ga-HBED-CC-PSMA (Figure 1).

^{123}I-MIP-1072 and ^{123}I-MIP-1095 have been clinically evaluated for their potential to visualize prostate, bone and soft-tissue PC lesions. Early results show potential for ^{123}I-MIP-1072 in imaging of (primary) PC, whilst MIP-1095 radiolabeled with ^{131}I will be further investigated for its therapeutic potential [18].
^{99m}Tc-MIP-1404 is currently evaluated in a multicenter phase II trial. Next to its high clinical potential and excellent sensitivity for imaging PC metastases, ^{99m}Tc-MIP-1404 has several other advantages over current imaging agents, such as the short time between injection and imaging, and the easy radiolabeling procedure enabling use of

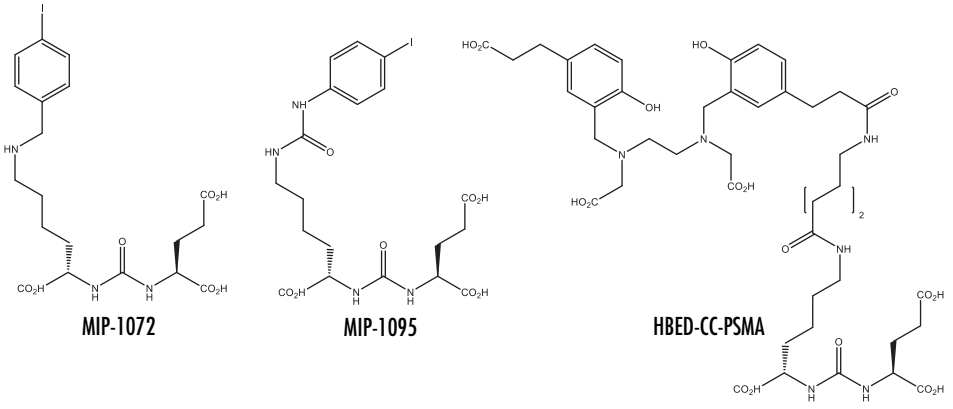

Figure 1. Structure of MIP-1072, MIP-1095 and HBED-CC-PSMA.

the tracer in nuclear medicine departments without specialized facilities [20].
^{68}Ga-HBED-CC-PSMA is another PSMA ligand currently under investigation for PET. The first clinical studies indicate that this tracer may have considerable advantages in detecting PC lesions in patients with recurrent disease, even in patients with low PSA levels [10, 21, 22]. Based on promising preclinical results, Afshar-Oromieh et al. investigated the role of ^{68}Ga-HBED-CC-PSMA in PET/CT imaging in a cohort of 37 patients. In 84% of the patients, PC-specific lesions could be identified. At PSA levels <2.2 ng/ml, PC-specific lesions were found in 60% of the patients. At PSA levels >2.2 ng/ml, PC-specific lesions were found in all patients. Afshar et al. have also shown superiority of this tracer over ^{18}F-choline in detecting PC lesions in patients with biochemical relapse. In this study, 86.5% of the patients showed at least one PC-specific lesion with ^{68}Ga-HBED-CC-PSMA PET/CT, whereas this was the case in only 70.3% when ^{18}F-fluorocholine was used as a tracer. At PSA values higher than 2.82 ng/ml, ^{68}Ga-HBED-CC-PSMA could detect at least one lesion in each patient, while ^{18}F-fluorocholine missed lesions in 10% of the patients. At PSA levels below 2.82 ng/ml at least one lesion could be detected in 68.8% and 43.8% of the patients using ^{68}Ga-HBED-CC-PSMA and ^{18}F-fluorocholine, respectively. Most importantly, all lesions visible in ^{18}F-fluorocholine-PET/CT were also visible using ^{68}Ga-HBED-CC-PSMA PET/CT, indicating that ^{68}Ga-HBED-CC-PSMA PET/CT can replace ^{18}F-fluorocholine PET/CT in these patients. No false-positives were found. Overall, this study suggests a significantly improved sensitivity of ^{68}Ga-HBED-CC-PSMA PET/CT compared to ^{18}F-fluorocholine PET/CT, especially at low PSA levels [22]. Recently, Eiber et al. reported the detection of PC lesions with ^{68}Ga-HBED-CC-PSMA-PET/CT in 248 patients with biochemical recurrence after radical prostatectomy. ^{68}Ga-HBED-CC-PSMA-PET/CT showed substantial higher detection rates than reported for other imaging modalities. Most importantly, a high number of positive findings in the clinically important range of low PSA values (<0.5 ng/ml) was

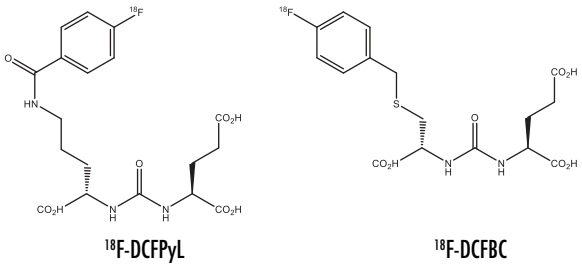

Figure 2. Structure of ^{18}F-DCFPyL and ^{18}F-DCFBC.

identified [23].

Recently, the ^{18}F-labeled PSMA-ligands ^{18}F-DCFBC and ^{18}F-DCFPyl were developed at Johns Hopkins University (Baltimore, MD, USA), enabling centralized production, thus eliminating the need for on-site manufacturing (Figure 2). This could markedly improve the accessibility of radiolabeled PSMA-ligands. Rowe at al. compared the first generation ^{18}F-PSMA ligand ^{18}F-DCFBC to conventional imaging modalities in both hormone naïve and castration resistant PC. In a lesion-by-lesion analysis, detection of lymph nodes, bone lesions and visceral lesions by ^{18}F-DCFBC was superior to conventional imaging, with superior sensitivity for the ^{18}F-ligand (92% *vs* 71%) [24]. Based on the positive results with ^{18}F-DCFBC, the second generation ^{18}F-PSMA ligand ^{18}F-DCFPyl was developed, with the advantage of lower blood pool activity most likely caused by binding of ^{18}F-DCFBC to plasma proteins. Dietlein et al. described a direct comparison between ^{68}Ga-HBED-CC-PSMA-PET/CT and ^{18}F-DCFPyL-PET/CT. In this study, 14 patients underwent both ^{68}Ga-HBED-CC-PSMA-PET/CT (1 h p.i.) and ^{18}F-DCFPyL-PET/CT (2 h p.i.). All lesions detected by ^{68}Ga-HBED-CC-PSMA-PET/CT were also detected by ^{18}F-DCFPyL-PET/CT. ^{18}F-DCFPyL-PET/CT detected additional lesions suspicious for PC in 3 out of 14 patients, suggesting a higher sensitivity using ^{18}F-DCFPyL. Furthermore, SUV_{max} and tumor-to-background lesions were significantly higher with ^{18}F-DCFPyL-PET/CT, possibly due to later acquisition times (with better signal-to-noise ratios) and faster clearance of the ^{18}F-PSMA ligand [25]. This highlights the potential of ^{18}F-labeled PSMA ligands in diagnosis of PC.

Therapy of prostate cancer

Dependent on the stage of the disease, determined by PSA levels and by means of Gleason score based on prostate biopsies, therapeutic options differ significantly. In patients with low risk PC, there is often no (direct) need for treatment. In pT1a-b patients, "watchfull waiting" is advised, whilst in T1c-2a (Gleason score <7, pretreatment PSA <10 ng/ml and <2 positive biopsies), "active surveillance" is indicated. In patients with localized or locally advanced prostate cancer, treatment options consist of (external) radiation therapy or radical prostatectomy. Treatment in this phase has a curative intent, but is accompanied with significant morbidity, such as relatively high risks for urinary incontinence and impotence. When PC has metastasized, treatment is no longer curative, but is aimed at slowing spread of the disease and optimal quality of life. Bilateral orchidectomy or hormonal therapy with LHRH antagonists and LHRH

agonists (with or without anti-androgens) are therapeutic options of choice in this phase of PC, although accompanied with severe side-effects. Eventually, the disease will progress to castration-resistant prostate cancer (CRPC), a phase in which progression occurs even though serum testosterone is at castration level. Therapeutic options in this phase are limited. A relatively new therapy for asymptomatic metastatic CRPC is sipuleucel-T (Provenge®), which is EMA approved since 2013. Sipuleucel-T is a dendritic cell vaccine manufactured from autologous leukocytes, activating the immune system of the patient to selectively kill PC cells. Although prolonged survival has been shown using this vaccine, it is not reimbursed in The Netherlands due to the negative advice of the Dutch Medicine Evaluation Board considering effectiveness.

First line chemotherapy in CRPC consists of docetaxel combined with prednisone. Second line options are chemotherapy using cabazitaxel and prednisone, or abiraterone. Abiraterone is a relatively new agent that inhibits CYP17, thus blocking testosterone synthesis entirely. Even in CRPC, complete testosterone blockade results in therapeutic effect comparable to that of cabazitaxel, but with less side-effects and the possibility of oral dosing. Third option is enzalutamide, an oral non-steroïd androgen receptor antagonist that prevents binding of activated androgen receptors to DNA.

Painful bone metastases may be palliatively treated with α-emitting radionuclide ^{223}Ra (Xofigo®), which has also shown overall survival benefit in a phase III clinical trial [26]. Prevention of Skeletal Related Events is done by means of bisphosphonate therapy or denosumab, an IgG2 monoclonal antibody that inhibits osteoclastic activity.

As is shown above, therapeutic options once the disease has spread beyond the prostate are limited, highlighting the need for new systemic therapies. One of the most promising class of therapeutic agents currently investigated in clinical trials consists of ^{177}Lu-labeled PSMA ligands. In these trials, new PSMA ligands are investigated which can be radiolabeled with both radionuclides used for diagnostic purposes (^{111}In/^{68}Ga), and nuclides suitable for therapy of PC, such as ^{177}Lu and ^{90}Y. The first clinical trials were performed with DOTA-conjugated PSMA, followed by DOTAGA-conjugated PSMA ligands with favourable tumor uptake compared to the DOTA-conjugated ligands. Baum et al. evaluated the therapeutic effects of DOTAGA conjugated PSMA ligand ^{177}Lu-DOTAGA-(ly)fk(Sub-KuE) (^{177}Lu-PSMA-I&T) in a group of 56 mCRPC patients. Of all patients, 33.3% reported significant improvement in pain after treatment with 1-5 cycles of therapy (5.7 ± 0.8 GBq/cycle), whereas the therapy was very well tolerated, showing no significant side effects nor hematological or renal toxicity. Of 25 patients included in this study, that were followed up at least 6 months after 2 or more cycles of therapy, 14 patients were reported to have partial remission. Stable disease was reported in 2 patients, and 9 patients revealed progressive disease according to EORTC response criteria [27]. A PSA decline of >50% was observed in 58.9% of patients.

These results of the first clinical studies indicate that PSMA ligands will have a high impact on both diagnostic and therapeutic procedures in PC patients in the near future.

Monoclonal antibodies

Monoclonal antibodies (mAbs) are antibodies that bind to the same epitope, and are currently used in the treatment of a wide range of malignancies. The first monoclonal antibodies were generated in 1975, and the first license for clinical use of a mAb was granted in 1986. Since then, development of mAb-based pharmacotherapy has risen to about 30 licensed mAb-based drugs. Humanized mAbs are nowadays the fastest growing group of biotechnology-derived molecules used in clinical trials [28]. The huge advantage of this class of pharmaceuticals is their specific targeting.
Next to the regular therapeutic use of mAbs, these pharmaceuticals can be radiolabeled in order to enable visualization of the target cells by means of immunoPET or immunoSPECT. In case of successful targeting of malignant tissue, these mAbs may also be used in RadioImmunoTherapy (RIT), when labeled with the β-emitting radionuclides ^{177}Lu or ^{90}Y. These are capable of destruction of malignant cells and, dependent on their specific properties, the cell layers surrounding the targeted tissue.
Currently, only two radiolabeled therapeutic antibodies are FDA approved, i.e. ^{90}Y-ibritumomab-tiuxetan (Zevalin®) and ^{131}I-tositumomab (Bexxar®) for the treatment of chemotherapy-refractive NHL. For the treatment of prostate cancer, the ^{177}Lu-labeled anti-PSMA mAb J591 was investigated in a phase II clinical trial [14], showing promising results that are further investigated in a phase III clinical trial.

Several antigens are overexpressed in prostate cancer cells, and are therefore potentially suitable for targeting prostate cancer using mAbs. We investigated the expression of 4 of the most common antigens in PC: PSMA, PSCA, MUC1 and TROP-2 in human prostate cancer tissue samples by means of immunohistochemical analysis. We investigated frozen samples of normal human prostate tissue, BPH tissue and prostate cancer tissue with increasing Gleason grades (n=2-3). All samples were stained with mAbs directed against the PC-associated antigens mentioned above. Sections were stained with diaminobenzidine and counterstained with hematoxylin. Gleason grade of the samples was scored. Intensity of staining was scored as - (no staining), ± (very weak staining), + (weak staining), ++ (moderate staining), +++ (strong staining) and ++++ (very strong staining). Staining intensity can be compared within samples from the same Ab, but not between different Abs, due to the inequality in sensitivity of the antibodies for their respective antigens. Tissue samples were collected according to national and institutional guidelines. Results are summarized in Table 1.

PSMA

PSMA is by far the most well-known target in PC imaging. PSMA is an integral, membrane glycoprotein (84 kD) that is highly expressed on prostate epithelial cells. It is a homologue of the protein N-acetyl-L-aspartyl-L-glutamate peptidase I (NAALADase I or

Table 1. Intensity of immunohistochemical staining of normal human prostate tissue and prostate cancer Gleason grade 8 samples using 4 different antibodies (PSMA, PSCA, TROP-2 and MUC1).

	PSMA	PSCA	TROP-2	MUC1
Normal*	+ / +++	- / +	++ / +++	-
BPH*	± / +++	- / ±	++ / +++	-
Gleason < 6**	++ / +++	-	+ / ++	-
Gleason 6*	++ / +++	-	+ / +++	- / ±
Gleason 7-8*	++ / ++++	- / ±	++ / +++	- / ±
Gleason 9-10*	+++ / ++++	- / ++	++ / +++	- / ±

*n=3, **n=2

folate hydrolase I), a protein which is active in the central nervous system. In malignant tissue, PSMA has been suggested to be involved in angiogenesis, as PSMA was found to be expressed in the endothelial cells lining the neovasculature of solid tumors, next to its expression in prostate cancer cells [5]. In our immunohistochemical studies, although with a limited number of prostate tissue samples, a clear intense staining of all prostate cancer samples was observed, with a trend of higher expression in PC with a higher Gleason score (Table 1, Figure 3). This is in accordance with other studies, which conclude that PSMA is strongly upregulated in prostate cancer (95% expression in PC cells and 100% in tumor positive lymph nodes and bone metastasis) [15]. PSMA expression levels are directly correlated to PC progression, expression increases with androgen independence, metastasis and cancer progression [29].

PSCA

PSCA (Prostate Stem Cell Antigen) is a small (10-24 kDa), anchored cell-surface glycoprotein, that is expressed on several epithelial cells among which epithelial cells of the prostate. It is expressed mainly in differentiating cells rather than in stem cells, contradictory to the suggestion of its name. Table 1 shows limited expression of PSCA in normal tissue, that increases with Gleason grade (Figure 3) which is in line with literature findings. PSCA is expressed extensively in PC: 90% in primary prostate cancer [30] and 95% in lymph node and bone metastasis [15]. Its expression increases with increasing Gleason score, tumor invasion, androgen independence and is related to poor prognosis. Expression is limited by androgen deprivation [29].

TROP-2

TROP-2, also known as EGP-1 (epithelial glycoprotein-1), GA733-1, gp50/T16, TACSTD2 (tumor-associated calcium signal transducer 2), is a 46 kDa transmembrane glycoprotein expressed in carcinomas of the lung, bladder, breast, cervix, ovary, stomach and prostate. Most normal human tissues do not express TROP-2, but it is found

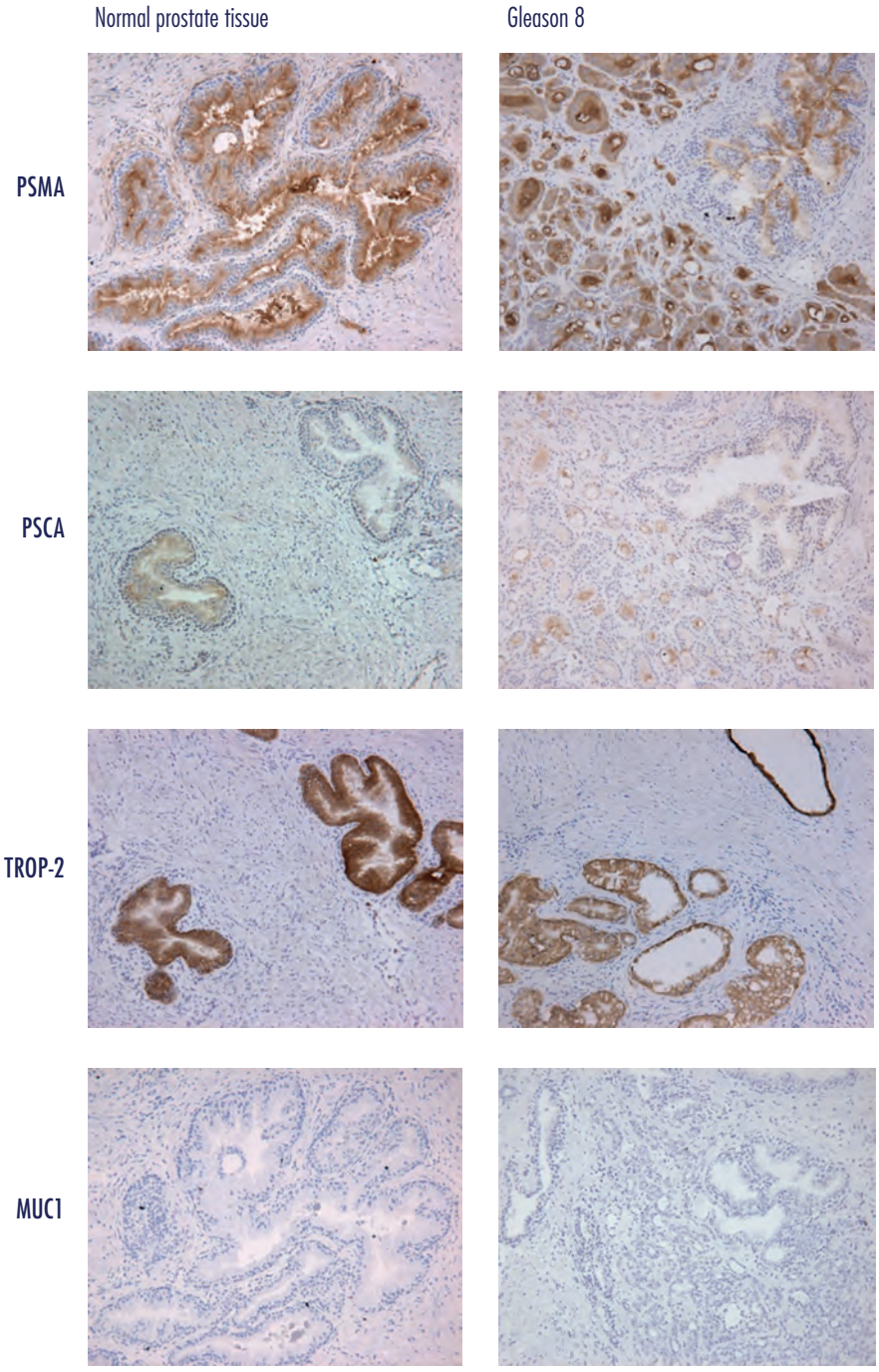

Figure 3. Immunohistochemical staining of normal human prostate tissue and prostate cancer Gleason grade 8 samples using 4 different antibodies (PSMA, PSCA, TROP-2 and MUC1).

in epithelial tissue and at low levels in several normal glandular cells, including glands in the bronchus, breast, prostate and skin, and ducts and acini of the pancreas [31]. Immunohistochemical analysis of the different samples of prostate tissue shows relatively high expression in normal prostate tissue and BPH as well as prostate cancer samples with different Gleason scores, without obvious increase with increasing Gleason scores (Table 1, Figure 3).

MUC1

MUC1 is a large mucin (122 kDa) expressed on the surface of most epithelial tissues. In PC tissue MUC1 is expressed equally over the tumor cell surface, as opposed to its apical expression in normal epithelial cells. Table 1 shows virtually no expression in healthy prostate tissue and BPH, together with limited expression in higher PC grades (Figure 3). Overexpression of MUC1 is seen in several cancer types such as ovarian, lung, pancreatic, colon and some types of prostate cancer, and has been related to tumor angiogenesis, proliferation, signal transduction, invasion, metastasis, and immunosuppression.

Due to their specificity, monoclonal antibodies can be used for cancer imaging and targeted therapy. However, there are several drawbacks to the use of mAbs in radioimmunoimaging and -therapy. Due to the long circulatory half-lives of intact antibodies (IgG), lesions can only be depicted several days after injection when the radiolabeled antibody has cleared from the background tissues. This is inconvenient for patients and for clinical practice. Next, this limits the use of this imaging modality when imaging is required directly before and after treatment [32]. In addition, monoclonal antibodies show nonspecific localization in tumors and inflamed tissues due to the Enhanced Permeability and Retention (EPR) effect.

Furthermore, in radioimmunotherapy, the long circulatory half-life of mAbs causes relatively high radiation doses to well-perfused tissues such as liver, spleen and bone marrow. The long exposure to the therapeutic radionuclide results in clinically relevant myelotoxicity limiting the activity dose that can be safely administered. To avoid toxicity related to slow clearance of radiolabeled antibodies from the circulation, various approaches can be applied. One of these approaches consists of the use of antibody fragments, because antibody fragments are cleared much faster from the blood. In general, tumor uptake of antibody fragments is lower than that of the intact antibody, while kidney uptake is higher. Another strategy to use the excellent targeting capability of mAbs and to overcome their disadvantages in imaging and RIT is pretargeting.

Pretargeting

In pretargeting, tumors are targeted by a non-radiolabeled targeting agent, allowing the unbound agent to clear from the circulation, followed by a second injection of a

radiolabeled small molecule that is recognized by the targeting agent. The unbound radiolabeled compound then rapidly accumulates in the tumor or clears quickly from the circulation (Figure 4). This concept was first published in 1984 by Goodwin et al. Two pretargeting approaches can be distinguished. The first approach is based on the ultra-high binding affinity (10^{-15} M) [33] of biotin to mammalian avidin or bacterial streptavidin. The biotin-avidin pretargeting system has been applied clinically, but is hampered by the inherent immunogenicity of (strept)avidin being a nonhuman protein. Next to that, due to the high affinity of biotin and (strept)avidin, both agents also complex in the circulation, thus causing longer circulatory half-life of the radiolabeled compound.

The second strategy uses bispecific antibodies (bsAbs) as targeting agents. Initially, these bispecific antibodies were developed by chemically coupling anti-tumor-antibody Fab-fragments with an anti-chelator antibody. Injection of this bsAb was followed by a radiolabeled chelator. Salaun et al [34] performed a phase II clinical trial in patients with metastatic medullary thyroid carcinoma (MTC) using an anti-CEA x anti-DTPA bsAb, followed by injection of an ^{131}I-di-DTPA-indium bivalent hapten. This pretargeted radioimmunotherapy approach showed antitumor activity, accompanied by severe but manageable toxicity in progressive MTC.

This system was improved by replacing the chelator by an HSG (Histamine-Succinyl-Glycine) hapten-peptide containing a DOTA moiety, which was suitable for

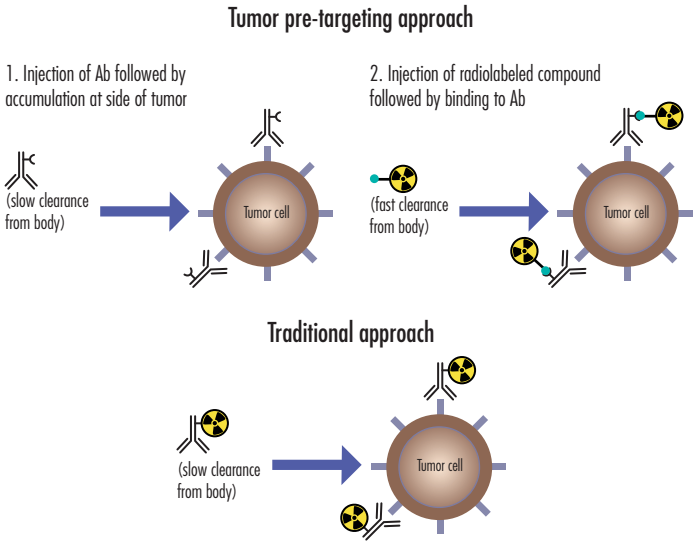

Figure 4. Pretargeting.
This figure was originally published in: Borrmann A, van Hest JCM. Bioorthogonal chemistry in living organisms. Chem Sci 2014; 5(6):2123–34. © by Chem Sci.

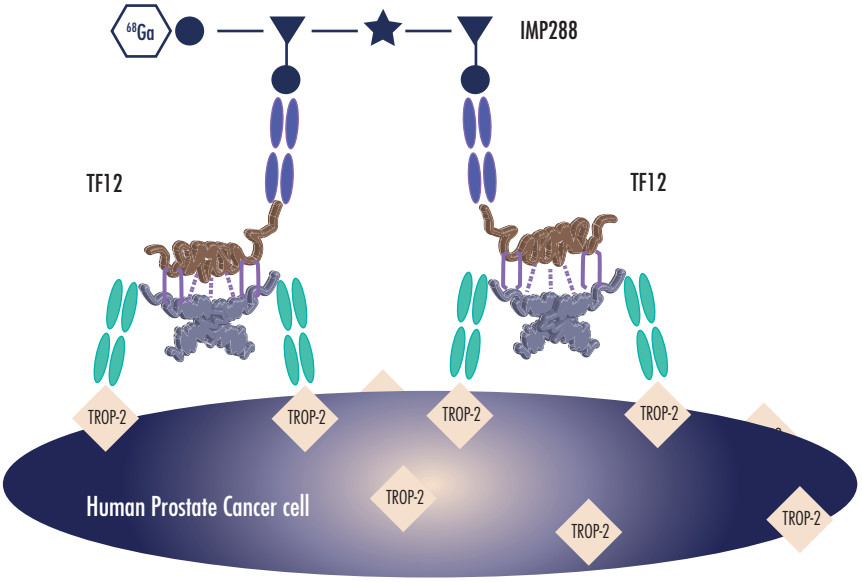

Figure 5. Pretargeting with TF12 and IMP288.
This figure was originally published in: Goldenberg DM, Rossi EA, Sharkey RM, McBride WJ, Chang CH. Multifunctional antibodies by the Dock-and-Lock method for improved cancer imaging and therapy by pretargeting. J Nucl Med 2008; 49(1):158-63. © by the Society of Nuclear Medicine and Molecular Imaging, Inc.

labeling with different radionuclides. The bsAb was further optimized by introducing the Dock-and-Lock (DNL) method developed by Rossi et al., efficiently joining two anti-tumor Fab fragments covalently with one anti-HSG-Fab fragment [35]. This trivalent bsAb provided higher tumor uptake and retention than Fab'- Fab'conjugates, and relatively rapid clearance from the circulation. The combination of one anti-HSG-Fab-fragment on the bsAb together with two HSG residues on the hapten-peptide provided optimal tumor retention of the radiolabeled peptide-hapten, a phenomenon referred to as affinity enhancement [33, 36]. Radiolabeled compounds bearing two haptens are more avidly bound at the tumor cell surface, since they can cross-link between two adjacent bsAbs at the tumor cell surface (Figure 5) [37]. This system allowed for high tumor-to-blood ratios within 1 h after injection of the radiolabeled peptide.
Using the DNL method, several recombinant bsAbs were produced including an anti-CEA bsAb (TF2), an anti-CD20 bsAb (TF4), an anti-EGP-1 bsAb (TF12) and an anti-MUC1 bsAb (bsPAM4) [38]. In a phase I/II clinical trial Schoffelen et al. have demonstrated the potential of such an approach to target colorectal carcinoma (CRC) in patients. The results showed rapid and specific tumor targeting of the ^{111}In- or ^{177}Lu-labeled hapten-peptide IMP288 after pretargeting with TF2. The study demonstrated that PRIT in CEA expressing CRC is feasible and safe [39].

For pretargeting of human carcinomas, the bsAb TF12 (Figure 5) was developed using the DNL method, based on the monoclonal antibody hRS7 in combination with the anti-HSG mAb. hRS7 is a humanized IgG1 monoclonal antibody directed against TROP-2, which is overexpressed in prostate cancer. The studies described in this thesis, aimed to provide proof-of-concept for pretargeting of prostate cancer, using TF12 together with the di-HSG-hapten IMP288 (Figure 6).

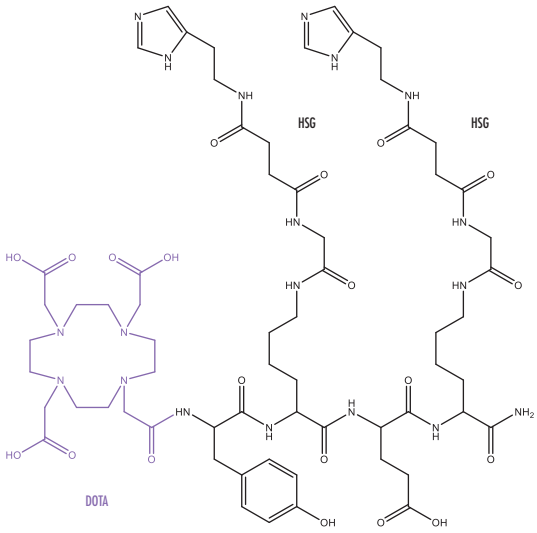

Figure 6. Structural formula of IMP288.

Aim of the studies

The aim of the studies described in this thesis was to investigate the potential of (pre) targeted radioimmunoimaging and radioimmunotherapy of prostate cancer using a radiolabeled humanized anti-TROP-2 monoclonal antibody (hRS7) and an anti-TROP-2 x anti-HSG bispecific monoclonal antibody (TF12) in combination with a radiolabeled di-HSG hapten-peptide (IMP288).

Acknowledgements

We gratefully thank Jack Schalken and Tilly Aalders (Department of Experimental Urology, Radboud University Medical Center, The Netherlands) for their valuable contribution to the immunohistochemical studies.

Thesis outline

Substantial progress has been made in the development of functional and molecular imaging modalities for prostate cancer, such as positron emission tomography using radiolabeled metabolic tracers, receptor-binding ligands, amino acids, peptides and antibodies. In chapter 2, the value of these novel radionuclide based molecular imaging techniques in the assessment of prostate cancer is reviewed.
In chapter 3, the characteristics of the anti-TROP-2 monoclonal antibody hRS7 for targeting prostate cancer are assessed. Its potential in both immunoSPECT and

immunoPET is investigated in nude mice with human prostate cancer xenografts.
In chapter 4, the internalizing properties of the anti-TROP-2 bispecific antibody TF12 are evaluated both in vitro and in vivo, to determine whether its internalizing properties would hamper its use in pretargeting.
In chapter 5, pretargeting of PC with anti-TROP-2 x anti-HSG bsAb TF12 and the radiolabeled di-HSG peptide IMP288 is investigated in mice with human prostate tumors. The optimal dose of both agents and optimal dose interval are determined, as well as the retention of the radiolabeled hapten-peptide in the tumor. After optimization, the potential for pretargeted radioimmunoimaging and radioimmunotherapy is assessed in the same mouse model.
Chapter 6 describes our studies investigating radioimmunoPET using TF12 and ^{68}Ga-IMP288 in mice with s.c. and i.p. human PC xenografts using ^{18}F-FDG as a reference.
In chapter 7, the efficacy of pretargeted radioimmunotherapy with multiple cycles of TF12 and ^{177}Lu-labeled IMP288 in mice with PC xenografts is investigated and compared with that of conventional radioimmunotherapy with ^{177}Lu-labeled hRS7.

References

1. IKNL. Landelijke Richtlijn Prostaatcarcinoom. 04-16; http://www.oncoline.nl/index.php? pagina=/richtlijn/item/pagina.php&id=37145&richtlijn_id=934&tab=1. Accessed 03-20, 2015.
2. NIH. SEER Stat Fact Sheets: Prostate Cancer. Surveillance, Epidemiology and End Results program [http://seer.cancer.gov/statfacts/html/prost.html. Accessed 03-20, 2015.
3. Cremers RG, Galesloot TE, Aben KK, et al. Known susceptibility SNPs for sporadic prostate cancer show a similar association with "hereditary" prostate cancer. Prostate 2015;75(5):474-483.
4. Lütje S, Boerman OC, van Rij CM, et al. Prospects in radionuclide imaging of prostate cancer. Prostate 2012; 72(11):1262-1272.
5. Lütje S, Heskamp S, Cornelissen AS, et al. PSMA Ligands for Radionuclide Imaging and Therapy of Prostate Cancer: Clinical Status. Theranostics 2015; 5(12):1388-1401.
6. Barentsz MW, Verkooijen HM, Pijnappel RM, et al. Sentinel lymph node localization with contrast-enhanced ultrasound and an ^{125}I seed: An ideal prospective development study. Int J Surg 2015; 14:1-6.
7. Ravizzini G, Turkbey B, Kurdziel K, et al. New horizons in prostate cancer imaging. Eur J Radiol 2009; 70(2):212-226.
8. Jadvar H. Molecular imaging of prostate cancer with PET. J Nucl Med 2013; 54(10):1685-1688.
9. Kitajima K, Murphy RC, Nathan MA. Choline PET/CT for imaging prostate cancer: an update. Ann Nucl Med 2013; 27(7):581-591.
10. Eder M, Eisenhut M, Babich J, et al. PSMA as a target for radiolabelled small molecules. Eur J Nucl Med Mol Imaging 2013; 40(6):819-823.
11. Bauman G, Belhocine T, Kovacs M, et al. ^{18}F-fluorocholine for prostate cancer imaging: a systematic review of the literature. Prostate Cancer Prostatic Dis 2012; 15(1):45-55.
12. Mohsen B, Giorgio T, Rasoul ZS, et al. Application of ^{11}C-acetate positron-emission tomography (PET) imaging in prostate cancer: systematic review and meta-analysis of the literature. BJU Int 2013; 112(8):1062-1072.
13. Pandit-Taskar N, O'Donoghue JA, Beylergil V, et al. ^{89}Zr-huJ591 immunoPET imaging in patients with advanced metastatic prostate cancer. Eur J Nucl Med Mol Imaging 2014; 41(11):2093-2105.
14. Tagawa ST, Milowsky MI, Morris M, et al. Phase II study of Lutetium-177-labeled anti-prostate-specific membrane antigen monoclonal antibody J591 for metastatic castration-resistant prostate cancer. Clin Cancer Res 2013; 19(18):5182-5191.
15. Ananias HJ, van den Heuvel MC, Helfrich W, et al. Expression of the gastrin-releasing peptide receptor, the prostate stem cell antigen and the prostate-specific membrane antigen in lymph node and bone metastases of prostate cancer. Prostate 2009; 69(10):1101-1108.
16. Kahkonen E, Jambor I, Kemppainen J, et al. In vivo imaging of prostate cancer using ^{68}Ga-labeled bombesin analog BAY86-7548. Clin Cancer Res 2013; 19(19):5434-5443.
17. Beer M, Montani M, Gerhardt J, et al. Profiling gastrin-releasing peptide receptor in prostate tissues: clinical implications and molecular correlates. Prostate 2012; 72(3):318-325.
18. Barrett JA, Coleman RE, Goldsmith SJ, et al. First-in-man evaluation of 2 high-affinity PSMA-avid small molecules for imaging prostate cancer. J Nucl Med 2013; 54(3):380-387.

19. Osborne JR, Akhtar NH, Vallabhajosula S, et al. Prostate-specific membrane antigen-based imaging. Urol Oncol 2013; 31(2):144-154.
20. Vallabhajosula S, Nikolopoulou A, Babich JW, et al. ^{99m}Tc-labeled small-molecule inhibitors of prostate-specific membrane antigen: pharmacokinetics and biodistribution studies in healthy subjects and patients with metastatic prostate cancer. J Nucl Med 2014; 55(11):1791-1798.
21. Eder M, Neels O, Muller M, et al. Novel Preclinical and Radiopharmaceutical Aspects of ^{68}Ga-PSMA-HBED-CC: A New PET Tracer for Imaging of Prostate Cancer. Pharmaceuticals 2014; 7(7):779-796.
22. Afshar-Oromieh A, Malcher A, Eder M, et al. PET imaging with a ^{68}Ga-labelled PSMA ligand for the diagnosis of prostate cancer: biodistribution in humans and first evaluation of tumour lesions. Eur J Nucl Med Mol Imaging 2013; 40(4):486-495.
23. Eiber M, Maurer T, Souvatzoglou M, et al. Evaluation of Hybrid ^{68}Ga-PSMA Ligand PET/CT in 248 Patients with Biochemical Recurrence After Radical Prostatectomy. J Nucl Med 2015; 56(5):668-674.
24. Rowe SP, Mana-Ay M, Javadi MS, et al. PSMA-Based Detection of Prostate Cancer Bone Lesions With ^{18}F-DCFPyL PET/CT: A Sensitive Alternative to ^{99m}Tc-MDP Bone Scan and Na^{18}F PET/CT? Clin Genitourin Cancer 2016; 14(1):e115-118.
25. Dietlein M, Kobe C, Kuhnert G, et al. Comparison of ^{18}F-DCFPyL and ^{68}Ga-PSMA-HBED-CC for PSMA-PET Imaging in Patients with Relapsed Prostate Cancer. Mol Imaging Biol 2015; 17(4):575-584.
26. Hoskin P, Sartor O, O'Sullivan JM, et al. Efficacy and safety of radium-223 dichloride in patients with castration-resistant prostate cancer and symptomatic bone metastases, with or without previous docetaxel use: a prespecified subgroup analysis from the randomised, double-blind, phase 3 ALSYMPCA trial. Lancet Oncol 2014; 15(12):1397-1406.
27. Baum RP, Kulkarni HR, Schuchardt C, et al. Lutetium-177 PSMA Radioligand Therapy of Metastatic Castration-Resistant Prostate Cancer: Safety and Efficacy. J Nucl Med 2016. Epub jan 21.
28. Liu JK. The history of monoclonal antibody development - Progress, remaining challenges and future innovations. Ann Med Surg 2014; 3(4):113-116.
29. Li Y, Cozzi PJ, Russell PJ. Promising tumor-associated antigens for future prostate cancer therapy. Med Res Rev 2010; 30(1):67-101.
30. Saeki N, Gu J, Yoshida T, et al. Prostate stem cell antigen: a Jekyll and Hyde molecule? Clin Cancer Res 2010; 16(14):3533-3538.
31. Basu A, Goldenberg DM, Stein R. The epithelial/carcinoma antigen EGP-1, recognized by monoclonal antibody RS7-3G11, is phosphorylated on serine 303. Int J Cancer 1995; 62(4):472-479.
32. Lütje S. Antibody-based imaging of Prostate Cancer. Nijmegen: Radiology and Nuclear Medicine, Radboud University Nijmegen; 2014.
33. Sharkey RM, Chang CH, Rossi EA, et al. Pretargeting: taking an alternate route for localizing radionuclides. Tumour Biol 2012; 33(3):591-600.
34. Salaun PY, Campion L, Bournaud C, et al. Phase II trial of anticarcinoembryonic antigen pretargeted radioimmunotherapy in progressive metastatic medullary thyroid carcinoma: biomarker response and survival improvement. J Nucl Med 2012; 53(8):1185-1192.
35. Rossi EA, Goldenberg DM, Cardillo TM, et al. Stably tethered multifunctional structures of defined composition made by the dock and lock method for use in cancer targeting. Proc Natl Acad Sci USA 2006; 103(18):6841-6846.

36. Goldenberg DM, Chang CH, Rossi EA, et al. Pretargeted molecular imaging and radioimmunotherapy. Theranostics 2012; 2(5):523-540.
37. Sharkey RM, Goldenberg DM. Cancer radioimmunotherapy. Immunotherapy 2011; 3(3):349-370.
38. van de Watering FC, Rijpkema M, Robillard M, et al. Pretargeted imaging and radioimmunotherapy of cancer using antibodies and bioorthogonal chemistry. Front Med 2014; 1:44.
39. Schoffelen R, Boerman OC, Goldenberg DM, et al. Development of an imaging-guided CEA-pretargeted radionuclide treatment of advanced colorectal cancer: first clinical results. Br J Cancer 2013; 109(4):934-942.

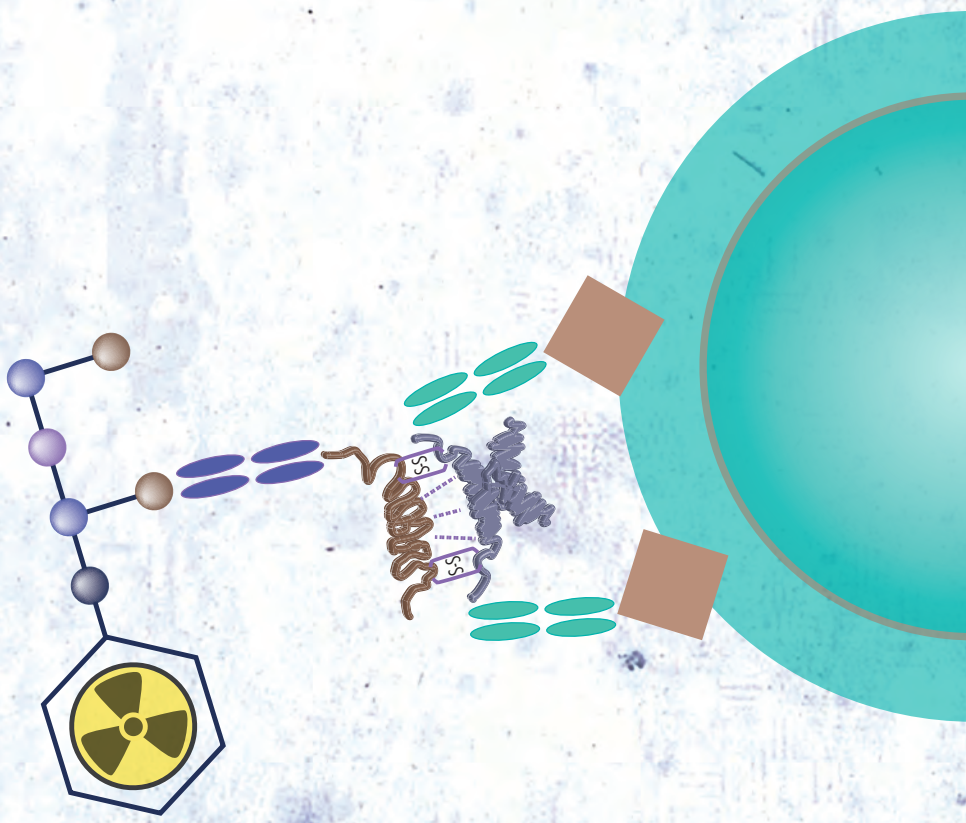

Prospects in radionuclide imaging of prostate cancer

2

Susanne Lütje
Otto C. Boerman
Catharina M. van Rij
Michiel Sedelaar
Wijnand Helfrich
Wim J.G. Oyen
Peter F.A. Mulders

Prostate 2012; 72(11):1262-1272

Abstract

Prostate cancer is the most common malignancy in men in the Western world and represents a major health problem with substantial morbidity and mortality. Sensitivity and specificity of digital rectal examination (DRE) and evaluation of prostate specific antigen (PSA) are excellent methods for diagnosis of prostate cancer, but have limited value for staging. Imaging of prostate cancer has become increasingly important to improve staging and management of prostate cancer patients. Conventional imaging modalities, such as transrectal ultrasound and computed tomography, show limited accuracy for a reliable assessment of prostate cancer. Diagnostic value of magnetic resonance imaging has improved by dynamic contrast enhancement (DCE-MRI) and diffusion-weighted magnetic resonance imaging (DWI). Recently, substantial progress has been made in the development of functional and molecular imaging modalities, such as positron emission tomography using radiolabeled metabolic tracers, receptor-binding ligands, amino acids, peptides, or antibodies. Here, we review the value of these novel radionuclide imaging techniques in the assessment of prostate cancer.

Introduction

Prostate cancer remains the most common malignancy in men in Europe, with an incidence of 382,000 cases and a mortality rate of 89,000 in 2008 [1]. In early stages of the disease, neoplastically transformed prostate cells are confined to the prostate gland. In later stages malignant cells metastasize to other parts of the body, typically including bones and lymphnodes. Currently, metastatic prostate cancer is essentially incurable. Therefore, early diagnosis represents the most effective strategy with a change for curative treatment options and consequently minimizes prostate cancer-related mortality [2].

At present, in the US screening for prostate cancer is advisable for men above 40 years of age by evaluation of the prostate-specific antigen levels (PSA) and by digital rectal examination (DRE). When abnormalities are found or suspected, further evaluation is commenced, typically by taking transrectal ultrasound (TRUS)-guided biopsy [3]. The most commonly used histopathological grading system for prostate cancer is the Gleason score. Together with other patient parameters, like age, health state, PSA levels, and biopsy pathology, the Gleason grading system predicts prognosis and helps to guide therapeutic management. Patients with a low Gleason score have well-to-moderately differentiated prostate cancer histology and usually have localized disease. These early-stage patients can have a very indolent course of the disease with low mortality rates and can be monitored by watchful waiting to prevent overtreatment and related morbidity.

Curative treatment of confined prostate cancer includes radical prostatectomy performed either as an open conventional procedure or by (robot-assisted) laparoscopic surgery and may be combined with various forms of radiation therapy (RT), including 3-dimensional conformal RT, intensity-modulated RT, or proton beam RT [4]. Other curative treatment options include brachytherapy combined with external- beam RT, high-intensity focused ultrasound, and cryosurgery. However, in a substantial proportion of prostate cancer patients, primary curative treatment fails, as becomes evident by frequent recurrences of the disease. In general, the first sign indicating treatment failure is a shorter doubling time of PSA serum levels that may occur months or even years before development of clinical symptoms or radiographic indications for recurrent disease.

However, the diagnostic use of PSA levels has several important drawbacks. Due to low sensitivity and specificity, the diagnostic value of PSA levels is limited and may yield both false-negative and false-positive results, leading to under- and overtreatment, respectively. Most notably, evaluation of PSA levels fails to differentiate between local and metastatic disease, which is in fact a prerequisite for appropriate management of the disease [5]. Therefore, new highly sensitive and specific imaging modalities for accurate visualization of prostate cancer and reliable monitoring of therapy response are urgently needed. Radionuclide imaging techniques such as PET and SPECT are

very sensitive imaging modalities as picomolar amounts of the tracer can be detected. Depending on the radiotracer used, these techniques can visualize specific molecular processes.
Here, we review conventional and novel imaging modalities in prostate cancer and discuss the new developments in radionuclide imaging of prostate cancer in more detail.

Conventional imaging methods

Transrectal Ultrasound

Today, transrectal ultrasound (TRUS) is the most commonly used technique for further clinical evaluation of size and anatomy of the prostate gland. TRUS has several advantages including high level of safety, favorable portability, relatively low costs, ease of use, and the possibility to perform real-time imaging. However, several disadvantages like low resolution, sensitivity, and specificity limit the reliability of TRUS. In particular, TRUS has a limited ability to delineate small cancer foci which usually are isoechoic and therefore cannot be detected. Moreover, the majority of hypoechoic foci detected by TRUS are not malignant, but rather represent conditions such as benign prostatic hyperplasia (BPH), atrophy, or inflammatory processes in the prostate gland [6].
Currently, several modulations of TRUS are clinically available, including Doppler TRUS and contrast-enhanced TRUS with microbubbles. Using Doppler TRUS, regions of tumors with hypervascularity can be detected. However, since many small tumors are not angiogenic, the sensitivity of Doppler TRUS is not significantly increased compared to TRUS [7]. In contrast-enhanced TRUS with microbubbles, sensitivity to detect tumor foci is higher than in conventional TRUS, still, imaging does not reliably discriminate between inflammatory and malignant processes in the prostate [8].

Computed Tomography

Due to its soft-tissue type tissue architecture, the prostate gland can only be visualized poorly by computed tomography (CT). An accurate distinction between neoplastic and healthy tissue by CT is currently not feasible. Therefore, the use of CT in prostate cancer is limited to providing an anatomic reference for functional imaging modalities and for the detection of metastatic bone involvement.

Magnetic Resonance Imaging

The soft-tissue resolution of Magnetic Resonance Imaging (MRI) is superior to CT. MRI accurately visualizes the anatomy of the prostate, which allows a more reliable detection of prostate cancer. Moreover, with innovative techniques such as diffusion weighted MRI (DWI), MR spectroscopy (MRS), and dynamic contrast-enhanced MRI (DCE-MRI), functional assessment of the disease is also possible, resulting in a more precise staging and follow-up of prostate cancer.

In malignant tumors with high cellular density diffusion of water molecules is restricted, a process that can be visualized by DWI [9]. Typically, prostate cancers have relatively tight glandular elements with increased cellular density and decreased extracellular space, producing high-signal-intensity foci on DWI [8]. Unfortunately, the specificity of this modality is relatively low since benign hyperplastic changes can also show low water diffusion [8].

MRS is a technique that provides information on aberrant levels of cellular metabolites. Prostate cancer is associated with locally elevated levels of choline and polyamine and decreased levels of citrate that can be evaluated by MRS. Recent reports indicate that MRS appears to be a promising functional imaging modality for the detection of prostate cancer [10, 11, 12]. Unfortunately, to obtain increased tumor detection rate MRS needs to be combined with MRI, which is technically challenging and therefore currently not widely available [13].

With DCE-MRI, tumor vascularization can be visualized by quantitative kinetic parameters that reflect blood flow and the vascular permeability [8]. DCE-MRI has higher specificity than MRI alone [14]. However, small low-grade tumors might be missed due to lack of angiogenesis. Furthermore, there is a concern regarding gadolinium-based contrast agents due to the risk for induction of nephrogenic systemic fibrosis in patients with renal failure [8].

More advanced imaging techniques include high-resolution MRI combined with lymphotropic superparamagnetic (ultra) small particles of iron oxide, (U)SPIO. Administered intravenously, (U)SPIO penetrate the vascular endothelium and enter the interstitial space and lymph vessels, finally reaching the lymph nodes. In the lymph nodes, the particles are phagocytised by macrophages which produces signal variations. In case of malignant involvement of the lymph node, absence of macrophage activity leads to signal modification. Consequently, affected lymph nodes will appear hyperintense on T2-weighted MRIs [15]. It has been found that USPIO-MRI has a significantly higher sensitivity than conventional MRI [16]. However, several disadvantages may limit the clinical use of USPIO-MRI, such as the requirement for particular expertise, its time-consuming nature, and the limited sensitivity of USPIO-MRI in small lymph nodes (<5 mm). Recently, the uptake of bombesin-functionalized iron oxide nanoparticles in PC3 prostate cancer cells has been evaluated and preclinical data indicate that this approach may yield a prostate cancer-selective imaging probe [17].

Radionuclide imaging

Positron Emission Tomography

Radiolabeled metabolite tracers

Today, positron emission tomography (PET) is emerging as an important functional imaging modality in various malignancies. Using PET, specific cellular and molecular processes, such as glucose metabolism and cell proliferation can be functionally visualized. The most commonly used tracer for PET imaging is ^{18}F-fluorodeoxyglucose (^{18}F-FDG). Tumor cells can be depicted by this technique by exploiting their enhanced glucose demand that is mainly due to increased aerobic glycolysis in malignant cells, allowing them to be distinguished from normal cells [18]. ^{18}F-FDG is taken up via glucose transporters. Intracellularly, ^{18}F-FDG is rapidly phosphorylated after which it cannot be metabolized any further. Consequently, ^{18}F-FDG is trapped inside metabolically active cells and can be visualized with PET.

For anatomic reference for the functional PET images, integrated PET/CT has become the standard technology. Unfortunately, in primary prostate cancer ^{18}F-FDG-PET with or without integration of CT has only limited sensitivity. A large fraction of prostate cancers expresses only low numbers of glucose transporters such as Glut-1, which limits ^{18}F-FDG uptake [19]. In addition, sensitivity of ^{18}F-FDG-PET is also limited since ^{18}F-FDG is excreted mainly via the urinary tract, obscuring the prostate gland, and restricting the identification of pelvic lymph node metastases [20].

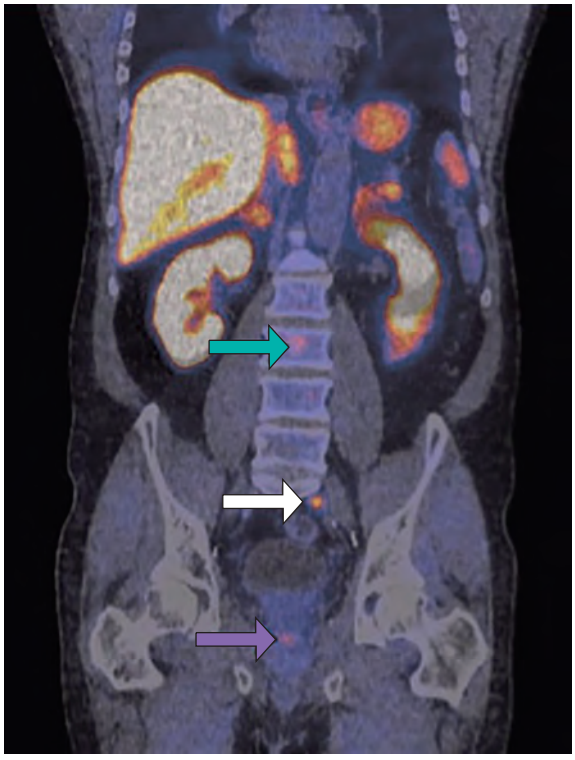

Figure 1. PET/CT image acquired after injection of ^{11}C-choline in a patient with prostate cancer. This image shows metastatic involvement of a lymph node (white arrow) and vertebra (green arrow).

3-Deoxy-3-^{18}F-fluorothymidine (FLT) radiolabeled with ^{18}F is another potential tracer for monitoring early effects of treatment of hormone-refractory prostate cancer. FLT has been introduced as a radiopharmaceutical for assessing tumor proliferation with PET imaging. Oyama et al. [21] demonstrated a significant decrease of FLT uptake in tumors after administration of docetaxel, while the changes of FDG uptake were minimal. Immunohistochemical analysis revealed that the changes of FLT uptake were correlated with those of proliferation activity.

Currently, choline radiolabeled with ^{11}C (Figure 1) or ^{18}F (Figure 2) is routinely used as PET tracer to image prostate cancer [22]. The use of choline is based on the fact that it is a key precursor in the biosynthesis of phosphatidylcholine, a major component of the cell membrane.

An explanation for increased choline uptake in prostate cancer might be the increased proliferation rate in tumors [23]. Another possible explanation is upregulation of choline kinase in cancer cells [24].

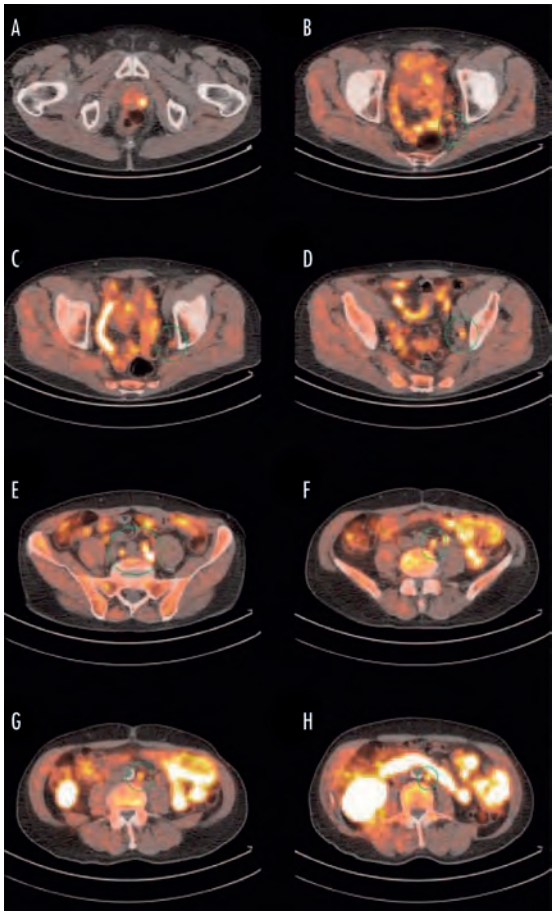

Figure 2. Transaxial slices of ^{18}F-choline PET/CT images of a patient with metastasized prostate cancer. Panel (**A**) shows local recurrence of prostate cancer in the left retrovesical area. Panels (**B-H**) show metastatic involvement of lymph nodes.

The major advantage of ^{11}C-choline PET is the limited excretion rate via the urinary system, which minimizes obscuring of the prostate and therefore enables imaging of the pelvis without confounding bladder activity [25]. Rinnab and coworkers [26] evaluated ^{11}C-choline PET/CT in 50 patients with biochemical recurrence and reported a sensitivity of 91% at PSA concentrations below 2.5 ng/ml and a specificity of 50%. Besides low specificity, the use of the tracer ^{11}C-choline is limited by the short half-life of ^{11}C (t½ 20 min), which requires the availability of an on-site cyclotron [22]. With a half-life of 110 min, ^{18}F-labeled choline (^{18}F-FCH) overcomes this limitation. However, urinary excretion of ^{18}F-FCH is higher than that of ^{11}C-choline and might confound image

interpretation. Eschmann et al. [27] compared ^{11}C-choline PET/CT with conventional whole-body MRI and reported a better overall diagnostic performance with ^{11}C-choline PET/CT due to higher detection rate of lymph node metastases and other local disease related alterations. However, for detection of bone metastases, the authors recommend a combination of both techniques to improve diagnostic accuracy.

Acetate is another commonly used tracer for PET imaging of prostate cancer. Intracellularly, acetate is converted into acetyl-CoA and incorporated into cholesterol and fatty acids, which finally form the cellular membrane. Recently, fatty acid synthesis was shown to be increased in prostate cancer with fatty-acid synthase being overexpressed [28]. Since acetate is excreted mainly via the pancreas [8], confounding bias through bladder activity is prevented which enables accurate imaging of the pelvis. Therefore, ^{11}C-acetate PET has been clinically evaluated for detection and follow-up of prostate cancer. A clinical trial by Albrecht et al. [29] suggested that ^{11}C-acetate PET might be useful for the detection of recurrent prostate cancer, especially in very early work-up of postoperative patients presenting with very low PSA values. Those data confirmed previous PET studies by Oyama et al. [30], who showed that ^{11}C-acetate uptake in the prostate bed as well as in lymph nodes was superior to that of ^{18}F-FDG. ^{18}F-fluoroacetate, an ^{18}F-labeled analogue of acetate, has also been developed for PET. Similar to acetate, ^{18}F-fluoroacetate is substrate for acetyl coenzyme A synthase, but with lower specificity. ^{18}F-fluoroacetate represents a new alternative for ^{11}C-acetate in PET imaging of prostate cancer with the benefit of using a positron emitter with a longer half-life [31]. Small-animal PET series with ^{18}F-fluoroacetate in CWR22 tumor-bearing mice showed clear delineation of tumor tissue compared to reference organs, suggesting that it might be a useful PET tracer for imaging of malignancies [31]. Matthies et al. [32] provided preliminary clinical data of a prostate cancer patient with rising PSA and progressive bone metastases. They showed that, compared to ^{11}C-acetate, ^{18}F-fluoroacetate PET offers the possibility of delayed imaging with the potential to further increase tumor to-background ratios.

For detection of malignant bone metastases, ^{18}F-sodium fluoride PET (Figure 3) has shown high sensitivity and specificity [33]. The uptake in malignant lesions represents the increase in local blood flow and osteoblast activity. ^{18}F-fluoride PET has been found to be more sensitive than ^{99m}Tc-methylene diphosphonate (^{99m}Tc-MDP) planar bone scintigraphy, especially in the early detection of metastases [33]. ^{18}F-fluoride PET is characterized by a twofold higher bone uptake than ^{99m}Tc-MDP, faster clearance from the blood pool and a higher target-to-background ratio [33]. Unfortunately, like ^{99m}Tc-MDP, ^{18}F-fluoride PET is not tumor-selective and false-positive rates may be high [34]. However, this limitation can be overcome by integration of ^{18}F-fluoride PET with CT, which provides higher specificity and sensitivity [35]. More recent data indicate ^{18}F-FCH PET/CT to be more specific than ^{18}F-fluoride PET/CT in the early detection of bone metastases [36].

Another potential tracer for PET imaging of prostate cancer is ^{18}F-fluoropropionic acid (^{18}F-FPA). It is hypothesized that, as discussed above for fluoroacetate, ^{18}F-FPA mimics acetate and therefore accumulates in tumor tissue [37]. Compared to ^{18}F-FDG, ^{18}F-FPA showed more accurate delineation of CWR22 prostate cancer xenografts in mice. However, further research is necessary to evaluate if ^{18}F-FPA offers further advantages over existing tracers for prostate cancer.

Figure 3. Coronal and sagittal slices of a Na-F-^{18} PET scan of a patient with bone metastases in clavicula (green arrow), lumbal spine (L2, white arrow), and left femur (purple arrow).

Radiolabeled androgen receptor binding ligands

Recently, the imaging agent ^{18}F-fluoro-5-alpha-dihydrotestosterone (^{18}F-FDHT) that binds to androgen receptors, has been developed. Functional androgen receptor expression is a key factor in anti-androgen-based treatment of prostate cancer. Consequently ^{18}F-FDHT PET/CT may be exploited to monitor viable and androgen-sensitive tumor tissue and for the evaluation of anti-androgen therapy response [38]. The major advantage of this modality is that androgen-sensitive tumors can be detected whereas androgen-resistant tumors cannot, predicting if antiandrogen-based approaches represent a therapeutic option for individual patients. ^{18}F-FDHT PET/CT seems to be more likely to be of use in advanced disease with metastatic bone involvement rather than in localized prostate cancer, since background uptake can be high [39]. However, so far, experience with ^{18}F-FDHT PET/CT is limited and more studies evaluating its role in prostate cancer are needed.

Radiolabeled bombesin- and gastrin-releasing peptide receptor binding ligands

Since bombesin- and gastrin-releasing peptide receptors (GRPR) are overexpressed in prostate cancer, they represent a potential target for molecular imaging. The first radiolabeled bombesin analog (Cu-64-DOTA-8-amino-octanoicacid-bombesin) was introduced by Rogers et al. [39]. In this study, specific tumor localization of ^{64}Cu-DOTA-Aoc-bombesin in mice with PC3 xenografts was demonstrated by microPET imaging and was confirmed by biodistribution studies. However, the high uptake of ^{64}Cu-labeled bombesin in normal tissues prevented its clinical implementation.

In a very recent study, the values of the ^{111}In-labeled bombesin agonists PESIN, AMBA, MP2346, and MP2653 and the ^{99m}Tc-labeled antagonist Demobesin-1 for SPECT/CT imaging of prostate cancer were evaluated in SCID mice xenografted with human GRPR-overexpressing PC3 tumors [40]. Schroeder et al. showed that Demobesin-1 was superior to the other agents with respect to in vivo stability, tumor uptake, and retention. Typically, renal and pancreatic clearance for Demobesin-1 was fast. The best GRPR agonists in this study were PESIN and AMBA with sufficient in vivo stability and relatively high tumor uptake and retention. However, further studies are needed to evaluate the clinical use of these agents in patients with prostate cancer.

In another study, novel series of [^{64}Cu-NO_2A-(X)-BBN(*7*-14)NH_2] agonists for the specific targeting of GRPR on human PC3 cells and tumor tissue have been evaluated [41]. The [^{64}Cu-NO_2A-(AMBA)-BBN(*7*-14)NH_2] conjugate exhibited the highest accumulation in tumor tissue and the most efficient whole-body clearance via the renal-urinary excretion pathway.

One of the first clinical studies for imaging androgen-dependent prostate cancer using ^{99m}Tc-[Leu13]BN has been performed by Scopinaro and colleagues in eight patients with primary prostate cancer. They were able to visualize eight cancers in the prostate fossa with SPECT. Moreover, they reported uptake in obturator nodes which were proven to be cancer-specific by histopathology in three patients that were negative on MRI and CT [42]. In another study, Vincentis et al. [43] reported detection of prostate cancer by ^{99m}Tc BN SPECT in 12 out of 12 patients with androgen-dependent prostate cancer and visualization of loco-regional lymph nodes in 4 out of 12 patients. These preliminary data suggest that ^{99m}Tc BN SPECT could be useful to detect primary prostate cancer and to evaluate loco-regional lymph node involvement.

Other strategies focus on imaging of the heterodimeric transmembrane glycoprotein $\alpha_v\beta_3$ integrin that plays an important role in angiogenesis, metastasis, and the development of bone metastases in prostate cancer [44]. To image expression of $\alpha_v\beta_3$, the PET tracer ^{18}F-galacto-RGD was developed. Compared to conventional bone scans, the detection rate of bone metastases was higher using tracer ^{18}F-galacto-RGD PET. However, uptake of ^{18}F-galacto-RGD was heterogeneous, which suggests a variation in $\alpha_v\beta_3$ expression in prostate cancer metastases [45].

During invasion, angiogenesis, and metastasis of GRPR-positive tumors, the endothelial cells around the tumor tissue are activated and express high levels of integrin $\alpha_v\beta_3$.

Thus, many GRPR-positive tumors are also positive for integrin $\alpha_v\beta_3$ [45]. Due to this, dual-receptor targeting of $\alpha_v\beta_3$ and GRPR represents another potential approach for detection of prostate cancer. Therefore, a BBN-RGD peptide heterodimer has been developed, that recognizes GRPR through the BBN motif and integrin through the RGD motif. In prostate cancer xenograft models, the BBN-RGD heterodimer labeled with ^{18}F exhibited excellent tumor uptake and favorable in vivo kinetics superior to the BBN and RGD analogues [46].

In a subsequent study, 1,4,7-triazacyclononane-1,4,7-triacetic acid (NOTA) has been used as a chelator and the potential advantages of ^{64}Cu-labeled NOTA-RGD-bombesin heterodimer above the monomeric analogues NOTA-RGD and NOTA-bombesin for imaging GRPR-positive tumors were demonstrated [47].

Radiolabeled antibody imaging

Currently, extensive research is focused on both imaging and therapy of several types of malignancies using radiolabeled monoclonal antibodies (mAbs) directed towards relevant tumor-associated cell surface antigens.

Recently, several anti-PSMA antibodies have been developed that target the prostate specific membrane antigen (PSMA). The first antibody used to target PSMA in prostate cancer is capromab (7E11). Capromab pendetide (Prostascint®) is a monoclonal antibody labeled with ^{111}Indium that specifically targets an intracellular epitope of PSMA. Capromab pendetide was approved by the FDA for imaging of soft-tissue sites in metastatic prostate cancer for presurgical staging. In addition, it was approved for the evaluation of PSA relapse after local therapy. In a low number of presurgical patients with high-risk disease that show no lesions on CT or MRI scans, capromab detected positive nodes, thereby sparing these patients unnecessary surgical procedures [48]. However, as indicated above, capromab binds to the intracellular domain of PSMA. Therefore, binding to viable tumor cells first requires internalization. Alternatively, capromab may only bind to dead cells with disrupted cellular membranes. In addition, localization of capromab uptake is limited by nonspecific binding and high activity in the blood [8]. However, due to the relatively long half-life of ^{111}Indium (2.8 days), SPECT images can be obtained several days after injection, allowing washout of background activity from blood and bowel. Using capromab, detection of recurrence of disease, lymph node metastases, and other metastatic involvement is possible and combination with CT to improve anatomical resolution increases its specificity. One of the major limitations of imaging with radiolabeled capromab is the poor penetration in bone, limiting the detection of metastatic bone involvement [49].

To overcome limitations due to intracellular binding of capromab, antibodies binding to the epitopes on the extracellular domain of PSMA, such as J591, J415, and J533, have been developed that show high affinity binding to viable PSMA-expressing LNCaP cells [50]. In a preclinical study, mice were treated with J591 radiolabeled with ^{131}Iodine, ^{177}Lutetium, and ^{90}Yttrium. ^{177}Lu and ^{90}Y provide better dosimetry due

to their longer biological half-lives [51]. However, due to development of human-anti-mouse antibody (HAMA) responses, repetitive dosing was restricted. Meanwhile, a humanized form of J591 has been developed, which was well-tolerated and showed high tumor targeting capacity [52]. The first clinical studies with ^{111}In-, ^{90}Y, and ^{177}Lu-radiolabeled humanized mAb J591 have been performed by Bander et al. [53]. Tumor targeting results of 53 patients that received radiolabeled humanized J591 in phase I trials have been analyzed. In 43 evaluable patients, J591 accurately targeted bone lesions in 94% and soft-tissue lesions in 72% of the patients, respectively. They also showed that the humanized antibody is less immunogenic and can be administered several times to the same patient with persistently accurate tumor targeting activity.

More recently, a phase-II clinical trial with ^{177}Lu-J591 for metastatic castration-resistant prostate cancer has been completed with excellent targeting of CT or MRI proven sites of prostate cancer metastases in 94% of the patients [54]. During this study, thrombocytopenia was the most commonly seen hematologic toxicity and limited the dose of ^{177}Lu-J591. Also, ^{90}Y-J591 is known for its hematologic toxicity causing significant myelosuppression.

Recently, three other antibodies were identified that are directed against alternative epitopes on PSMA that appear to have diagnostic potential for prostate cancer [55]. Wolf et al. characterized monoclonal antibodies 3/A12, 3/E7, and 3/F11 in vitro and demonstrated a high affinity binding to PSMA-positive C4-2 cells for all three antibodies. A subsequent study focused on in vivo behavior, biodistribution, and tumor uptake of the ^{64}Cu-DOTA-labeled antibodies 3/F11 and 3/E7 and fragments of 3/A12 [52]. PET imaging demonstrated specific tumor uptake of these monoclonal antibodies in PSMA-positive C4-2 tumors in SCID mouse xenografts models, which further confirmed possible use of those antibodies in imaging of prostate cancer. Very recently, another group studied the potential targeting ability of the humanized IgG1 mAb hRS7 which is directed against EGP-1. The epithelial glycoprotein-1 (EGP-1) is a pancarcinoma marker that is expressed at high levels on virtually all prostate carcinomas. They evaluated the biodistribution of ^{111}In-, ^{125}I-, and ^{89}Zr-labeled hRS7 and performed immunoPET and immunoSPECT with ^{111}In-hRS7 and ^{89}Zr-hRS7 in mice with s.c. and intraprostatic PC3 xenografts. They showed that specific tumor uptake of hRS7 is high with high tumor-to- blood ratios, which allowed excellent immunoPET/CT and immunoSPECT imaging of the PC3 xenografts [56].

Another recent study developed a pretargeting approach for localizing advanced prostate cancer based on an anti-EGP-1 antibody in subcutaneous and orthotopic PC3 mouse models [57]. The pretargeting approach resulted in high uptake in the tumor, rapid blood clearance, and excellent tumor-to-blood ratios for ^{111}In-IMP288 in the PC3 tumors. Already 1 h after injection of the radiolabeled peptide, pretargeted immunoPET images clearly visualized the subcutaneous and orthotopic tumors with minimal activity in the kidneys. Van Rij et al. showed that pretargeting with TF12 in combination with radiolabeled IMP288 is an excellent approach for specific, fast, high-contrast imaging

of prostate cancer.

Another important cell surface target for molecular imaging of prostate cancer is the prostate stem cell antigen (PSCA), which is over-expressed in a majority of prostate cancers and has low levels of expression in a very limited number of normal tissues. PSCA has been detected in approximately 60% of lymph node and liver metastases [58] and strong PSCA staining has been observed in 87–100% of bone metastases [56]. Elevated PSCA expression has also been shown to correlate with increased tumor stage, grade, and progression to androgen independence. Olafsen et al. studied a humanized anti-PSCA monoclonal antibody 1G8 (hu1G8) in preclinical models [59] and showed that PET evaluation in LAPC-9-xenografted mice following radioiodination with the positron emitter ^{124}I provided high contrast PET images. Due to the slow clearance kinetics of the antibody, enhanced target-to-background images were not obtained until 1 week after administration of ^{124}I-hu1G8. To facilitate and accelerate clearance from blood, antibody fragments of various sizes were used in subsequent studies.

Leyton et al. evaluated the role of the from hu1G8 antibody derived minibody 2B3 labeled with ^{131}I or ^{124}I for imaging prostate cancer xenograft-bearing mice. The 2B3 minibody showed fast blood clearance in comparison to the intact hu1G8 monoclonal antibody, which resulted in the ability to image prostate cancer xenografts within 21 h in contrast to 168 h with the intact antibody [60]. Remarkably, the 2B3 minibody mimicked the tumor uptake of the intact hu1G8 monoclonal antibody in the LAPC-9 model despite its rapid elimination from the circulation. Due to the ability of the 2B3 antibody to image androgen-independent as well as androgen-dependent xenografts, 2B3 has promising potential as a rapid imaging agent for high-risk prostate cancer patients [60].

Another recent study evaluated the tumor targeting activity of an internalizing human single-chain antibody fragment (scFv) UA20 that is directed against a still unknown antigen. UA20 was labeled with ^{99m}Tc to target human prostate carcinoma in DU145 xenograft mouse models [61]. In this study, UA20 scFv showed rapid and specific internalization in prostate tumor cells in vitro and accumulation in prostate tumor xenografts in vivo. SPECT/CT showed significant tumor uptake as early as 1 h after injection and at 3 h after injection, tumor uptake was 4.4% ID/g. In contrast, the control antibody N3M2 showed a tumor uptake of only 0.26% ID/g that was similar to nonspecific uptake in muscle and fat. These data indicated the potential of UA20 scFv for future development for prostate cancer imaging.

Radiolabeled amino acid imaging

Radiolabeled amino acids may be alternative tracers for imaging of prostate cancer, since their uptake is frequently increased in rapidly proliferating cells [28].

A potential tracer for PET imaging of prostate cancer is the radiolabeled amino acid methionine. Since accumulation of ^{11}C-methionine in tumor cells reflects transport of amino acids and protein synthesis, enhanced metabolism of tumors can be visualized

with ^{11}C-methionine. Methionine is mainly metabolized in liver and pancreas, without excretion via the urinary tract [3].

The few studies available that investigated the role of ^{11}C-methionine PET in prostate cancer indicate superiority of ^{11}C-methionine PET over ^{18}F-FDG PET in the detection of metastatic bone and soft-tissue lesions [62]. Nunez et al. obtained a relatively high sensitivity (72.1%) of ^{11}C-methionine PET for the detection of bone and soft-tissue metastases, which compared favorably with the sensitivity of 48% for ^{18}F-FDG PET. A possible explanation for this difference in sensitivity of detection of metastatic lesions might be the relatively high activity of ^{18}F-FDG in the bladder, interfering with the evaluation of the prostate and nearby tissues. In contrast, only a minimal amount of ^{11}C-methionine is excreted via the urinary system allowing more reliable evaluation of pelvic structures. As a consequence ^{18}F-FDG may have limited ability to detect abdominal retroperitoneal metastases [37]. Nunez et al. also found that the agreement between ^{11}C-methionine PET and conventional imaging methods exceeds the agreement of conventional methods with ^{18}F-FDG PET.

In a pilot study, L-leucine analogue anti-1-amino-3-^{18}F-fluorocyclobutyl-1-carboxylic acid (anti-^{18}F-FACBC) showed uptake in primary and metastatic prostate cancer. Bladder excretion of anti-^{18}F-FACBC was found to be low and data indicate a potential role for anti-^{18}F-FACBC in the differentiation between BPH and malignant transformation of the prostate gland [63]. However, anti-^{18}F-FACBC needs to be further evaluated in clinical studies.

Since tumors express specific antigens, radiolabeled antibodies can target the antigens and can be of diagnostic value. However, due to the long circulatory half-life of radiolabeled antibodies high target to background ratios are only obtained several days after injection. Therefore, peptides that target those antigens represent alternatives for imaging of prostate cancer [64]. PET imaging of xenografted tumors overexpressing PSMA was achieved with the PSMA inhibitor labeled with ^{11}C. This ^{11}C-DCMC compound specifically binds with high affinity to the extracellular domain of PSMA [65]. ^{11}C-DCMC showed clear delineation of the tumor at 30 min after injection. This PSMA inhibitor was also labeled with ^{18}F. High uptake of ^{18}F-DCFBC was observed in the PSMA-positive tumors whereas uptake in PSMA-negative tumors was low [66].

Conclusion and future perspectives

Since conventional approaches have limited value in the early detection, staging, and follow-up of prostate cancer, extensive research currently focuses on the development of highly sensitive and specific imaging modalities for accurate visualization of prostate cancer.

Improvements on conventional MR imaging have yielded promising new approaches such as DWI, MRS, or DCE-MRI, which allows for more accurate disease staging and

follow-up of prostate cancer.

Substantial progress has been made in the development of radionuclide imaging techniques and the value of numerous radioactive tracers for the detection of prostate cancer has been evaluated. Since sensitivity of ^{18}F-FDG-PET for imaging of prostate cancer is limited, tracers like ^{11}C-choline, ^{18}F-FCH, ^{11}C-acetate, and ^{11}C-methionine represent more appropriate alternatives. ^{11}C-methionine PET is superior to ^{18}F-FDG-PET in both the detection of soft-tissue lesions and the early detection of bone metastases. For evaluation of tumor bed and lymph nodes, ^{11}C-acetate PET was superior to ^{18}F-FDG-PET. However, in progressive disease and detection of bone metastases, ^{18}F-fluoroacetate might be superior to ^{11}C-acetate. In this case, ^{18}F-fluoride PET represents another appropriate tracer for detection of bone involvement with high sensitivity and specificity. The relatively novel tracer ^{18}F-FPA appears to be superior to ^{18}F-FDG in the detection of prostate cancer; however, more preclinical and clinical data are needed for further evaluation. Receptor binding ligands like ^{18}F-FDHT may have a value in the detection of androgen-sensitivity of the tumor, which would direct therapeutic strategies towards anti-androgen-based approaches. During the last decade, a wide range of antibodies and antibody fragments, such as capromab, 3/A12, 3/E7, 3/F11, 2B3, and UA20 have been developed which show promising potential for targeted imaging of prostate cancer.

More studies are necessary to accurately compare novel imaging modalities and their tracers for optimal suitability in the early detection of (recurrent) prostate cancer, metastatic manifestations, and response to therapy.

References

1. Ferlay J, Parkin DM, Steliarova-Foucher E. Estimates of cancer incidence and mortality in Europe in 2008. Eur J Cancer 2010; 46(4):765–781.
2. Kularatne SA, Wang K, Santhapuram HKR, et al. Prostatespecific membrane antigen targeted imaging and therapy of prostate cancer using a PSMA inhibitor as a homing ligand. Mol Pharm 2009; 6(3):780–789.
3. Turkbey B, Albert PS, Kurdziel K, et al. Imaging localized prostate cancer: Current approaches and new developments. Am J Roentgenol 2009;192(6):1471–1480.
4. Choi M, Hung AY. Technological advances in radiation therapy for prostate cancer. Curr Urol Rep 2010; 11(3):172–179.
5. Beer AJ, Eiber M, Souvatzoglou M, et al. Radionuclide and hybrid imaging of recurrent prostate cancer. Lancet Oncol 2011; 12(2):181–191.
6. Hricak H, Choyke PL, Eberhardt SC, et al. Imaging prostate cancer: A multidisciplinary perspective. Radiology 2007; 243(1):28–53.
7. Cornud F, Hamida K, Flam T, et al. Endorectal color Doppler sonography and endorectal MR imaging features of nonpalpable prostate cancer: Correlation with radical prostatectomy findings. Am J Roentgenol 2000; 175(4):1161–1168.
8. Turkbey B, Pinto PA, Choyke PL. Imaging techniques for prostate cancer: Implications for focal therapy. Nat Rev Urol 2009; 6(4):191–203.
9. Kwee TC, Takahara T, Ochiai R, et al. Diffusion-weighted whole-body imaging with background body signal suppression (DWIBS): Features and potential applications in oncology. Eur J Radiol 2008; 18(9):1937–1952.
10. Costello LC, Franklin RB, Feng P. Mitochondrial function, zinc, and intermediary metabolism relationships in normal prostate and prostate cancer. Mitochondrion 2005; 5(3):143–153.
11. Ramirez de Molina A, Rodriguez-Gonzalez A, et al. Overexpression of choline kinase is a frequent feature in human tumor-derived cell lines and in lung, prostate, and colorectal human cancers. Biochem Biophys Res Commun 2002; 296(3):580–583.
12. Shukla-Dave A, Hricak H, Moskowitz C, et al. Detection of prostate cancer with MR spectroscopic imaging: An expanded paradigm incorporating polyamines. Radiology 2007; 245(2):499–506.
13. Casciani E, Polettini E, Bertini L, et al. Contribution of the MR spectroscopic imaging in the diagnosis of prostate cancer in the peripheral zone. Abdom Imaging 2007; 32(6):796–802.
14. Ocak I, Bernardo M, Metzger G, et al. Dynamic contrast-enhanced MRI of prostate cancer at 3T: A study of pharmacokinetic parameters. Am J Roentgenol 2007; 189(4):849.
15. Heesakkers RA, Hovels AM, Jager GJ, et al. MRI with a lymph node-specific contrast agent as an alternative to CT scan and lymph-node dissection in patients with prostate cancer: A prospective multicohort study. Lancet Oncol 2008; 9(9):850–856.
16. Harisinghani MG, Barentsz J, Hahn PF, et al. Noninvasive detection of clinically occult lymph-node metastases in prostate cancer. N Engl J Med 2003; 349(10):1010.

17. Martin AL, Hickey JL, Ablack A, et al. Synthesis of bombesin-functionalized iron oxide nanoparticles and their specific uptake in prostate cancer cells. J Nanoparticle Res 2010; 12(5):1599–1608.
18. Van der Heiden MG, Cantley LC, Thompson CB. Understanding the Warburg effect: The metabolic requirements of cell proliferation. Science 2009; 324(5930):1029–1033.
19. Jana S, Blaufox MD. Nuclear medicine studies of the prostate, testes, and bladder. Semin Nucl Med 2006; 36(1):51–72.
20. Liu IJ, Zafar MB, Lai YH, et al. Fluorodeoxyglucose positron emission tomography studies in diagnosis and staging of clinically organ-confined prostate cancer. Urology 2001; 57(1):108–111.
21. Oyama N, Hasegawa Y, Kiyono Y, et al. Early response assessment in prostate carcinoma by ^{18}F-fluorothymidine following anticancer therapy with docetaxel using preclinical tumour models. Eur J Nucl Med Mol Imaging 2011; 38(1):81–89.
22. Bouchelouche K, Tagawa ST, Goldsmith SJ, et al. PET/CT imaging and radioimmunotherapy of prostate cancer. Semin Nucl Me 2011;41(1):29–44.
23. Breeuwsma AJ, Pruim J, Jongen MM, et al. In vivo uptake of ^{11}C-choline does not correlate with cell proliferation in human prostate cancer. Eur J Nucl Med Mol Imaging 2005; 32(6):668–673.
24. Zheng QH, Gardener TA, Raikwar S, et al. ^{11}C-choline as a PET biomarker for assessment of prostate cancer tumor models. Bioorg Med Chem 2004; 12(11):2887–2893.
25. de Jong IJ, Pruim J, Elsinga PH, et al. Visualization of prostate cancer with ^{11}C-choline positron emission tomography. Eur Urol 2002; 42(1):18–23.
26. Rinnab L, Mottaghy FM, Blumstein NM, et al. Evaluation of ^{11}C-choline positron-emission/computed tomography in patients with increasing prostate-specific antigen levels after primary treatment for prostate cancer. Br J Urol Int 2007; 100(4):786–793.
27. Eschmann SM, Pfannenberg AC, Rieger A, et al. Comparison of ^{11}C-choline-PET/CT and whole body-MRI for staging of prostate cancer. Nuklearmedizin 2007; 46(5):161–168.
28. Apolo AB, Pandit-Taskar N, Morris MJ. Novel tracers and their development for the imaging of metastatic prostate cancer. J Nucl Med 2008; 49(12):2031–2041.
29. Albrecht S, Buchegger F, Soloviev D, et al. ^{11}C-acetate PET in the early evaluation of prostate cancer recurrence. Eur J Nucl Med Mol Imaging 2007; 34(2):185–196.
30. Oyama N, Miller TR, Dehdashti F, et al. ^{11}C-acetate PET imaging of prostate cancer: Detection of recurrent disease at PSA relapse. J Nucl Med 2003; 44(4):549–555.
31. Ponde DE, Dence CS, Oyama N, et al. ^{18}F-fluoroactetate: A potential acetate analog for prostate tumor imaging—In vivo evaluation of ^{18}Ffluoroactetate versus ^{11}C-acetate. J Nucl Med 2007; 48(3):420–428.
32. Matthies A, Ezziddin S, Ulrich EM, et al. Imaging of prostate cancer metastases with ^{18}F-fluoroacetate using PET/CT. Eur J Nucl Med Mol Imaging 2004; 31(5):797.
33. Even-Sapir E, Metser U, Mishani E, et al. The detection of bone metastases in patients with high-risk prostate cancer: ^{99m}Tc-MDP planar bone scintigraphy, single- and multi-field-of-view SPECT, ^{18}F-fluoride PET, and ^{18}F-fluoride PET/CT. J Nucl Med 2006; 47(2):287–297.

34. Fogelman I, Cook G, Israel O, et al. Positron emission tomography and bone metastases. Semin Nucl Med 2005; 35(2):135–142.
35. Even-Sapir E, Metser U, Flusser G, et al. Assessment of malignant skeletal disease: Initial experience with ^{18}F-fluoride PET/CT and comparison between ^{18}F-fluoride PET and ^{18}F-fluoride PET/CT. J Nucl Med 2004; 45(2):272–278.
36. Beheshti M, Vali R, Waldenberger P, et al. Detection of bone metastases in patients with prostate cancer by ^{18}F fluorocholine and ^{18}F fluoride PET-CT: A comparative study. Eur J Nucl Med Mol Imaging 2008; 35(10):1766–1774.
37. Pillarsetty N, Punzalan B, Larson SM. 2-^{18}F-Fluoropropionic acid as a PET imaging agent for prostate cancer. J Nucl Med 2009; 50(10):1709–1714.
38. Dehdashti F, Picus J, Michalski JM, et al. Positron tomographic assessment of androgen receptors in prostatic carcinoma. Eur J Nucl Med Mol Imaging 2005; 32(3):344–350.
39. Rogers BE, Bigott HM, McCarthy DW, et al. MicroPET imaging of a gastrin-releasing peptide receptor-positive tumor in a mouse model of human prostate cancer using a ^{64}Cu-labeled bombesin analogue. Bioconjug Chem 2003; 14(4):756–763.
40. Schroeder RP, Müller C, Reneman S, et al. A standardised study to compare prostate cancer targeting efficacy of five radiolabelled bombesin analogues. Eur J Nucl Med Mol Imaging 2010; 37(7):1386–1396.
41. Lane SR, Nanda P, Rolde TL, et al. Optimization, biological evaluation and microPET imaging of copper-64-labeled bombesin agonists, [^{64}Cu-NO2A-(X)-BBN(7–14)NH_2], in a prostate tumor xenografted mouse model. Nucl Med Biol 2010; 37(7):751–761.
42. Scopinaro F, De Vincentis G, Varvarigou AD, et al. ^{99m}Tc-bombesin detects prostate cancer and invasion of pelvic lymph nodes. Eur J Nucl Med Mol Imaging 2003; 30(10):1378–1382.
43. De Vincentis G, Remediani S, Varvarigou AD, et al. Role of ^{99m}Tc-bombesin scan in diagnosis and staging of prostate cancer. Cancer Biother Radiopharm 2004; 19(1):81–84.
44. Cooper CR, Chay CH, Pienta KJ. The role of alpha(v)beta(3) in prostate cancer progression. Neoplasia 2002;4(3):191–194.
45. Haubner R, Weber WA, Beer AJ, et al. Noninvasive visualization of the activated alphavbeta3 integrin in cancer patients by positron emission tomography and ^{18}F-Galacto-RGD. PLoS Med 2005; 2(3):e70.
46. Li ZB, Wu Z, Chen K, et al. ^{18}F-labeled BBN-RGD heterodimer for prostate cancer imaging. J Nucl Med 2008; 49(3):453–461.
47. Liu Z, Li ZB, Cao Q, et al. Small-animal PET of tumors with ^{64}Cu-labeled RGD-bombesin heterodimer. J Nucl Med 2009; 50(7):1168–1177.
48. Bander NH. Technology insight: Monoclonal antibody imaging of prostate cancer. Nat Clin Pract Urol 2006; 3(4):216–225.
49. Schettino CJ, Kramer EL, Noz ME, et al. Impact of fusion of indium-111 capromab pendetide volume data sets with those from MRI or CT in patients with recurrent prostate cancer. Am J Roentgenol 2004; 183(2):519–524.
50. Liu H, Rajasekaran AK, Moy P, et al. Constitutive and antibody-induced internalization of prostate-specific membrane antigen. Cancer Res 1998; 58(18):4055–4060.

51. Smith-Jones PM, Vallabhajosula S, Navarro V, et al. Radiolabeled monoclonal antibodies specific to the extracellular domain of prostate-specific membrane antigen: Preclinical studies in nude mice bearing LNCaP human prostate tumor. J Nucl Med 2003; 44(4):610–617.
52. Alt K, Wiehr S, Ehrlichmann W, Reischl G, et al. High-resolution animal PET imaging of prostate cancer xenografts with three different ^{64}Cu-labeled antibodies against native cell-adherent PSMA. Prostate 2010; 70(13):1413–1421.
53. Bander NH, Trabulsi EJ, Kostakoglu L, et al. Targeting metastatic prostate cancer with radiolabeled monoclonal antibody J591 to the extracellular domain of prostate specific membrane antigen. J Urol 2003; 170(5):1717–1721.
54. Tagawa ST, Milowsky MI, Morris MJ, et al. Phase II trial of ^{177}Lutetium radiolabeled anti-prostate-specific membrane antigen (PSMA) monoclonal antibody J591 (^{177}Lu-J591) in patients with metastatic castrate-resistent prostate cancer. J Clin Oncol 2008; 26(15S): 5140.
55. Wolf P, Freudenberg N, Bühler P, et al. Three conformational antibodies specific for different PSMA epitopes are promising diagnostic and therapeutic tools for prostate cancer. Prostate 2010; 70(5):562–569.
56. Gu Z, Thomas G, Yamashiro J, et al. Prostate stem cell antigen (PSCA) expression increases with high gleason score, advanced stage and bone metastasis in prostate cancer. Oncogene 2000; 19(10):1288–1296.
57. van Rij C, Franssen G, Sharkey R, et al. Pretargeted immunoPET imaging and radioimmunotherapy (RIT) of prostate cancer with an anti-EGP1 x anti-HSG bispecific antibody (bsAb). J Nucl Med 2010; 51(Suppl 2):501.
58. Lam JS, Yamashiro J, Shintaku IP, et al. Prostate stem cell antigen is overexpressed in prostate cancer metastases. Clin Cancer Res 2005; 11(7):2591–2596.
59. Olafsen T, Gu Z, Sherman MA, et al. Targeting, imaging, and therapy using a humanized antiprostate stem cell antigen (PSCA) antibody. J Immunother 2007; 30(4):396–405.
60. Leyton JV, Olafsen T, Lepin EJ, et al. Humanized radioiodinated minibody for imaging of prostate stem cell antigen-expressing tumors. Clin Cancer Res 2008; 14(22):7488–7496.
61. He J, Wang Y, Feng J, et al. Targeting prostate cancer cells in vivo using a rapidly internalizing novel human single-chain antibody fragment. J Nucl Med 2010; 51(3):427–432.
62. Nunez R, Macapinlac HA, Yeung HW, et al. Combined ^{18}F-FDG and ^{11}C-methionine PET scans in patients with newly progressive metastatic prostate cancer. J Nucl Med 2002; 43(1):46–55.
63. Schuster DM, Votaw JR, Nieh PT, et al. Initial experience with the radiotracer anti-1-amino-3-^{18}F-fluorocyclobutane-1-carboxylic acid with PET/CT in prostate carcinoma. J Nucl Med 2007; 48(1):56–63.
64. Hong H, Zhang Y, Sun J, et al. Positron emission tomography imaging of prostate cancer. Amino Acids 2010; 39(1):11–27.
65. Foss CA, Mease RC, Fan H, et al. Radiolabeled small-molecule ligands for prostate-specific membrane antigen: In vivo imaging in experimental models of prostate cancer. Clin Cancer Res 2005; 11(11):4022–4028.
66. Mease RC, Dusich CL, Foss CA, et al. N-[N-[(S)-1,3-Dicarboxypropyl]carbamoyl]-4-^{18}F-fluorobenzyl-L-cysteine, ^{18}F-DCFBC: A new imaging probe for prostate cancer. Clin Cancer Res 2008; 14(10):3036–3043.

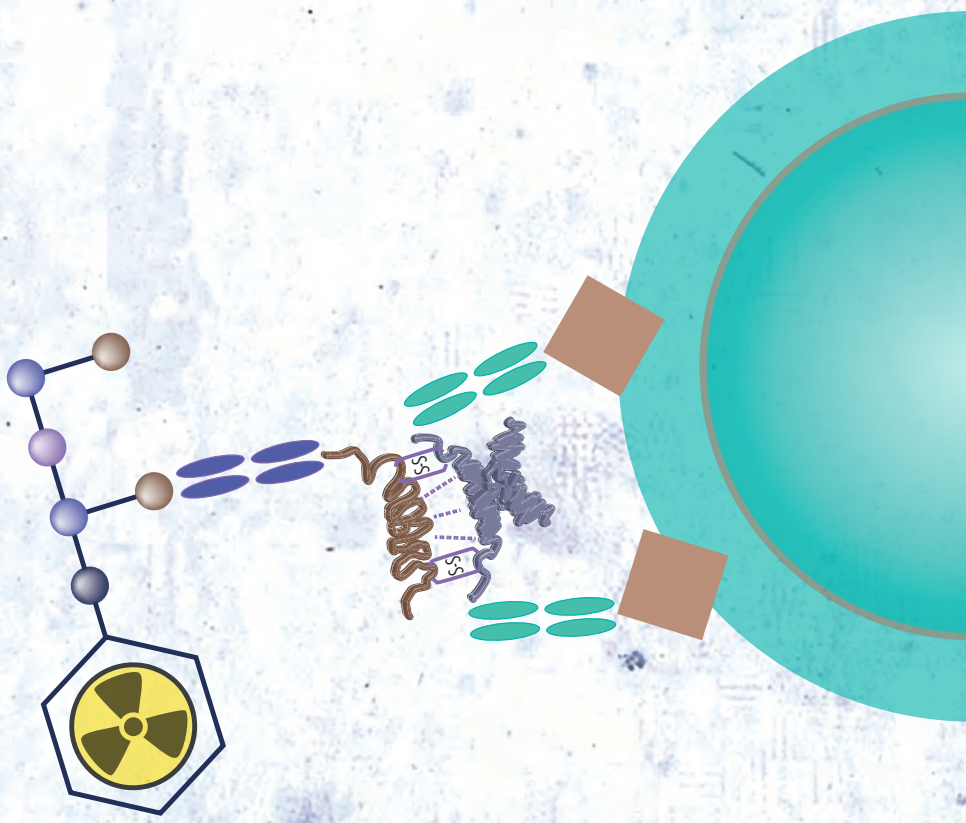

Imaging of prostate cancer with immunoPET and immunoSPECT using a radiolabeled anti-EGP-1 monoclonal antibody

3

Catharina M. van Rij
Robert M. Sharkey
David M. Goldenberg
Cathelijne Frielink
Janneke D.M. Molkenboer
Gerben M. Franssen
Wietske M. van Weerden
Wim J.G. Oyen
Otto C. Boerman

J Nucl Med 2011; 52(10):1601-7.

Abstract

hRS7 is a humanized IgG1 monoclonal antibody directed against the Epithelial Glycoprotein-1 (EGP-1; also known as TROP-2). This antigen is found in many epithelial cancers, including prostate cancer, and therefore this antibody could be suitable for targeting this cancer. In this study, the characteristics of hRS7 to target prostate cancer were examined. The potential for immunoPET with ^{89}Zr-hRS7 and immunoSPECT with ^{111}In-hRS7 was assessed using nude mice with human prostate cancer xenografts.

Methods

EGP-1 expression was assessed by immunohistology in human primary and metastatic prostate cancer samples and in PC3 xenografts. The optimal antibody protein dose for prostate cancer targeting was examined in nude mice with s.c. PC3 xenografts and then the biodistribution of ^{111}In-, ^{125}I- and ^{89}Zr-labeled hRS7 was determined in s.c. PC3 xenografts at 1, 3 and 7 days p.i. ImmunoPET and immunoSPECT were performed with ^{89}Zr-hRS7 and ^{111}In-hRS7 in mice with s.c. and intraprostatic PC3 xenografts, respectively.

Results

Immunohistochemical analysis showed abundant EGP-1 expression in human primary and metastatic prostate cancers and in PC3 xenografts. ^{111}In-hRS7 and ^{89}Zr-hRS7 preferentially and specifically accumulated in PC3 xenografts, with tumor uptake as high as 60% ID/g at a protein dose of 0.1 μg per mouse. PC3 tumors in nude mice were clearly visualized with both tracers with immunoPET and immunoSPECT.

Conclusion

hRS7 shows excellent in vivo tumor targeting in human PC xenografts. Therefore, hRS7 is a potent vehicle for targeting PC.

Introduction

Despite ongoing improvement in both detection and treatment of prostate cancer (PC), it is the second leading cause of cancer-related deaths in men in the Western world. PC causes significant morbidity, especially when metastasized. While treatable in early, hormone-dependent stages, PC can only be managed palliatively in the later, hormone-refractory phase of the disease.

At diagnosis, imaging of PC aims at differentiating between malignant and non-malignant tissue. Diagnosis is usually performed effectively with imaging modalities like Trans Rectal Ultrasound (TRUS) combined with biopsies or Magnetic Resonance Imaging (MRI), which are usually able to adequately detect and localize primary PC [1]. In advanced PC, however, it is essential to differentiate between metastatic and non-metastatic disease, to predict disease outcome, and to determine treatment options. TRUS and conventional MRI are less effective in detecting metastatic spread.

Positron Emission Tomography (PET) imaging is a useful imaging modality to detect metastatic disease in several cancers. ^{18}F-FDG-PET is not suitable for staging patients with PC, since sensitivity is low due to poor ^{18}F-FDG uptake in most well-differentiated PC lesions and due to the elimination of ^{18}F-FDG via the kidneys and the urinary bladder [2,3]. ^{18}F-Fluorocholine has been investigated extensively, but also has a low sensitivity for detecting PC metastases [2,3]. ^{11}C-acetate is a promising radiotracer for PC, but it requires an on-site cyclotron [1,2,3].

Several radiolabeled monoclonal antibodies (mAbs) have been developed and tested for PC imaging. The anti-PSMA antibody, ^{111}In-capromab pendetide (Prostascint®, EUSA Pharma, Oxford, UK), has been approved for pre-surgical staging and evaluation of recurrence after focal therapy of PC, but has several limitations. These include the suboptimal visualization of bone metastases and the inability to discern viable from non-viable cancer cells, most likely because this antibody is directed against an intracellular epitope [3]. However, the use of ^{111}In-capromab pendetide in combination with SPECT/CT showed improved results [4]. J591, a humanized anti-PSMA monoclonal antibody, has been reported to have better characteristics to detect bone metastases [3].

hRS7 is a humanized IgG1 monoclonal antibody directed against the Epithelial Glycoprotein-1 (EGP-1; also known as TROP-2). EGP-1 is a transmembrane glycoprotein with a molecular mass of approximately 46 kDa [5]. hRS7 was originally raised against human non-small cell carcinoma of the lung [6], and was found to be reactive with carcinomas of the lung, bladder, breast, cervix, ovary, stomach and prostate. Most normal human tissues do not express EGP-1, including lymph nodes, heart, connective

tissues, blood vessels, stomach, jejunum and duodenum, but it is found at low levels in several normal glandular cells, including glands in the bronchus, breast, prostate and skin, and ducts and acini of the pancreas [6]. Given its expression in prostate cancer, we studied the potential targeting ability of hRS7 IgG in a nude mouse-human prostate cancer model, examining the antibody radiolabeled with radioiodine or radiometals, and applying SPECT and PET imaging modalities.

Materials and methods

The monoclonal antibody hRS7

The production and characterization of hRS7 (the humanized version of the murine monoclonal antibody RS7-3G11) have been described previously [7]. As a control antibody the humanized anti-CD22 antibody, hLL2 (not reactive with prostate cancer), was used. Both antibodies were supplied by Immunomedics, Inc. (Morris Plains, NJ, USA).

Cell culture

The human prostate cancer cell line, PC3, is an androgen-independent cell line, originally derived from a PC bone metastasis. Cells were obtained from ATCC (CRL-1435) and grown in complete RPMI 1640 medium, supplemented with 10% FCS (fetal calf serum, Life Technologies, Grand Island, NY). Before s.c. inoculation of mice to induce PC3 xenografts, tumor cells were washed with 0.9% NaCl, disaggregated with trypsin, and resuspended in 67% complete RPMI 1640 medium with 33% Matrigel (BD Biosciences, San Jose, CA) to the appropriate concentration (3 x 10^6 cells/200 µL).

Murine models

Nude mice (Central Animal Facility, Radboud University Medical Center Nijmegen, The Netherlands), 8–9 weeks old, were adapted to laboratory conditions for at least one week before experimental use. They were housed under non-sterile standard conditions in filter-topped cages (5 mice per cage), with free access to animal chow (Sniff Voer®) and water.

Male BALB/*c* nude mice were inoculated s.c. in the shoulder with 3 x 10^6 PC3 cells suspended in 200 µL of 67% complete RPMI 1640 medium with 33% Matrigel (BD Biosciences, San Jose, CA). The s.c. PC3 tumors grew to approximately 0.1 g in 10 days after tumor cell inoculation as determined by caliper measurements in three

dimensions using the formula: V =4/3π (length/2 x width/2 x height/2), assuming that the density of tumor tissue is 1 g/cm^3. For an orthotopic mouse model, NMRI-foxn1 nude mice (Charles River) were used, because their prostate is larger and allows injection of 20 µL of cell suspension. NMRI-foxn1 mice were anesthetized and the abdomen was opened via a 1-cm midline mini-laparotomy. The prostate was gently lifted out of the abdomen and placed on gauze. Using a 29-G needle and a 1-ml syringe, 20 µL of a cell suspension containing 2 × 10^6 PC3 cells in Matrigel was injected into one of the dorsal lobes of the prostate. After 7-21 days, palpable tumors developed in the prostate.

All experiments were approved by the national Animal Welfare Committee through the institutional Animal Welfare Committee of the Radboud University Medical Center, and were conducted in accordance with the principles set forth by the Revised Dutch Act on Animal Experimentation.

Radiolabeling of hRS7

mAb hRS7 was radioiodinated according to the iodogen method [8]. Ten µL of 0.5 mol/L phosphate buffer, pH 7.4, 86 µL 50 mmol/L phosphate buffer, pH 7.4, 3.5 µL hRS7 (5.8 mg/mL), and 3.7 MBq Na^{125}I (GE Healthcare Europe, Den Bosch, The Netherlands) were added to an Eppendorf vial coated with 50 µg of iodogen (1,3,4,6-tetrachloro-3,6-diphenylglycoluril; Pierce Biotechnology, Inc.). The mixture was incubated for 10 min at room temperature, immediately followed by purification on a PD-10 column (GE Healthcare) eluted with PBS, 0.5% bovine serum albumin (BSA).

Conjugation of hRS7 with p-isothiocyanatobenzyl-DTPA (Macrocyclics, Dallas, TX) was done essentially as described by Ruegg et al. [9]. Briefly, 0.5 mL mAb hRS7 (10 mg/mL) was mixed with 50 µL 1.0 M $NaHCO_3$, pH 9.5, and a 50-fold molar excess of p-isothiocyanatobenzyl-DTPA (1.1 mg). Following incubation at room temperature for 1 h, the reaction mixture was dialyzed for 3 days in a Slide-A-Lyzer (20 kDa cutoff, Pierce, Rockford, IL) against 0.25 M NH_4Ac, pH 5.4. Determination of the substitution ratio, as described by Hnatowich et al. [10], revealed that 2 DTPA chelates were conjugated per hRS7 antibody molecule. Subsequently, the hRS7-DTPA conjugate was diluted in 0.25 M NH_4Ac, pH 5.4, to 1 mg/mL, and aliquots were stored at –20°C. hRS7-DTPA was labeled with $^{111}InCl_3$ by adding 0.37 MBq/µg hRS7-DTPA in 0.25 M NH_4Ac, pH 5.4. The mixture was incubated at room temperature for 30 min. The radiolabeled hRS7 preparation was purified by gel filtration on a PD-10 column. The radiochemical purity was determined by Instant Thin Layer Chromatography (ITLC) using 0.1 M sodium citrate, pH 6, as the mobile phase.

hRS7 was conjugated with desferrioxamine (Df) (Novartis, Basel, Switzerland) via an amide linkage and labeled with ^{89}Zr as described previously [11]. The antibody and N-succinyldesferrioxamine-tetrafluorphenol (VU Medical Center, Amsterdam, The Netherlands) were conjugated at room temperature for 30 min. On average, one Df-chelate per mAb molecule was conjugated. After conjugation, the pH was adjusted to 4.4 by adding 4 µl of 0.25 M H_2SO_4 and the iron was removed from the chelator by adding 50 µl of a 25 mg/ml EDTA solution and incubation for 30 min at 35°C. The hRS7-Df conjugate was purified on a PD-10 column that was eluted with 5 mg/mL gentisic acid in 0.9% NaCl pH 5. hRS7-Df was radiolabeled using 120 MBq ^{89}Zr oxalate (IBA Molecular, Louvain-le-Neuve, Belgium). The pH of the ^{89}Zr oxalate solution was adjusted to 4.1 using a 2.0 M Na_2CO_3 solution. After 3 min the pH of the ^{89}Zr oxalate solution was adjusted to 6.9 using a 0.5 M HEPES solution and the purified hRS7-Df was added. The solution was incubated for 90 min at 37 °C. Labeling efficiency was 60%, as determined by ITLC. The radiolabeled hRS7 preparation was purified by gel filtration on a PD-10 column and the radiochemical purity (>95%) was determined by ITLC using 20 mM citrate buffer, pH 6 as the mobile phase. Labeling efficiency varied considerably (15-80%), depending on the batch ^{89}Zr oxalate used. The desired amount of ^{89}Zr-hRS7-desferal (20 µg hRS7-Df labeled with 11 MBq ^{89}Zr) was diluted in 5 mg/mL gentisic acid, pH 5, to a volume of 200 µL. The control antibody hLL2, an anti-CD22 monoclonal antibody was conjugated with desferrioxamine and labeled with ^{89}Zr as described above.

Immunoreactivity

The immunoreactive fraction of the radiolabeled hRS7 was determined using freshly trypsinized PC3 cells, as described by Lindmo et al. [12] with minor modifications. Briefly, a fixed amount of radiolabeled antibody (200 Bq) was incubated with increasing concentrations of PC3 tumor cells in 0.5 mL binding buffer (RPMI 1640 medium, 0.5% BSA). A duplicate of the lowest cell concentration was incubated in the presence of an excess of unlabeled antibody to correct for nonspecific binding. After 1 h at 37°C, the activity in the total vial was determined in a gamma counter (Wallac wizard 3'' 1480 automatic gamma counter). Cells were spun down and washed once with 500 µL of binding buffer and the activity in the cell pellet was determined in the gamma counter. The immunoreactive fractions of all radiolabeled preparations used in the experiments exceeded 80%.

Immunohistochemical studies

Frozen 5-µm sections of PC3 tumor xenografts were air-dried and fixed in cold acetone for 10 minutes. After fixation, the slides were dried overnight and incubated with 4 µg/ml hRS7 in PBS, 1% BSA, for 1 h at room temperature. Slides were rinsed with PBS, and

were incubated with rabbit-anti-human-IgG-peroxidase (DAKO, Glostrup, Denmark) in PBS, 1% BSA (preincubated in 10% Normal Mouse Serum) for 30 min. After washing with PBS, the sections were stained with 3,3'-diaminobenzidine (Powervision DAB, Immunologic, Duiven, The Netherlands). All slides were counterstained with Mayer's hematoxylin (Fluka Chemie, Buchs, Switzerland) and mounted in Permount (Fisher Scientific, Breda, The Netherlands). Human tumor sections were stained similarly except that these sections were incubated with the murine RS7 antibody, and rabbit-anti-mouse-IgG-peroxidase was used as the second antibody. Tissue samples were collected according to national and institutional guidelines.

Biodistribution studies

The effect of the antibody dose on the biodistribution of ^{111}In-hRS7 in mice with s.c. PC3 tumors was determined in groups of 5 mice that received escalating protein doses of ^{111}In-hRS7 (0.1, 1, 10, 30 and 100 µg hRS7/mouse, 0.4 MBq). Three days after injection of the radiolabeled mAb, mice were euthanized by CO_2/O_2 asphyxiation and a blood sample was obtained by heart puncture. Tissues (tumor, muscle, femur, lung, spleen, kidney, liver, duodenum and colon) were dissected, weighed, and the radioactivity content was determined in a gamma counter (Wallac wizard 3'' 1480 automatic gamma counter). To permit calculation of the radioactive uptake in each organ as a fraction of the injected dose, an aliquot of the injection dose was counted simultaneously.

In another study,^{111}In-hRS7 (0.4 MBq, 5 µg) and ^{125}I-hRS7 (0.2 MBq, 5 µg of hRS7) were coinjected in groups of 5 mice that were killed by CO_2 asphyxiation and dissected at 3 days p.i. (post injection). Tissue samples were counted in a gamma counter for ^{111}In and ^{125}I activity. ^{125}I activity was corrected for crossover with ^{111}In activity. To check the accuracy of the ^{125}I activity in the samples, samples were counted again one month later. Results of the biodistribution experiments were expressed as a percentage of the injected dose per gram of tissue (% ID/g).

ImmunoPET and ImmunoSPECT imaging

Groups of 5 mice with s.c. PC3 tumors were injected with 11 MBq (20 µg) ^{89}Zr-hRS7. Although optimal protein dose was established at ≤10 µg hRS7, a higher amount was chosen due to the higher activity that is needed for imaging. At 1, 3 or 7 days after injection, mice underwent immunoPET using a small-animal PET/CT scanner (Inveon®, Preclinical Solutions, Siemens Healthcare Molecular Imaging, Knoxville, TN, USA), while anesthetized with a mixture of isoflurane, N_2O and oxygen. One additional group was coinjected with an excess of 500 µg of unlabeled hRS7 and one group received ^{89}Zr-labeled hLL2 (20 µg, 6 MBq) to determine the nonspecific uptake in the

tissues. Animals were placed in a supine position in the PET/CT scanner. Emission scans were acquired over 15 (day 1), 20 (day 3) or 30 minutes (day 7), followed by a CT scan for anatomical reference (spatial resolution 113 µm, 80 kV, 500 µA). Scans were reconstructed using Inveon Acquisition Workplace software version 1.2, with an ordered set expectation maximization-3D/maximum a posteriori (OSEM3D/MAP) algorithm having the following parameters: matrix 256 x 256 x 159, pixel size 0.43 x 0.43 x 0.8 mm^3 and a beta-value of 0.1. Images were analyzed quantitatively by drawing regions of interest and tumor-to-liver ratios were calculated. After imaging, mice were killed by CO_2 asphyxiation and dissected to determine tissue uptake by gamma counting.

Orthotopically implanted mice were scanned using a U-SPECT II microSPECT scanner (Milabs, Utrecht, The Netherlands). All mice were injected with ^{111}In-hRS7 (37 MBq, 10 µg) 3 days before the SPECT images were acquired. Four groups of 5 mice were imaged at 10, 13, 17 and 24 days after intraprostatic PC3 cell inoculation. A control group of 3 mice without surgery and without PC3 tumor was imaged simultaneously. The second control group of mice with PC3 tumors received 500 µg of unlabeled hRS7 along with the injection of ^{111}In-hRS7 on day 17, in order to block specific uptake of the radiolabeled antibody. Thirty min before scanning, the mice received 0.5 mg of furosemide s.c. to promote voiding of the bladder. Mice were killed and scanned for 30 min using the 1.0 mm diameter pinhole collimator tube. After scanning, biodistribution of the ^{111}In-label was determined as described above. Scans were reconstructed with MILabs reconstruction software, which uses an ordered-subset expectation maximization algorithm, with a voxel size of 0.375 mm. Tumor-to-liver ratios were calculated with the PMOD software (version 3.15, PMOD technologies Ltd, Zürich, Switzerland).

Statistical analysis

Statistical analysis was performed using GraphPad Prism version 4.00 and InStat version 3.05 (San Diego, CA) for Windows®. Differences in uptake of radiolabeled RS7 were tested for significance using the nonparametric Mann Whitney test for two groups. A *P*-value below 0.05 was considered significant. For multiple comparisons the Bonferroni correction was applied.

Results

Immunohistochemical studies

Figure 1 shows that EGP-1 was expressed heterogeneously throughout the PC3 tumor (A, B). EGP-1 expression was membranous and cytoplasmic. Immunohistochemical analysis of three human primary prostate tumors with varying Gleason scores showed high homogeneous and consistent expression of EGP-1 in all three PC tumors analyzed (D, E and F). Normal human prostate (C) showed EGP-1 expression of the glandular epithelium. Immunohistochemistry also showed abundant expression of EGP-1 in PC metastases in a lymph node (G, H) and in the liver (I).

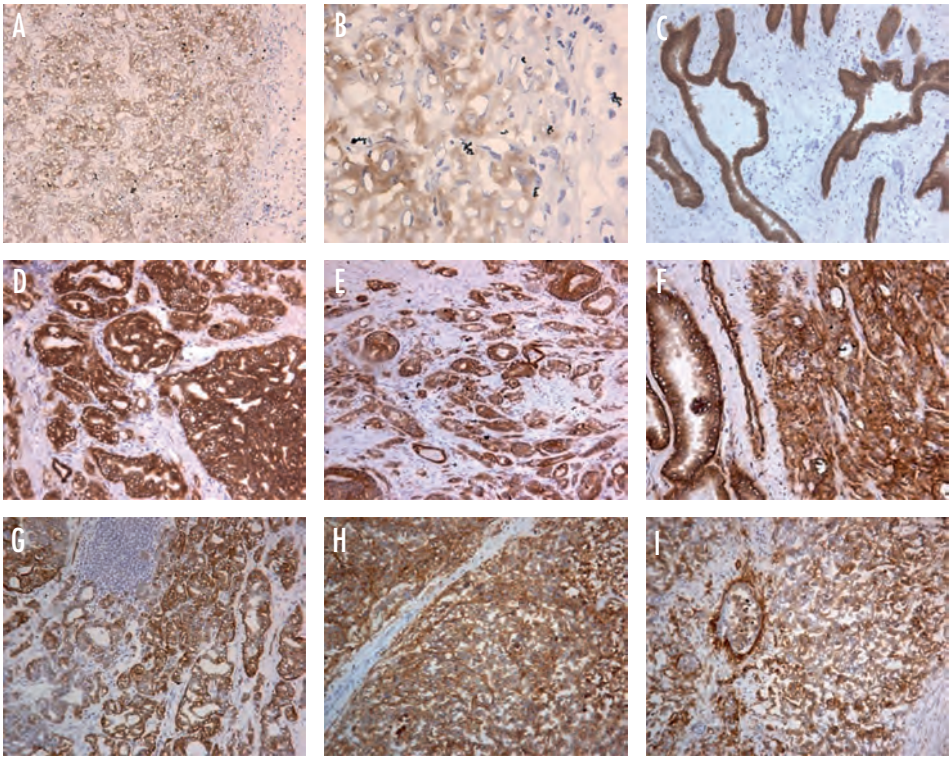

Figure 1A-B. hRS7 staining of PC3 mouse xenografts, magnified 100x (A) and 400x (B).
Figure 1C-F. mRS7 staining of human prostate tissue with different Gleason scores: normal prostate (C), Gleason 6 (D), Gleason 7-8 (E) and Gleason 9-10 (F) (magnified 100x).
Figure 1G-I. mRS7 staining of two human lymph node (G,H) and one liver (I) metastases (magnified 100x).

Biodistribution studies

A protein dose study showed maximum tumor uptake (>50% ID/g) following injection of ≤10 µg of ^{111}In-hRS7 at 3 days after injection (Figure 2A). Tumor uptake of ^{111}In-hRS7 decreased significantly with increasing doses of mAb from 60.8 ± 14.8% ID/g at 0.1 µg/mouse to 22.2 ± 7.1% ID/g at 100 µg/mouse (*P*=0.004). Protein dose did not affect concentrations in the blood or normal tissues. Tumor-to-blood ratios ranged from 3.0 (at 100 µg/mouse) to 7.2 (at 0.1 µg/mouse). Tumor weights were 0.08 ± 0.043 g and did not differ significantly between groups.

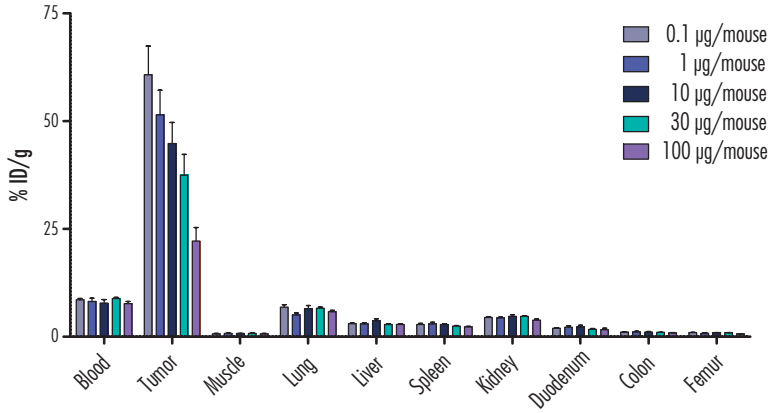

Figure 2A. Biodistribution of escalating ^{111}In-hRS7 doses (0.1-100 µg, 0.4 MBq) in BALB/*c* nude mice with a subcutaneous PC3 xenograft at 3 days after injection (n=5).

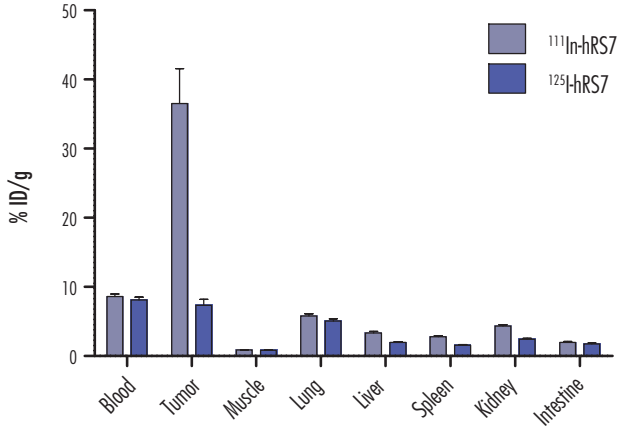

Figure 2B. Biodistribution of ^{125}I-hRS7 (5 µg, 0.2 MBq) and ^{111}In-hRS7 (5 µg, 0.4 MBq) in BALB/*c* nude mice with a subcutaneous PC3 xenograft at 3 days after injection (n=5).

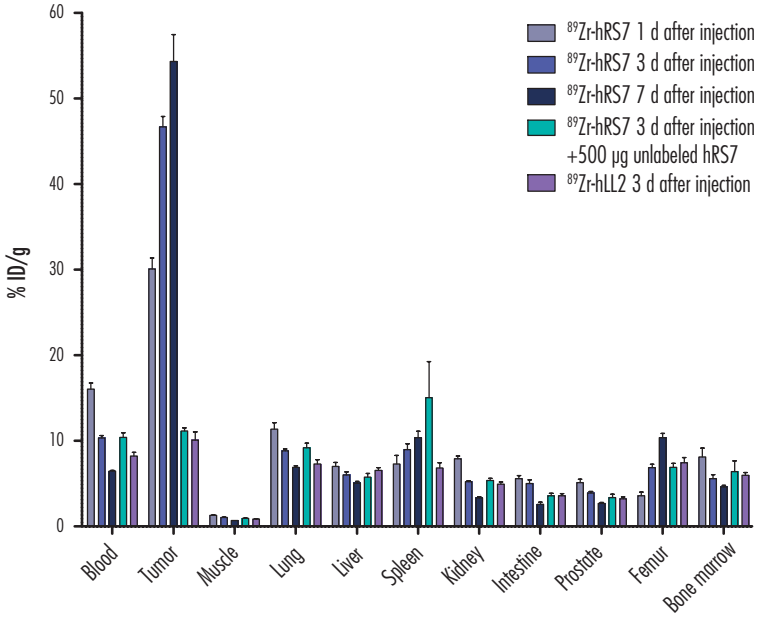

Figure 3. Biodistribution of ^{89}Zr-hRS7 (20 µg, 11 MBq) in BALB/*c* nude mice with a subcutaneous PC3 xenograft at increasing time after injection (1, 3 and 7 days after injection, n=5). One group of mice was coinjected with an excess of 500 µg of unlabeled hRS7, one group received 20 µg (6 MBq) of a control antibody not reactive with prostate cancer (^{89}Zr-hLL2).

Figure 2B shows that uptake of ^{111}In-hRS7 in tumor tissue at 3 days after injection was significantly higher than that of ^{125}I-hRS7 (36.5 ± 13.3% ID/g *vs* 7.3 ± 2.3%ID/g, *P*=0.0003, weight of the tumors 0.28 ± 0.11 g), yet normal tissue uptake was similar. This confirmed earlier studies with the murine RS7 antibody that showed residualizing radionuclides would be better retained with this internalizing antibody [13]. The biodistribution of ^{89}Zr-hRS7 was determined at 1, 3 and 7 days p.i. Figure 3 shows that tumor uptake of ^{89}Zr-hRS7 at 3 days after injection was comparable to that of 10 µg of ^{111}In-hRS7 (46.7 ± 2.7% ID/g *vs* 44.8 ± 11.0% ID/g). The same applies for the tissue uptake in all other organs (<9% ID/g for ^{89}Zr-hRS7), except for femur uptake which is significantly higher for ^{89}Zr-hRS7 (6.9 ± 0.9% *vs* 1.0 ± 0.2% ID/g, *P*<0.0001). Tumor uptake increased significantly with time from 30.1 ± 2.8% ID/g at 1 day p.i. to 54.3 ± 7.0% ID/g at 7 days p.i., consequently the tumor-to-blood ratio increased with time to a ratio exceeding 8 at 7 days after injection (*P*=0.0001). Tumor uptake was blocked by coinjection of an excess of unlabeled antibody, resulting in nonspecific (non-antigen-mediated) tumor uptake of 11.2 ± 0.8% ID/g at 3 days p.i. Tumor uptake of ^{89}Zr-labeled control anti-CD22 antibody at 3 days p.i. was low as well: 10.1 ± 2.1% ID/g.

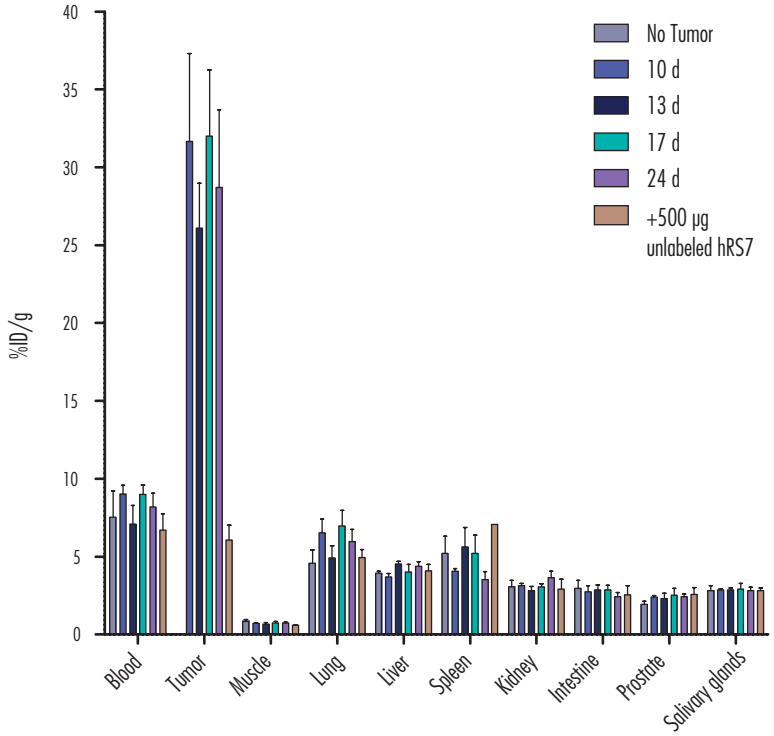

Figure 4. Biodistribution of ^{111}In-hRS7 (10 µg, 37 MBq) in NMRI nude mice with an orthotopic PC3 xenograft at increasing time after cell inoculation (10, 13, 17 and 24 days p.i, n=5). One group of mice without PC3 xenograft received the same amount of ^{111}In-hRS7. The second control group of mice with an orthotopic PC3 tumor additionally received an excess of 500 µg of unlabeled hRS7 (n=3).

Figure 4 shows that tumor uptake of ^{111}In-hRS7 in the orthotopic mouse model at 3 days after injection was constant in the time period investigated and on average was slightly lower than that detected in the s.c. model (31.7 ± 9.8% ID/g at 10 days, 23.6 ± 3.8 at 13 days, 32.0 ± 12.9% ID/g at 17 days and 19.3 ± 8.5% ID/g at 24 days after inoculation). Tissue uptake in all other organs was low (<7% ID/g). Tumor uptake could be blocked by coinjection of an excess of unlabeled antibody, resulting in nonspecific tumor uptake of 6.1 ± 1.7% ID/g. Mean weight of the tumors in this experiment was 0.042 ± 0.026 g, there was no significant tumor weight difference between the experimental groups.

ImmunoPET/CT and immunoSPECT imaging

MicroPET/CT imaging of ^{89}Zr-hRS7 was performed in mice with s.c. PC3 tumors at 1, 3 and 7 days p.i. One day after injection of the radiolabeled antibody, the PET/CT image showed high activity in blood. At 3 days p.i., blood levels were lower and

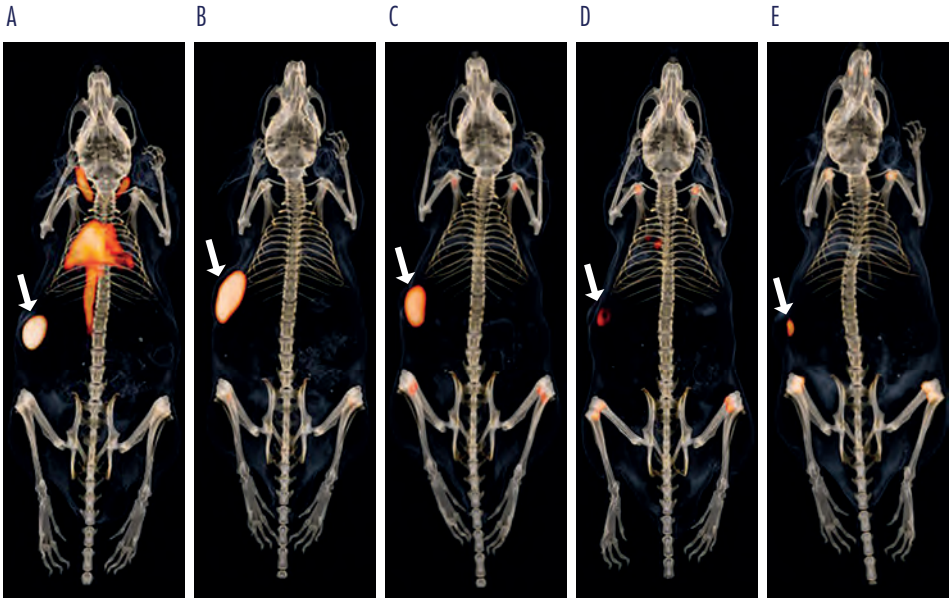

Figure 5. Anterior 3D volume-rendering projections of PET/CT scans of mice with a subcutaneous PC3 tumor on the shoulder injected with ^{89}Zr-hRS7 (20 μg, 11 MBq) acquired 1 (A), 3 (B,D,E) or 7 (C) days after injection. One control group was coinjected with an excess of 500 μg of unlabeled hRS7 (D), a second control group (E) received the same dose of an antibody not reactive with prostate cancer (^{89}Zr-hLL2, 20 μg, 6 MBq). Arrows indicate tumor.

the tumor was clearly visible. At 7 days p.i., ^{89}Zr-hRS7 was retained in the tumor and had cleared from the rest of the body, with some activity in the skeleton (Figure 5). PET/CT imaging at 7 days after injection showed high uptake of the ^{89}Zr-labeled hRS7 antibody in the PC3 tumor. There was no accumulation of radioactivity in the other organs, and some uptake in the skeleton (nose, the joints of the knees and shoulders and the spine) was observed. Accumulation of ^{89}Zr-hRS7 in the tumor was significantly reduced when an excess of unlabeled hRS7 was coinjected (Fig. 5D). The same low uptake in the tumor was observed after injection of the ^{89}Zr-labeled control antibody hLL2 (Figure 5E). Tumor-to-liver ratios were determined by ROI analysis at each time point: the tumor-to-liver ratio was 2.9 ± 0.2, 6.5 ± 0.6 and 7.7 ± 1.3 at 1, 3 and 7 days after injection, respectively. The tumor-to-liver ratio increased significantly between 1 and 3 days after injection (P<0.0001).

MicroSPECT imaging of ^{111}In-hRS7 was performed in mice at 10, 13, 17, and 24 days after inoculation of tumor cells in the prostate. Representative coronal sections through the center of the tumor are displayed in Figure 6. The mice in the control group without PC3 tumors showed no uptake of ^{111}In-hRS7. Uptake in PC3 tumors in the prostate could be blocked by coinjection of an excess of unlabeled hRS7. Tumors were clearly visualized in the prostate in all mice. There was no visual difference in SPECT

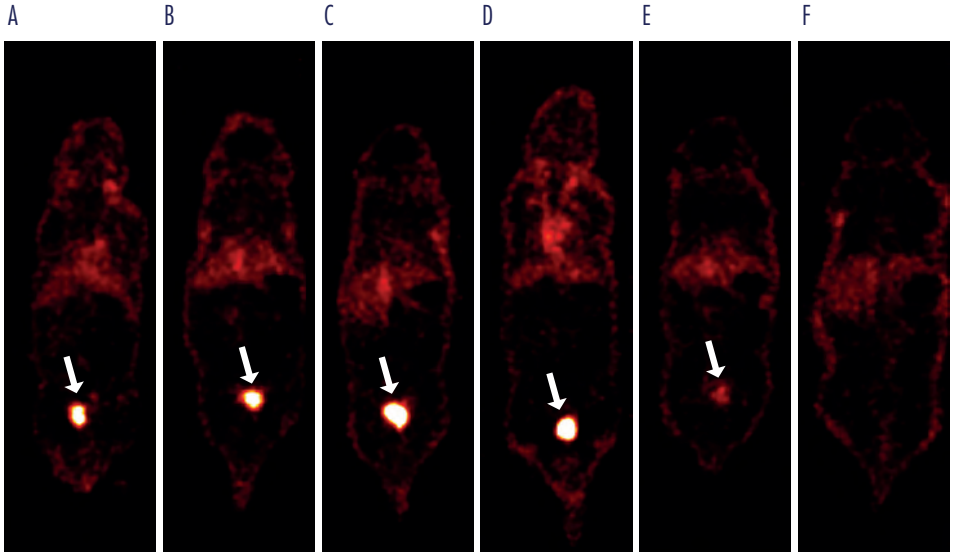

Figure 6. Anterior projections of SPECT scans of NMRI nude mice with an orthotopic PC3 tumor in the prostate injected with ^{111}In-hRS7 (10 µg, 37 MBq) at 10 (A), 13(B), 17(C) and 24(D) days after tumor cell inoculation respectively. One control group of mice with an orthotopic PC3 tumor was coinjected with an excess of 500 µg of unlabeled hRS7 (E). The second control group received ^{111}In-hRS7 and consisted of mice without PC3 xenograft (F). Arrows indicate tumor. Scans were acquired 3 days after injection.

images acquired 10, 13, 17, or 24 days after tumor cell inoculation. Tumor-to-liver ratios were determined by ROI analysis at each time point. The tumor-to-liver ratio at 10 days after inoculation was 6.9 ± 0.3, 4.4 ± 0.6 at 13 days, 7.3 ± 3.8 at 17 days, and 7.5 ± 3.5 at 24 days. There was no significant increase in tumor-to-liver ratio with time. Tumors weights were 0.047 ± 0.017 g at 10 days, 0.028 ± 0.015 g at 13 days, 0.046 ± 0.012 g at 17 days, and 0.067 ± 0.042 g at 24 days after intraprostatic cell injection, and there was no significant tumor weight difference between the experimental groups.

Discussion

In the present study, the potential of hRS7 for radioimmunoimaging of PC was investigated. Immunohistochemical analysis showed that EGP-1 is expressed on the epithelial cells of the normal prostate and is abundantly expressed on human primary prostate tumors and human PC metastases, indicating that EGP-1 is a potential target for PC imaging. Expression of EGP-1 in normal prostate tissue does not necessarily disqualify the use of hRS7 for specific imaging of PC. Firstly, in situations where distant

metastases are being examined, EGP-1 expression in the normal prostate is irrelevant. Secondly, it has yet to be determined whether EGP-1 would be accessible to the antibody in the intact tissue architecture of the normal prostate, as has been described for other antibodies [14]. Since EGP-1 is not expressed in the prostate of mice, we could not assess this issue.

The antibody protein dose escalation study with ^{111}In-hRS7 revealed that the highest tumor uptake was obtained at ≤10 µg, with progressively less uptake as the dose was increased to 100 µg. This likely reflects a gradual saturation of antigen. The antigen was not fully saturated at the 100 µg dose, because when a 500 µg blocking dose was administered, tumor uptake was as low as 10% ID/g (*vs* 20% ID/g at 100 µg). Uptake in normal tissue was low (<6%), as expected, since murine tissues do not express cross-reactive antigen, and was not affected by the protein dose.

Simultaneous injection of ^{111}In-hRS7 and ^{125}I-hRS7 showed a much higher tumor uptake of ^{111}In-hRS7 compared to the ^{125}I-labeled mAb (36.5 ± 13.3% ID/g *vs* 7.3 ± 2.3% ID/g, *P*=0.0003). This is in agreement with previous reports that show murine RS7 internalization [15]. Internalization causes catabolism of the labeled antibody in the lysosomes with subsequent wash-out of the ^{125}I-labeled metabolite. Upon internalization, the ^{111}In- and ^{89}Zr-labeled metabolites are retained intracellularily in the lysosomes. Uptake of ^{111}In-hRS7 and ^{125}I-hRS7 in normal tissues was relatively low (all <6%).

The biodistribution of ^{89}Zr-hRS7 in mice with s.c. PC3 xenografts was similar to that of ^{111}In-hRS7, except for femur uptake which was significantly higher for the ^{89}Zr-labeled hRS7. Tumor uptake increased significantly from 24 to 72 h p.i. (from 26.6 ± 7.9% ID/g to 43.6 ± 11.5% ID/g, *P*=0.0003). Between 3 and 7 days p.i., tumor uptake stabilized (54.3 ± 7.0% ID/g at 7 days p.i.), but due to the blood clearance of the radiolabeled mAb, tumor-to-blood ratios increased from 2 at 24 h to >8 at 7 days p.i. Tumor uptake was specific, as blocking the EGP-1 antigens in vivo with an excess of unlabeled hRS7 resulted in a much lower uptake of the radiolabeled hRS7 antibody in the tumor (11.2 ± 0.8% ID/g, 3 days p.i.). The same low nonspecific uptake (10.1 ± 2.1% ID/g) was observed when ^{89}Zr-hLL2 was injected. The specific accumulation of ^{89}Zr-hRS7 could be clearly visualized with PET/CT. Some ^{89}Zr activity in the skeleton was observed, most likely due to incorporation of released ^{89}Zr from the internalized and catabolized antibody into the bone, as has been described for a ^{89}Zr-anti-EGFR antibody [16]. ROI analysis of the PET images revealed a significant increase of the tumor-to-liver ratio between 1 and 3 days after injection of ^{89}Zr-hRS7 (2.9 ± 0.2% *vs* 6.5 ± 0.6% ID/g).

SPECT imaging of PC3 tumors in the mouse prostate clearly visualized the intraprostatic tumors with very low background activity levels. Metastatic spread of the tumor was not observed. Both imaging and biodistribution results showed that uptake could be

blocked by an excess of unlabeled antibody. A few mice showed accelerated mAb clearance from the blood, which occurs occasionally in BALB/*c* mice, as described previously [17]. Tumor uptake in the intraprostatic tumors was slightly lower than that in the s.c. tumors and was not affected by time after tumor inoculation.

Previous studies with hRS7 have demonstrated high antigen expression on a wide range of human tumor types, including breast and lung tumors [18,19]. Our studies suggest that radiolabeled hRS7 may also be a useful agent for targeting prostate cancer. To further improve PC imaging, a pretargeting strategy with an EGP-1 targeted bispecific antibody would be desirable. Future experiments will be aimed at the use of this bispecific antibody.

Conclusion

hRS7 showed high and specific accumulation in PC3 xenografts in nude mice. Immunohistochemical staining of human prostate tumor samples disclosed abundant EGP-1 expression in primary prostate tumors and PC metastases. Biodistribution studies showed high and specific tumor uptake and high tumor-to-blood ratios, especially at later time points. These properties of hRS7 result in excellent immunoPET and immunoSPECT images of PC3 xenograft mouse models. hRS7 is a promising candidate for imaging of EGP-1 expressing prostate tumors.

Acknowledgements

We thank Bianca Lemmers and Kitty Lemmens (Central Animal Facility, Radboud University Nijmegen Medical Center, The Netherlands) for their excellent technical assistance in the animal experiments, and Corrina de Ridder (Erasmus Medical Center Rotterdam, The Netherlands) for sharing her valuable expertise in setting up the orthotopic PC3 mouse model.

References

1. Zaheer A, Cho SY, Pomper MG. New Agents and Techniques for Imaging Prostate Cancer. J Nucl Med 2009; 50:1387-1390.
2. Beheshti M, Langsteger W, Fogelman I. Prostate Cancer: Role of SPECT and PET in Imaging Bone Metastases. Semin Nucl Med 2009; 39:396-407.
3. Ravizzini G, Turkbey B, Kurdziel K, et al. New horizons in prostate cancer imaging. Eur J Radiol 2009; 70:212-226.
4. Sodee DB, Sodee AE, Bakale G. Synergistic value of single-photon emission computed tomography/computed tomography fusion to radioimmunoscintigraphic imaging of prostate cancer. Semin Nucl Med 2007; 37:17-28.
5. Basu A, Goldenberg DM, Stein R. The epithelial/carcinoma antigen EGP-1, recognized by monoclonal antibody RS7-3G11, is phosphorylated on serine 303. Int J Cancer 1995; 62:472-479.
6. Stein R, Basu A, Chen S, Shih LB, et al. Specificity and properties of MAb RS7-3G11 and the antigen defined by this pancarcinoma monoclonal antibody. Int J Cancer 1993; 55:938-946.
7. Stein R, Basu A, Goldenberg DM, et al. Characterization of cluster 13: the epithelial/carcinoma antigen recognized by MAb RS7. Int J Cancer Suppl 1994; 8:98-102.
8. Fraker PJ, Speck JC, Jr. Protein and cell membrane iodinations with a sparingly soluble chloroamide, 1,3,4,6-tetrachloro-3a,6a-diphrenylglycoluril. Biochem Biophys Res Commun 1978; 80:849-857.
9. Ruegg CL, Anderson-Berg WT, Brechbiel MW, et al. Improved in vivo stability and tumor targeting of bismuth-labeled antibody. Cancer Res. 1990; 50:4221-4226.
10. Hnatowich DJ, Childs RL, Lanteigne D, et al. The preparation of DTPA-coupled antibodies radiolabeled with metallic radionuclides: an improved method. J Immunol Methods 1983; 65:147-157.
11. Verel I, Visser GW, Boellaard R, et al. ^{89}Zr immunoPET: comprehensive procedures for the production of ^{89}Zr-labeled monoclonal antibodies. J Nucl Med 2003; 44:1271-1281.
12. Lindmo T, Boven E, Cuttitta F, et al. Determination of the immunoreactive fraction of radiolabeled monoclonal antibodies by linear extrapolation to binding at infinite antigen excess. J Immunol Methods 1984; 72:77-89.
13. Stein R, Govindan SV, Mattes MJ et al. Improved iodine radiolabels for monoclonal antibody therapy. Cancer Res. 2003;63:111-118.
14. Hilgers J, Zotter S, Kenemans P. Polymorfic epithelial mucin and CA 125-bearing glycoprotein in basic and applied carcinoma research. Cancer Reviews. 1989;11-12:3-10.
15. Shih LB, Xuan H, Aninipot R, et al. In vitro and in vivo reactivity of an internalizing antibody, RS7, with human breast cancer. Cancer Res 1995; 55(Suppl):5857s-5863s.
16. Perk LR, Visser GW, Vosjan MJ et al. ^{89}Zr as a PET surrogate radioisotope for scouting biodistribution of the therapeutic radiometals ^{90}Y and ^{177}Lu in tumor-bearing nude mice after coupling to the internalizing antibody cetuximab. J Nucl Med 2005; 46:1898-1906.
17. Reddy N, Lin Ong G, Behr TM, et al. Rapid blood clearance of mouse IgG2a and human IgG1 in many nude and nu /+ mouse strains is due to low IgG2a serum concentrations. Cancer Immunology, Immunotherapy 1998; 46:25-33.

18. Stein R, Chen S, Sharkey RM, et al. Murine monoclonal antibodies raised against human non-small cell carcinoma of the lung: specificity and tumor targeting. Cancer Res 1990; 50:1330-1336.
19. Stein R, Chen S, Haim S, et al. Advantage of yttrium-90-labeled over iodine-131-labeled monoclonal antibodies in the treatment of a human lung carcinoma xenograft. Cancer 1997; 80(Suppl):2636-2641.

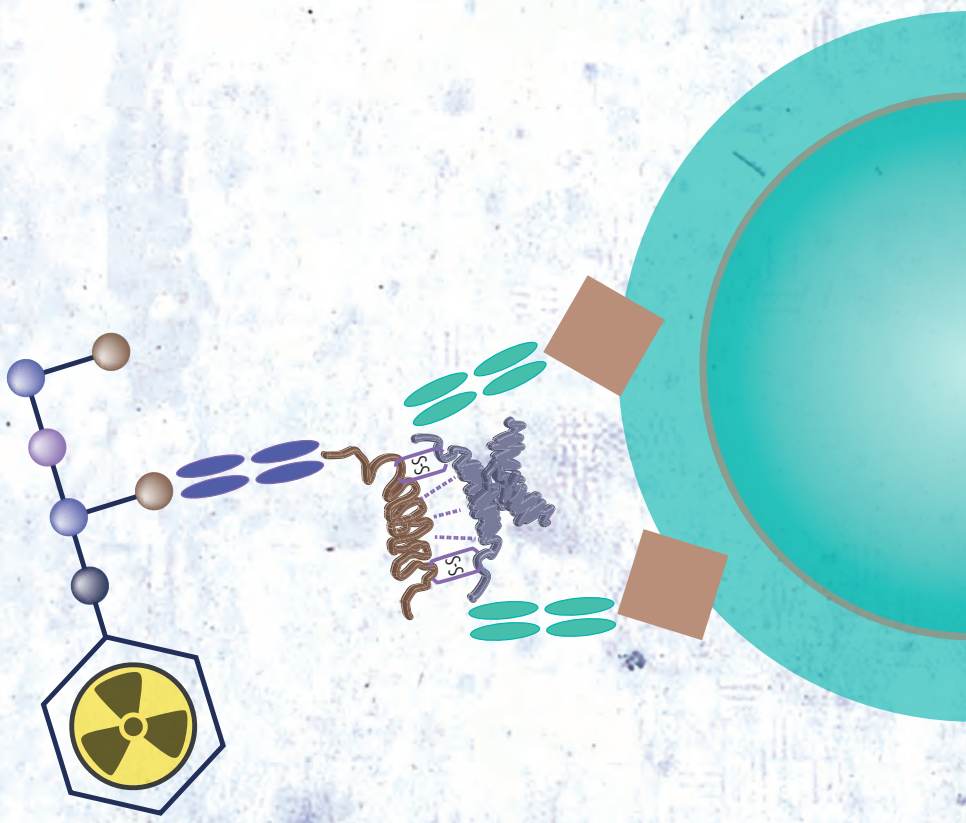

A new tri-Fab bispecific antibody for pretargeting TROP-2-expressing epithelial cancers

4

Robert M Sharkey,
Catharina M. van Rij,
Habibe Karacay,
Edmund A Rossi,
Cathelijne Frielink,
Celeste Regino,
Thomas M Cardillo,
William J. McBride,
Chien-Hsing Chang,
Otto C. Boerman,
David M Goldenberg

Nucl Med 2012; 53(10):1625-32.

Abstract

RS7 is an internalizing anti-TROP-2 pancarcinoma antibody capable of targeting most epithelial cancers. Since pretargeting strategies could improve tumor localization of radionuclides, a new anti-TROP-2 x anti-hapten bispecific antibody (bsAb) for pretargeting, based on humanized RS7 (hRS7) was prepared and evaluated with a radiolabeled hapten-peptide in vitro and in vivo to determine if its internalization properties would interfere with pretargeting.

Methods

The anti-TROP-2 x anti-hapten bsAb, TF12, was prepared using the modular Dock-and-Lock method. TF12 and hRS7 binding was assessed by cell binding assays and FACScan in a variety of human carcinoma cell lines. TF12's internalization was evaluated in vitro using a fluorescent TF12 conjugate or hapten-peptide, as well as ^{111}In-labeled TF12 and RS7. TF12's biodistribution and use as a pretargeting agent with an ^{111}In-labeled hapten-peptide were assessed in several human epithelial cancer xenografts. Dose optimization was examined in 2 cell lines.

Results

TF12 internalizes, but a substantial fraction remained accessible on the tumor surface. FACScan analysis showed only a minor change in fluorescent signal when probed with a fluorescent hapten-peptide over 4 h, and microscopy showed substantial membrane staining when reassessed 24 hours after TF12 exposure. Only 40.1% of ^{111}In-TF12 was internalized after 24 h. In vivo, excellent tumor localization of the ^{111}In-labeled peptide was observed in several tumor models.

Conclusion

TF12 was retained sufficiently on the cell surface in a number of epithelial cancers, thereby making it suitable for pretargeted imaging and therapy of various TROP-2-expressing carcinomas.

Introduction

Radioimmunotherapy is an effective therapeutic option for follicular non-Hodgkin lymphoma [1-3], but with challenges in solid tumors, efforts continue to search for new targets and procedures to improve imaging and therapeutic prospects [3]. In the search for new targets, TROP-2 (also known as EGP-1, epithelial glycoprotein-1; GA733-1, gastric antigen 733-1; and TACSTD2, tumor-associated calcium signal transducer 2) is of interest [4]. TROP-2 is a 47.8-kD integral membrane glycoprotein that is highly expressed on the majority of epithelial cancers originating from the breast, prostate, lungs, ovaries, gastrointestinal tract, pancreas, and skin, as well as selective expression in some normal tissues [5, 6]. TROP-2 expression is associated with poor prognosis, tumor aggressiveness and metastasis [4]. RS7 is an anti-TROP-2 monoclonal IgG antibody that targets epithelial cancers, including lung, breast, colon, pancreas, and prostate cancers [6-13]. Previous studies showed RS7 is internalized rapidly after binding TROP-2 on the target cell surface, with an estimate of 50% internalized within 70 min in a breast cancer cell line, while even faster internalization rates were determined in a lung cancer cell line [6, 8]. In vitro and in vivo studies showing that radiometal-labeled RS7 (e.g., ^{111}In or ^{90}Y) is retained at a much higher level than radioiodinated RS7 also are consistent with RS7's internalization [10, 11]. More recently, this property led to an evaluation of RS7 as a targeting agent for drugs [14]. However, unconjugated humanized RS7 (hRS7) showed potent ADCC (antibody-dependent cell-mediated cytotoxicity) activity in gynecological cancers, suggesting that some portion of hRS7 is retained on the surface to allow immune effector cell interaction.

Numerous studies have shown various pretargeting strategies are superior to directly radiolabeled antibodies in generating high tumor/non-tumor ratios quickly, with tumor uptake frequently rivaling that of a directly radiolabeled F(ab')$_2$ or even an IgG [15]. With its pancarcinoma targeting capability, the anti-TROP-2 antibody, RS7, is an interesting antibody for pretargeting, but with previous reports indicating RS7 is internalized [6, 8], its utility in pretargeting, where the primary targeting agent must remain accessible for some time to allow binding of the secondary compound, was in question. Nevertheless, with the ease of making bispecific antibodies (bsAb) with the Dock-and-Lock technology [16], an RS7-based anti-TROP-2 x anti-hapten Tri-Fab bsAb, designated TF12, was prepared (Figure 1). In this report, the potential for using TF12 in a pretargeting setting with a radiolabeled hapten-peptide was evaluated in vitro and in vivo in various epithelial cancer cell lines. The results show TF12 provides excellent localization of the radiolabeled hapten-peptide in vivo, illustrating the internalization properties of this bsAb/target combination do not impede its development for pretargeting applications.

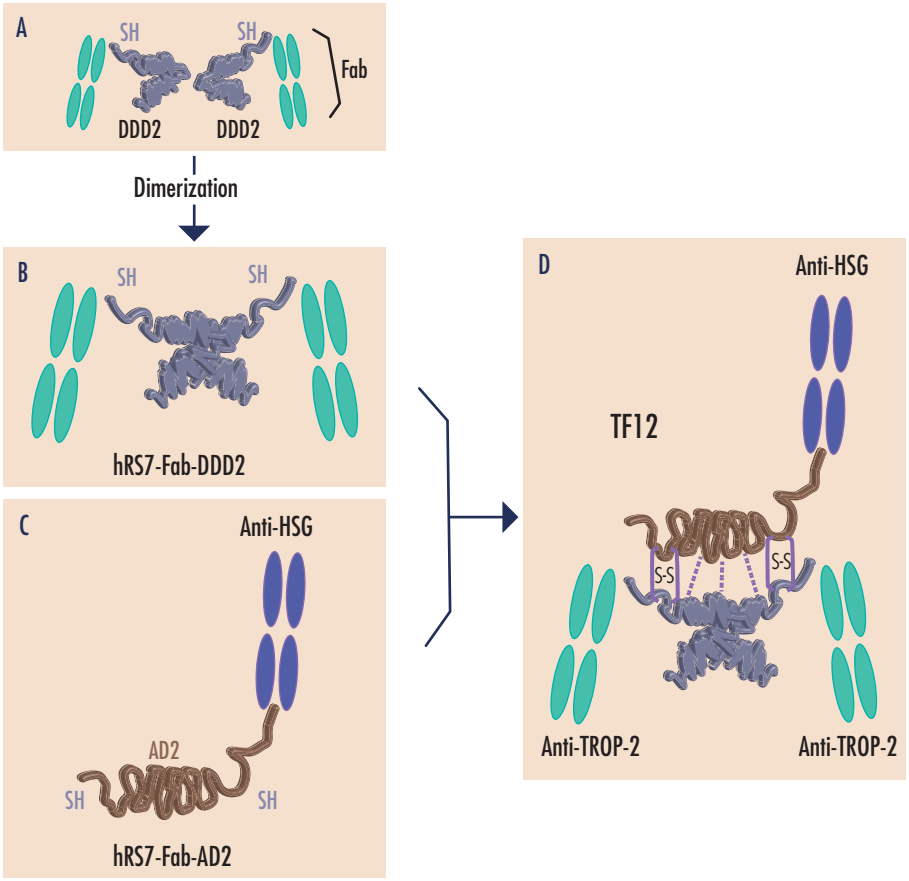

Figure 1. Schematic representation of the TF12 DNL construct (A). The hRS7-Fab-DDD2 (DDD, dimerization and docking domain) module forms homodimers (B). The h679 anti-HSG Fab is fused with the AD2 sequence (AD, anchoring domain) (C). When these 2 proteins are brought together, the AD2 portion docks to the docking domain of the DDD2 module, forming the tri-Fab anti TROP-2 x anti HSG bsAb TF12 (D). Disulfide bridges form between the strategically placed cysteines to link the 2 modules covalently.

Materials and methods

Cell Lines

MDA-MB-468 (breast cancer), SK-OV-3 (ovarian cancer), PC3 (prostate cancer), Calu-3 (lung cancer), HT29 (colon cancer), LS174T (colon cancer), Capan-1 (pancreatic cancer), and Raji (Burkitt lymphoma) were purchased from American Type Culture Collection (Manassas, VA).

Antibodies and Other Agents

The TF12 Tri-Fab bsAb (molecular weight 157 kDa) was prepared by the Dock-and-Lock procedure [16], using a humanized version of the murine RS7 as the partner with the humanized anti-HSG (histamine-succinyl-glycine) hapten antibody, 679 [17] (Figure 1). Purified TF12 and hRS7, as well as other antibodies that were used as controls, including veltuzumab [Vmab; humanized anti-CD20 IgG [18]] and TF8 (humanized anti-CD22 [based on epratuzumab [19]] x anti-HSG DNL Tri-Fab bsAb construct), were all provided by Immunomedics Inc., or IBC Pharmaceuticals, Inc., Morris Plains, NJ.
Unconjugated AffiniPure goat-anti-human (GAH) IgG (heavy and light chain specific) and FITC-conjugated AffiniPure GAH IgG (Fc-specific; FITC-GAH IgG) were purchased from Jackson ImmunoResearch, West Grove, PA. GAH IgG, TF12, hRS7, and Vmab, were conjugated with AlexaFluor® 488 (Invitrogen, Carlsbad, CA) according to manufacturer's instructions. The AlexaFluor® conjugates were designated AF-[antibody name].
IMP288, the di-HSG hapten-peptide (DOTA-D-Tyr-D-Lys(HSG)-D-Glu-D-Lys(HSG)-NH_2; MW: 1,453 Da), was prepared and radiolabeled with ^{111}In as described previously [20]. Radioiodinated TF12 and hRS7 were made by the iodogen method [21]. ^{125}I and ^{111}In were provided by either Perkin Elmer (Waltham, MA, USA) or Covidien (Petten, The Netherlands). Instant thin-layer chromatography showed <5% unbound radionuclide. Immunoreactivity of radiolabeled TF12 or hRS7 was determined by Lindmo assays [22] or by size-exclusion high performance liquid chromatography (SE-HPLC) using an excess of an anti-hRS7 idiotype antibody, as described previously [17].
A fluorescent-conjugated peptide, designated RDC017, was used to assess the accessibility of the bsAb bound to the surface of several cell lines. RDC017 was prepared from a thiol-containing derivative of the IMP288 (see Supplemental Data*).

Fluorescence-Activated Cell Sorting (FACS) Analysis

FACS analysis was performed to determine hRS7 and TF12 binding to TROP-2 expressing tumor cell lines. Cell suspensions were incubated with 5 μg/mL of RS7 and TF12 AF-conjugates for 30 min at room temperature (RT), and were analyzed by FACS (BD FACSCalibur, Becton Dickinson, San Jose, CA) after washing and fixing with 10% formalin. For each cell line, AF-Vmab was used as a negative control with the same procedures.

*http://jnm.snmjournals.org/content/suppl/2012/09/12/53.10.1625.DC1/104364_Supplemental_Data.pdf

Internalization Assays

MDA-MB-468 and PC3 were incubated with TF12 (5 µg/mL) for 1 h at 4°C. After washing to remove the unbound antibody, fresh medium was added and incubation was continued at 37°C. At 1, 2, and 4 h, the presence of surface-bound TF12 was then probed using a molar excess RDC017 for 30 min at 4°C before being washed and then fixed with 10% buffered formalin. As an internalizing control, Raji cells were incubated with the Tri-Fab bsAb, TF8 (anti-CD22 x anti-HSG), using the same procedure and probing with the RDC017 peptide. Non-specific binding was examined by incubating samples only with the fluorescent agent.
In a second approach, internalization assays using ^{111}In-radiolabeled RS7 and TF12 with PC3 cells in culture were performed as described previously [23, 24]. Briefly, cells were grown to confluence in 6-well plates, and incubated in triplicate with either 6.15 ng ^{111}In-radiolabeled hRS7, 4.02 ng ^{111}In-TF12, or a combination of 4.02 ng of ^{111}In-TF12 and 1.74 ng of unlabeled IMP288 in 2 mL of media plus 0.5% bovine serum albumin (all wells received 50,000 cpm in 100 µl PBS). As a control, separate wells were incubated in triplicate in the presence of 2 µg of unlabeled antibody before adding the radiolabeled product. After 1, 2, 4, 9 and 24 h incubation at 37°C, the cells were washed twice with cold PBS. To remove the membrane-associated fraction, the cells were incubated with an acid-buffer (0.1 M acetic acid, 154 nM NaCl, pH 2.6) for 10 min. Then, after washing the cells twice with PBS, they were removed from the plate with a cotton swab. The percentage of radioactivity in the two fractions, the membrane-associated and internalized fractions, with and without the addition of excess unlabeled antibody, was determined in triplicate.

Microscopic Evaluation of Internalization

An assessment of internalization of TF12 by fluorescent microscopy was performed in MDA-MB-468 cells following the procedure by Pirker et al. [25]. Briefly, 5 x 10^5 MDA-MB-468 cells were incubated with 5 µg/mL of TF12 or control TF8 anti-CD22 for 1 h at 4°C. CD22-expressing Raji human Burkitt lymphoma cells incubated with TF8 served as a positive control for internalization, since TF8 was based on epratuzumab, a rapidly internalizing, humanized anti-CD22 antibody [19]. After washing cells with ice-cold PBS, 0.1% BSA, 0.1% NaN_3 to remove excess unbound bsAb, the cells were re-suspended in fresh media, and a T_0 sample was collected, with the remaining cells allowed to incubate at 37°C for 1 or 24 h. At the prescribed times, the cells were washed with cold media, then probed using either the fluorescent di-HSG-peptide RDC 017 (3.2 nmoles/mL) or AF-conjugated AffiniPure GAH IgG (AF-GAH IgG). The set of cells probed with AF-GAH IgG were first fixed with 4% formalin in PBS and then permeabilized with 0.1% Triton-X-100 (5 min, RT) before adding the AF-GAH IgG.

This allowed the secondary agent to localize both surface and internalized TF12. Both the RDC017 and AF-GAH IgG were incubated for 30 min at 4°C before the cells underwent a final wash in PBS, followed by a brief fixation in PBS/formalin, and then a sample was placed on a slide for microscopic examination.

Biodistribution Studies

Studies were performed at either the Radboud University Medical Centre (Nijmegen, The Netherlands) or the Center for Molecular Medicine and Immunology (CMMI, United States) after receiving approval from their respective animal welfare committees. Mice were obtained from either Taconic (Hudson, NY, USA) or Janvier (Le Genest Saint Isle, France), and were acclimated to laboratory conditions for at least 1 week before implantation of tumors. They were housed under non-sterile standard conditions in cages with free access to food and water.
A typical study involved nude mice that were inoculated subcutaneously with 1 x 10^6 – 1 x 10^7 MDA-MB-468, SK-OV-3, PC3 or Capan-1 cells for assessment of targeting with radiolabeled TF12 or hRS7 IgG, or pretargeting with TF12. Pretargeting was also assessed using TF8 anti-CD22 bsAb with subcutaneously-grown Raji human Burkitt lymphoma cells. Once tumors were palpable, the studies were initiated (tumors generally averaged 0.1 to 0.3 g at the time of necropsy). The specific details for each study are given in the RESULTS. Animals were anesthetized and bled intracardially before euthanizing by CO_2/O_2 asphyxiation at various time points. After necropsy, tumors and organs of interest were excised, weighed, and counted in a scintillation counter. The percentage-injected dose per gram (% ID/g) was calculated based on a standard of the injected product co-counted with the tissues.

Results

In Vitro Characterization of TF12 Binding

The molecular characterization and binding properties of TF12 are given in Supplemental Figure 1.* Size-exclusion HPLC, SDS-PAGE confirmed purity, and its binding properties using Biacore to anti-rat hRS7 idiotype antibody as a surrogate for TROP-2 and the hapten, HSG, were confirmed. Binding analysis to MDA-MB-231 and SK-OV-3 breast and ovarian carcinoma cell lines showed similar affinity. By flow cytometry, TF12 and hRS7 bound in a similar manner to 4 cell lines of different origin shown in Table 1. TROP-2 expression in two other cell lines using hRS7 also is shown.

*http://jnm.snmjournals.org/content/suppl/2012/09/12/53.10.1625.DC1/104364_Supplemental_Data.pdf

Table 1. FACS analysis of TROP-2 expression in several epithelial cancer cell lines.*

		hRS7	TF12
MDA-468	Breast	824	865
Capan-1	Pancreatic	66	71
HT29	Colonic	98	109
SK-OV-3	Ovarian	283	273
PC3	Prostate	169	ND
Calu-3	Lung	144	ND

*TROP-2 expression is given as a normalized Mean Fluorescence Intensity (MFI), subtracting corresponding negative controls MRI from the TF12 or hRS7 binding.

In Vitro Assessment of Internalization

The internalization rate of murine RS7 in Calu-3 or MBA-MD-468 previously indicated 50% of the bound antibody was internalized in ~ 1 h or less [6, 8]. MDA-MB-468 cells that were pre-incubated with TF12 at 4°C before being washed and incubated at 37°C showed continued evidence of binding the fluorescent hapten-peptide RDC017 over 4 h (Figure 2). This was in sharp contrast to Raji lymphoma cells incubated with TF8, an anti-CD22 bsAb. Even after just 1 h, the RDC017 no longer bound to the cells, suggesting TF8 had internalized completely. It is important to emphasize that this assay does not account for bsAb that might otherwise be released from the cells into the media rather than being internalized. However, given the reported rapid internalization of the epratuzumab anti-CD22 antibody [19, 26, 27], it is reasonable to assume the inability of the peptide to bind to the Raji cells pre-incubated with TF8 was due to its internalization and not its release into the media. By microscopy, MBA-MD-468 cells pre-incubated with TF12 and probed with RDC017 showed intense membrane localization through 24 h, indicating that TF12 was still present on the surface (Figure 3). However, when the cells were probed with a fluorescent-conjugated anti-human IgG after fixing and permeabi-

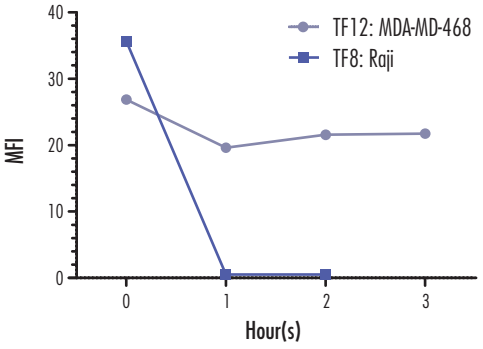

Figure 2. Analysis of internalization of TF12 anti-TROP-2 or TF8 anti-CD22 bsAb in MDA-468 and Raji cells, respectively. Cells were probed with the fluorescent hapten-peptide RDC017 after incubation with each bsAb. Fluorescence, as determined by FACScan, is expressed as Mean Fluorescent Intensity (MFI), normalizing data by subtracting the MFI for RDC 017 alone, which was minimal.

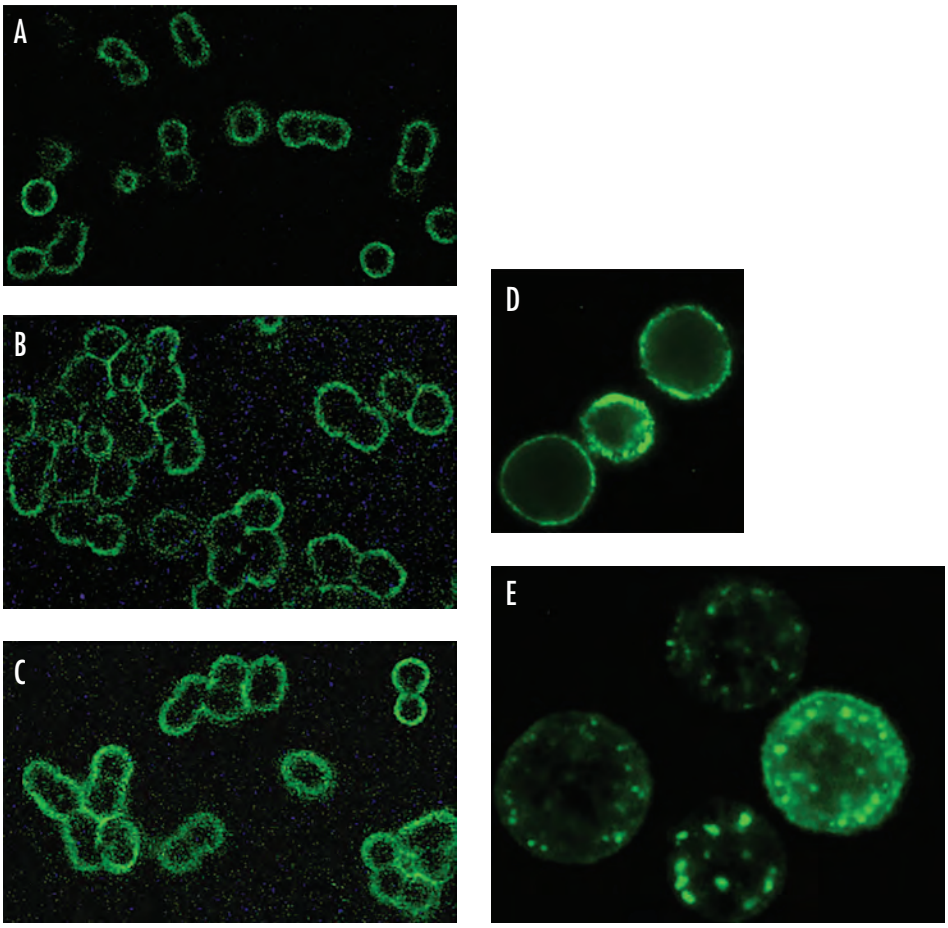

Figure 3. Visualization of TF12 internalization. MDA-MB-468 cells were incubated for 1 h at 4°C with TF12 before replacing with fresh media, and raising the incubation temperature to 37°C. (A-C) The cells were then probed with fluorescent RDC017 immediately after the 1-h 4°C incubation (A), after 1 h at 37°C (B), or 24 h at 37°C (C). D and E represent specimens of the same MDA-MB-468 cells first incubated with TF12 for 1 h at 4°C, but in this case, TF12 binding was revealed using AF-GAH IgG after fixing and permeabilizing the cells. (D) immediately following the 1-h 4°C incubation; (E) after 1-h 37°C incubation. Images were brightened and the contrast enhanced using Adobe® Photoshop®.

lizing cells to allow the fluorescent conjugate to penetrate inside the cells, staining was seen within the cells (Figures 3D and 3E), indicating that some portion had internalized. Microscopic examination of Raji cells incubated with TF8 and probed with RDC017 immediately after the 4°C incubation showed a patchy distribution that became more diffuse and faint (nearly absent) when probed after a 1-h incubation at 37°C, again suggesting that most of the anti-CD22 bsAb had internalized (not shown).

In order to provide a more quantitative estimate of how much TF12 is internalized,

Table 2. Internalization of ^{111}In-labeled RS7, TF12 and TF12 + IMP288 in PC3 cells in culture.

	% Internalized antibody* (mean ± SD)		
Time (h)	RS7	TF12	TF12+IMP288
1	14.9 ± 0.97	13.6 ± 3.09	22.2 ± 9.79
2	16.6 ± 1.02	16.3 ± 1.13	22.2 ± 2.49
4	18.6 ± 0.58	22.8 ± 1.47	23.2 ± 0.46
9	25.3 ± 0.18	28.3 ± 2.54	30.2 ± 2.34
24	32.0 ± 2.09	40.1 ± 4.99	38.4 ± 4.68

*Internalized antibody is expressed as a percentage [internalize ÷ (internalized + membrane-bound) x (100)]. In the presence of excess unlabeled antibody, the % internalized antibody at 24 h ranged from 2.6 to 4.1%.

TF12 and hRS7 were radiolabeled with ^{111}In and the fractional amount internalized over 24 h was evaluated in the PC3 prostate cell line. One hour after cells were incubated with the antibodies, ~14% of the antibody had internalized (Table 2). Over the next 8 h, the percent internalized increased nearly 2-fold, to 25.3 ± 0.18% for the hRS7 IgG and to 28.3 ± 2.54% for TF12. By 24 h, 40.1 ± 4.99% of the TF12 bsAb had internalized, while about one-third of the hRS7 IgG was inside the cell. Thus, in this cell line, ~60% of the bsAb is retained on the surface of the cells. When divalent hapten-peptide IMP288 was co-administered with radiolabeled TF12, uptake over the first 2 h was higher than with the bsAb alone. These data suggest that cross-linked TF12 initiates an earlier spurt of internalization that seems to plateau, achieving the same maximum uptake as TF12 alone (not cross-linked by the hapten-peptide). As expected, pre-incubating cells with unlabeled antibody blocked binding of the radiolabeled antibody to TROP-2, illustrating that internalization of the radiolabeled antibody was related to its binding to TROP-2.

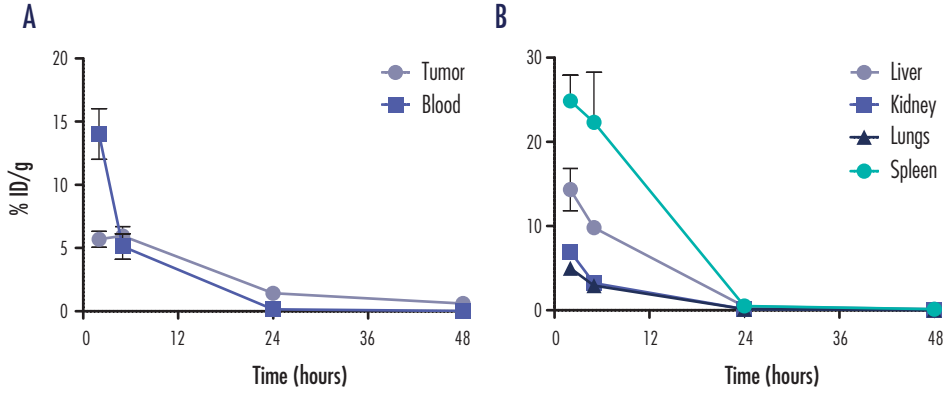

Figure 4. Biodistribution of ^{125}I-TF12 in nude mice bearing Capan-1 human pancreatic cancer xenografts. Percent injected dose per gram tumor and blood (A), other tissues (B).

Biodistribution Studies with Antibody Alone

A biodistribution study performed in animals bearing the Capan-1 human pancreatic xenograft showed radioiodinated TF12 cleared rapidly from the blood, with 0.15 ± 0.03% ID/g in the blood at 24 h (Figure 4), which is in agreement with the rapid clearance found with other tri-Fab bsAb [16]. Tumor uptake peaked at 2 h post-injection (5.6 ± 0.63% ID/g), falling to 1.43 ± 0.09% ID/g at 24 h. Similar levels of ^{125}I-TF12 were found in MBA-MD-468 breast and SK-OV-3 ovarian cancer cell lines 1 day after injection (0.91 ± 0.018% ID/g and 1.29 ± 0.33% ID/g, respectively), with blood concentrations averaging ≤0.4% ID/g. The spleen was the only tissue that showed an unusual early uptake, averaging ~20 to 25% ID/g at 2 and 5 h post injection, but like all the other normal tissues, TF12 cleared quickly, being equal to that in the liver (~ 0.5% ID/g) at 24 h.

The rapid clearance of the TF12 bsAb and its relatively low tumor uptake was in sharp contrast to the slow blood clearance of the hRS7 IgG and its higher uptake. For example, in PC3-bearing nude mice, tumor uptake of ^{125}I-hRS7 on day 3 was 7.3 ± 2.3% ID/g, while the concentration in the blood was 8.1 ± 1.1% ID/g. However, it is important to note that in PC3-bearing mice given ^{111}In-hRS7, tumor uptake was 36.5 ± 13.3% ID/g, whereas the blood concentration was similar to radioiodinated hRS7 IgG on day 3. These results are indicative of an internalizing antibody binding to a stable chelate-radiometal, where the percent uptake accounts for the cumulative binding of hRS7, its internalization, and entrapment of the ^{111}In-activity over time. However, the uptake of radioiodinated IgG or bsAb is expected to reveal only the amount of antibody that remains accessible (i.e., has not been internalized and catabolized).

Pretargeting Studies

Despite in vitro evidence that some portion of TF12 is internalized, biodistribution studies in mice bearing different s.c. tumor xenografts and pretargeted the day before with TF12 showed reasonably high (~10-15% ID/g) uptake of the ^{111}In-labeled peptide in the tumors (Table 3). Tissue uptake and blood concentrations were low, with tumor-to-blood ratios ranging from ~60:1 to 1000:1.

Additional studies examined several doses of TF12 (40, 79, and 158 µg) given with a fixed amount of IMP288 (0.026 nmole; TF12:IMP288 mole ratios = 10, 20, and 40:1) in the SK-OV-3 and MDB-MD-468 models (Figure 5). ^{111}In-IMP288 uptake in SK-OV-3 at 3 h increased from 5.3 ± 1.2% ID/g at the 10:1 ratio to as high as 21.3 ± 6.2% ID/g at the 40:1 ratio. Tumor uptake for TF12 in these animals (as measured by ^{125}I-TF12 added to TF12) was similar in the groups, ranging from 1.1 to 1.5% ID/g. In contrast, MDA-MB-468 uptake was only modestly increased from 11.6 ±

Table 3. Biodistribution of pretargeted ^{111}In-IMP288 in MDA-468, SK-OV-3 and PC3 3 h after injection.

	MBA-MD-468	SK-OV-3	PC3
Tumor	14.8 ± 3.4	13.6 ± 2.6	9.8 ± 1.6
Blood	0.02 ± 0.00	0.04 ± 0.02	0.16 ± 0.02
Spleen	0.17 ± 0.03	0.56 ± 0.34	0.31 ± 0.07
Kidney	2.45 ± 0.55	2.51 ± 0.64	1.49 ± 0.29
Liver	0.10 ± 0.02	0.20 ± 0.06	0.21 ± 0.03
Tumor to blood	1037 ± 303	378 ± 126	62 ± 4
Tumor weight (g)	0.06 ± 0.02	0.20 ± 0.09	0.07 ± 0.01

Nude mice were injected intravenously with 79 µg (0.5 nmol) ^{125}I-TF12 (0.37 MBq) and 0.025 nmol ^{111}In-IMP288, with exception of PC3 studies, where 462 µg (~3 nmol) of ^{125}I-TF12 and 0.11 nmol ^{111}In-IMP288. In all cases, ^{111}In-IMP288 was given 16 h after the TF12 injection. Data are expressed as % ID/g (mean ± SD; n=5).

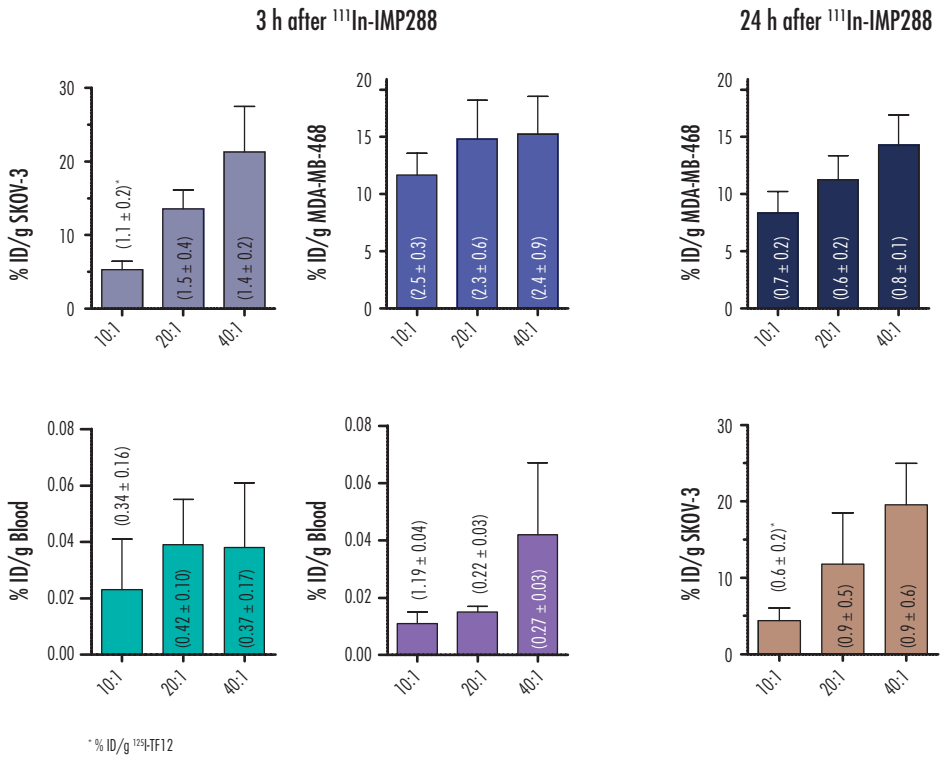

Figure 5. Optimizing IMP288 uptake in SK-OV-3 human ovarian cancer and MDA-MB-468 human breast cancer xenografts in nude mice. Animals (n=5/interval) were given 40, 79, or 158 µg of TF12 (containing trace ^{125}I-TF12) and then 16 h later, they received 0.026 nmoles (~40 µCi) of ^{111}In-IMP288. Animals were necropsied at 3 (A) and 24 h (B). Tumor and blood concentrations for the ^{111}In-IMP288 (bars) and the ^{125}I-TF12 (in parentheses) at the 3-h necropsy, as well as the 24-h tumor data. Tumors averaged between 0.1 to 0.3 g.

1.9 to 15.2 ± 3.3% ID/g over this same range of TF12. Interestingly, tumor uptake of the ^{125}I-TF12 was nearly 2-fold higher in the MDA-MB-468 xenografts than in the SK-OV-3 tumors, yet the breast cancer xenograft did not have a higher IMP288 uptake commensurate with the higher TF12 level. By 24 h, tumor uptake for the ^{111}In-IMP288 plateaued in both models, even though the uptake of the ^{125}I-TF12 decreased nearly 2- to 4-fold.

These targeting results are in sharp contrast to those obtained with the TF8 anti-CD22 bsAb in BALB/*c* nude mice bearing CD22-expressing Ramos or Raji tumors. In this study, animals were given 0.25 nmoles (40 µg) of TF8 followed 24 h later with 0.025 nmoles of ^{111}In-IMP288. Three hours later, uptake in Raji tumors was just 0.17 ± 0.07% ID/g and in Ramos, 0.15 ± 0.08 (n=4 in each). The low tumor uptake was predicted by the earlier in vitro studies that indicated efficient internalization within 1 h. Thus, even though tumor/blood ratios were high (e.g., averaging 38:1 in Raji-bearing mice), the low tumor uptake indicated unfavorable pretargeting with this bsAb.

Discussion

Pretargeting procedures for localizing radionuclides are very attractive, because they are able to localize the radiolabeled product (e.g., hapten-peptide or biotin) very quickly, developing very high tumor/nontumor ratios rapidly, and often with tumor uptake that can rival a directly radiolabeled IgG or F(ab')$_2$ fragment [15]. Bispecific antibody pretargeting procedures have typically relied on the bsAb's natural clearance from the blood and tissues, requiring a delay of several days before the hapten-peptide is given [15]. It is imperative that the bsAb remain accessible in the tumor (e.g., not internalized) in order for the radiolabeled hapten-peptide to be localized. Thus, if the pretargeting agent binds an antigen that triggers internalization, this target likely would not be suitable for pretargeting. For example, anti-CD22 antibodies are known to internalize rapidly, making these antibodies attractive candidates for targeting drugs or toxins that exert their effects intracellularly [27-32]. Pantelias et al. [33] compared the pretargeting of 3 different antigens associated with hematopoietic malignancies, anti-CD20, CD22, and HLA-DR, finding the anti-CD22 pretargeting agent had the lowest uptake of the 3 conjugates. However, CD22 also had the lowest density of the 3 antigens in the various cell lines examined, and thus this result may have merely reflected the lower antigen density. Herein, we included an evaluation of the TF8 tri-Fab bsAb that binds to CD22, suspecting its rapid internalization would affect its utility in pretargeting. We first noted that in vitro, the TF8 anti-CD22 bsAb was no longer accessible within just 1 h of its binding, and then in vivo, no appreciable localization of the radiolabeled hapten-peptide was observed. Thus, we agree that bsAbs to CD22 are not suitable for pretargeting, but not because it is insufficiently

expressed on target cells, but because the bsAb is efficiently internalized. Instead, we previously recommended the TF4 anti-CD20 tri-Fab bsAb be used for pretargeting B-cell malignancies [34]. It is interesting to note that in those studies, ^{111}In-TF4 had substantially higher uptake in tumor xenografts than radioiodinated TF4, suggesting some internalization over the 1-day pretargeting interval.

While antibody-based therapeutics (unconjugated and conjugated) are widely studied in hematological malignancies, it has been more challenging to find suitable targets for epithelial cancers [3]. In this regard, TROP-2 represents a promising new target for cancer, being expressed on the surface of many carcinomas [4]. Early in its development, the anti-TROP-2 antibody, RS7, was reported to internalize, and therefore most studies have focused on developing targeting strategies that take advantage of RS7's internalization properties [7, 10, 14, 35]. Shih et al. [8] examined internalization in MDA-MD-468 cells in vitro over 30 min and reported an extrapolated internalization rate of 0.0147 min^{-1}, indicating that under saturating conditions, surface-bound antibody will be internalized over ~70 min. Other studies in the Calu-3 human lung cancer cell line suggested an even faster rate of internalization, with most of the antibody being internalized within 45 min [6]. This compares to the anti-CD22 antibody, where 50% of the antibody was reported to be internalized within 10 min, with data indicating that nearly all the antibody had internalized within 2 h [27]. In vivo studies comparing RS7 labeled with a radiometal with RS7 labeled by the more traditional non-covalent radioiodination procedures showed substantially higher tumor retention when the antibody was labeled with a residualizing radionuclide, supporting the internalization capability of the RS7 antibody [7, 10, 11]. Thus, these data gave pause to developing a pretargeting procedure for TROP-2 localization. However, given TROP-2's presence in many carcinomas, and because the modular Dock-and-Lock method greatly simplifies bsAb preparation [16], TF12 was prepared for evaluation.

Our findings with the hRS7 IgG and the TF12 bsAb indicate that despite some initial internalization, sufficient residual bsAb remains on the surface of tumor cells to capture the hapten-peptide after ~1-day delay. Some of the in vitro studies were performed with the washed cells placed in fresh media before probing with the fluorescent hapten-peptide. Thus, it is unlikely that re-expression of antigen with re-engagement by the bsAb contained in the media explained the continued presence of TF12 on the cell surface. Because TF12 clears so quickly from the blood, it is equally unlikely that there would be considerable replenishing of the bsAb after the internalization process had occurred. Therefore, although there have been reports that internalization is nearly complete within ~1 h, our studies with TF12 and hRS7 radioconjugates found a smaller portion of the antibody, perhaps as low as 10-20%, is internalized over the first hour, but thereafter, internalization proceeds at a much slower rate (i.e., it is not linear). Indeed, it appears that after an initial spurt of internalization, some cell lines only had ~50% of the antibody internalized over 24 h.

These observations are very important, because antibodies are often characterized as

being internalizing or non-internalizing, when in fact there are varying rates among antibodies that are "actively" internalized, as well as rates for those "passively" taken into the cell. At least in the case of TF12, the in vitro studies using the fluorescent hapten-peptide were helpful for illustrating the continued capacity to bind the hapten-peptide after several hours and even 1 day. This type of assay should be useful for predicting which bsAb would have suitable surface retention for in vivo targeting, but it is unlikely it will be useful for predicting the actual quality of a given pretargeting agent, because there are other parameters that impact tumor localization [36]. With recent clinical studies, using the TF2 anti-CEACAM5 tri-Fab bsAb, also finding the bsAb is cleared sufficiently within just 1 day to allow efficient localization of the radiolabeled hapten-peptide [37, 38], we are encouraged to continue developing the TF12 bsAb for future clinical evaluation.

Conclusion

TF12 is a suitable bsAb for pretargeting different cancers that express TROP-2, primarily because after an initial spurt of internalization, sufficient bsAb remains on the surface to allow efficient capture of the hapten-peptide. With recent preclinical studies showing hRS7 targeting of prostate cancer [13], and with the need for developing better imaging procedures for this disease, this clinical indication should be considered. However, hRS7-SN-38 drug conjugates also have been proven to be effective in several cancer cell lines, including lung, pancreatic, colorectal, and breast cancers [6, 7, 12, 14, 39], and thus developing a highly sensitive imaging procedure for these cancers, perhaps to be used in concert with the therapeutic agent, is of interest as well.

Acknowledgements

Supported in part by NJ Cancer Commission grant 10-8-CCR-EO to RMS and the Dutch Cancer Society grant KUN-2010-4820 to OCB.

We thank Jayson Jebsen, Ali Mostafa, Lenka Muskova, Preeti Trisal, Anke Reuser, Gerben Franssen, Annemarie Eek, Kitty Lemmens, and Bianca Lemmers for their excellent technical assistance.

Disclaimer

EA Rossi, C Regino, TM Cardillo, WJ McBride, C-H Chang, and DM Goldenberg are employed or have financial interests in Immunomedics, Inc. or IBC Pharmaceuticals, Inc. Other authors declare no financial interests.

References

1. Hohloch K, Delaloye AB, Windemuth-Kieselbach C, et al. Radioimmunotherapy confers long-term survival to lymphoma patients with acceptable toxicity: registry analysis by the International Radioimmunotherapy Network. J Nucl Med 2011; 52:1354-1360.
2. Illidge T, Morschhauser F. Radioimmunotherapy in follicular lymphoma. Best Pract Res Clin Haematol 2011; 24:279-293.
3. Sharkey RM, Goldenberg DM. Cancer radioimmunotherapy. Immunotherapy 2011; 3:349-370.
4. Cubas R, Li M, Chen C, Yao Q. TROP-2: a possible therapeutic target for late stage epithelial carcinomas. Biochim Biophys Acta 2009; 1796:309-314.
5. Stepan LP, Trueblood ES, Hale K, et al. Expression of TROP-2 cell surface glycoprotein in normal and tumor tissues: potential implications as a cancer therapeutic target. J Histochem Cytochem 2011; 59:701-710.
6. Stein R, Basu A, Chen S, et al. Specificity and properties of MAb RS7-3G11 and the antigen defined by this pancarcinoma monoclonal antibody. Int J Cancer 1993; 55:938-946.
7. Govindan SV, Stein R, Qu Z, et al. Preclinical therapy of breast cancer with a radioiodinated humanized anti-EGP-1 monoclonal antibody: advantage of a residualizing iodine radiolabel. Breast Cancer Res Treat 2004; 84:173-182.
8. Shih LB, Xuan H, Aninipot R, et al. In vitro and in vivo reactivity of an internalizing antibody, RS7, with human breast cancer. Cancer Res 1995; 55:5857s-5863s.
9. Stein R, Blumenthal R, Sharkey RM, et al. Comparative biodistribution and radioimmunotherapy of monoclonal antibody RS7 and its $F(ab')_2$ in nude mice bearing human tumor xenografts. Cancer 1994; 73:816-823.
10. Stein R, Chen S, Haim S, et al. Advantage of yttrium-90-labeled over iodine-131-labeled monoclonal antibodies in the treatment of a human lung carcinoma xenograft. Cancer 1997; 80:2636-2641.
11. Stein R, Goldenberg DM, Thorpe SR, et al. Advantage of a residualizing iodine radiolabel for radioimmunotherapy of xenografts of human non-small-cell carcinoma of the lung. J Nucl Med 1997;38:391-395.
12. Stein R, Govindan SV, Chen S, et al. Successful therapy of a human lung cancer xenograft using MAb RS7 labeled with residualizing radioiodine. Crit Rev Oncol Hematol. 2001; 39:173-180.
13. van Rij CM, Sharkey RM, Goldenberg DM, et al. Imaging of prostate cancer with immunoPET and immunoSPECT using a radiolabeled anti-EGP-1 monoclonal antibody. J Nucl Med 2011; 52:1601-1607.
14. Cardillo TM, Govindan SV, Sharkey RM, Trisal P, Goldenberg DM. Humanized anti-TROP-2 IgG-SN-38 conjugate for effective treatment of diverse epithelial cancers: preclinical studies in human cancer xenograft models and monkeys. Clin Cancer Res 2011; 17:3157-3169.
15. Goldenberg DM, Chatal JF, Barbet J, et al. Cancer imaging and therapy with bispecific antibody pretargeting. Update Cancer Ther 2007; 2:19-31.
16. Rossi EA, Goldenberg DM, Cardillo TM, et al. Stably tethered multifunctional structures of defined composition made by the dock and lock method for use in cancer targeting. Proc Natl Acad Sci USA 2006; 103:6841-6846.

17. Sharkey RM, McBride WJ, Karacay H, et al. A universal pretargeting system for cancer detection and therapy using bispecific antibody. Cancer Res 2003; 63:354-363.
18. Goldenberg DM, Rossi EA, Stein R, et al. Properties and structure-function relationships of veltuzumab (hA20), a humanized anti-CD20 monoclonal antibody. Blood 2009; 113:1062-1070.
19. Leung SO, Goldenberg DM, Dion AS, et al. Construction and characterization of a humanized, internalizing, B-cell (CD22)-specific, leukemia/lymphoma antibody, LL2. Mol Immunol 1995; 32:1413-1427.
20. Karacay H, Sharkey RM, Gold DV, et al. Pretargeted radioimmunotherapy of pancreatic cancer xenografts: TF10-^{90}Y-IMP288 alone and combined with gemcitabine. J Nucl Med 2009; 50:2008-2016.
21. Fraker PJ, Speck JC, Jr. Protein and cell membrane iodinations with a sparingly soluble chloroamide, 1,3,4,6-tetrachloro-3a,6a-diphrenylglycoluril. Biochem Biophys Res Commun 1978; 80:849-857.
22. Lindmo T, Boven E, Cuttitta F, et al. Determination of the immunoreactive fraction of radiolabeled monoclonal antibodies by linear extrapolation to binding at infinite antigen excess. J Immunol Methods 1984; 72:77-89.
23. de Jong M, Breeman WA, Bakker WH, et al. Comparison of ^{111}In-labeled somatostatin analogues for tumor scintigraphy and radionuclide therapy. Cancer Res 1998; 58:437-441.
24. van Oosterhout YV, van den Herik-Oudijk IE, Wessels HM, et al. Effect of isotype on internalization and cytotoxicity of CD19-ricin A immunotoxins. Cancer Res 1994; 54:3527-3532.
25. Pirker R, FitzGerald DJ, Hamilton TC, et al. Characterization of immunotoxins active against ovarian cancer cell lines. J Clin Invest 1985; 76:1261-1267.
26. Carnahan J, Wang P, Kendall R, et al. Epratuzumab, a humanized monoclonal antibody targeting CD22: characterization of in vitro properties. Clin Cancer Res 2003; 9:3982S-3990S.
27. Shih LB, Lu HH, Xuan H, Goldenberg DM. Internalization and intracellular processing of an anti-B-cell lymphoma monoclonal antibody, LL2. Int J Cancer. 1994;56:538-545.
28. Ghetie V, Engert A, Schnell R, Vitetta ES. The in vivo anti-tumor activity of immunotoxins containing two versus one deglycosylated ricin A chains. Cancer Lett 1995; 98:97-101.
29. Newton DL, Hansen HJ, Mikulski SM, et al. Potent and specific antitumor effects of an anti-CD22-targeted cytotoxic ribonuclease: potential for the treatment of non-Hodgkin lymphoma. Blood 2001; 97:528-535.
30. Kreitman RJ, Pastan I. Immunotoxins in the treatment of hematologic malignancies. Curr Drug Targets 2006; 7:1301-1311.
31. Polson AG, Calemine-Fenaux J, Chan P, et al. Antibody-drug conjugates for the treatment of non-Hodgkin's lymphoma: target and linker-drug selection. Cancer Res. 2009;6 9:2358-2364.
32. Sharkey RM, Govindan SV, Cardillo TM, et al. Epratuzumab-SN-38: a new antibody-drug conjugate for the therapy of hematological malignancies. Mol Cancer Ther 2012; 11:224-234.
33. Pantelias A, Pagel JM, Hedin N, et al. Comparative biodistributions of pretargeted radioimmunoconjugates targeting CD20, CD22, and DR molecules on human B-cell lymphomas. Blood 2007; 109:4980-4987.
34. Sharkey RM, Karacay H, Johnson CR, et al. Pretargeted versus directly targeted radioimmunotherapy combined with anti-CD20 antibody consolidation therapy of non-Hodgkin lymphoma. J Nucl Med 2009; 50:444-453.

35. Chang CH, Gupta P, Michel R, et al. Ranpirnase (frog RNase) targeted with a humanized, internalizing, anti-TROP-2 antibody has potent cytotoxicity against diverse epithelial cancer cells. Mol Cancer Ther 2010; 9:2276-2286.
36. van Schaijk FG, Oosterwijk E, Molkenboer-Kuenen JD, et al. Pretargeting with bispecific anti-renal cell carcinoma x anti-DTPA(In) antibody in 3 RCC models. J Nucl Med 2005; 46:495-501.
37. Sharkey RM, Rossi EA, McBride WJ, et al. Recombinant bispecific monoclonal antibodies prepared by the dock-and-lock strategy for pretargeted radioimmunotherapy. Semin Nucl Med 2010; 40:190-203.
38. Schoffelen R, Boerman OC, van der Graff WT, et al. Phase I clinical study of the feasibility of pretargeted radioimmunotherapy (PT-RAIT) in patients with colorectal cancer (CRC): First results. J Nucl Med 2011; 52:107p.
39. Sharkey RM, Karacay H, Govindan SV, et al. Combination radioimmunotherapy and chemoimmunotherapy involving different or the same targets improves therapy of human pancreatic carcinoma xenograft models. Mol Cancer Ther 2011; 10:1072-1081.

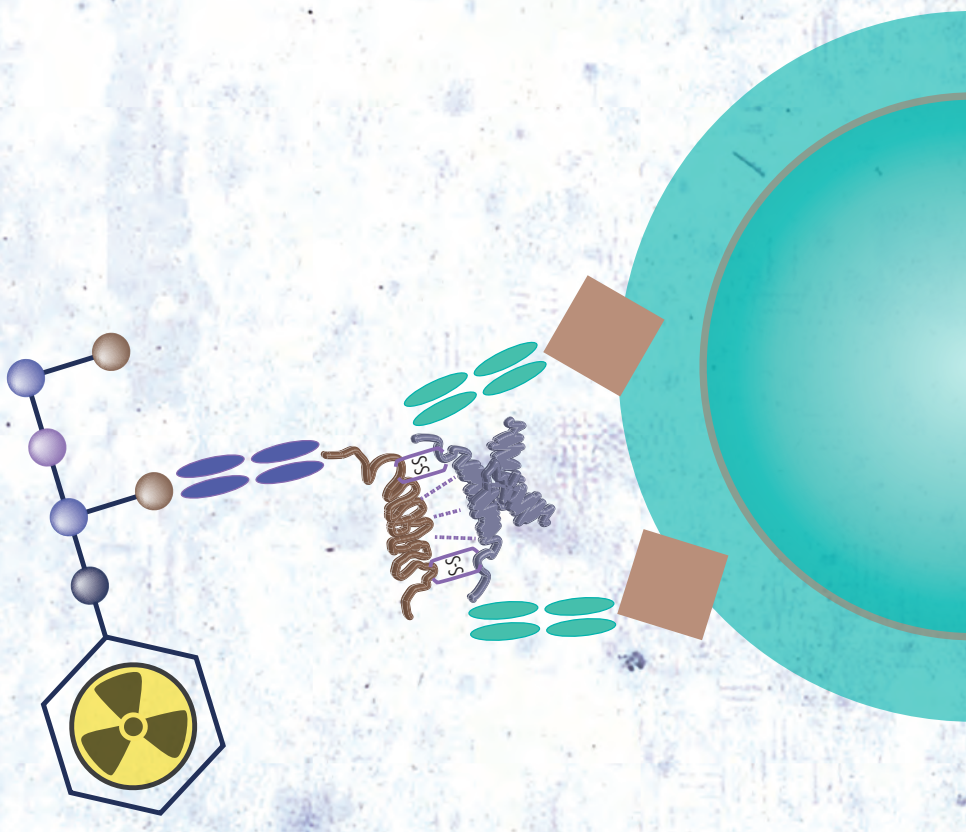

Pretargeted immunoPET and radioimmunotherapy of prostate cancer with an anti-TROP-2 x anti-HSG bispecific antibody

5

Catharina M. van Rij,
Susanne Lütje,
Cathelijne Frielink,
Robert M. Sharkey,
David M. Goldenberg,
Gerben M. Franssen,
William J. McBride,
Edmund A. Rossi,
Wim J.G. Oyen,
Otto C. Boerman

Eur J Nucl Med Mol Imaging 2013; 40(9):137-83.

Abstract

TF12 is a trivalent bispecific antibody that consists of two anti-TROP-2 Fab fragments and one anti-HSG (histamine-succinyl-glycine) Fab fragment. The TROP-2 antigen is found in many epithelial cancers, including prostate cancer (PC), and therefore this bispecific antibody could be suitable for pretargeting in this cancer. In this study, the characteristics and the potential for pretargeted radioimmunoimaging and radioimmunotherapy with TF12 and the radiolabeled di-HSG peptide IMP288 in mice with human PC were investigated.

Methods

The optimal TF12 protein dose, IMP288 peptide dose, and dose interval for prostate cancer targeting were assessed in nude mice with s.c. PC3 xenografts. ImmunoPET/CT was performed using TF12/^{68}Ga-IMP288 at optimized conditions. The potential of pretargeted radioimmunotherapy (PRIT) using the TF12 pretargeted ^{177}Lu-IMP288 was determined.

Results

TF12 and ^{111}In-IMP288 showed high and fast accumulation in the tumor (20.4 ± 0.6% ID/g at 1 h p.i.) at optimized conditions, despite the internalizing properties of TF12. The potential for PRIT was shown by retention of fifty percent of the ^{111}In-IMP288 in the tumor at 48 h p.i. One cycle of treatment with TF12 and ^{177}Lu-IMP288 showed significant improvement of survival compared to treatment with ^{177}Lu-IMP288 alone (90 *vs* 67 days, P <0.0001) with no renal or hematologic toxicity.

Conclusion

TROP-2-expressing prostate cancer can be pretargeted efficiently with TF12, with very rapid uptake of the radiolabeled hapten-peptide, IMP288, sensitive immunoPET, and effective therapy.

Introduction

Prostate cancer (PC) causes significant morbidity, and still is the second leading cause of cancer-related deaths in men in the Western world. Approximately 17% of American men will be diagnosed with PC during their lifetime, and 20% of them will die of the disease. While curable when diagnosed in an early stage and treatable in the hormone-dependent stage, PC treatment options are limited in advanced stages. In view of this, it is essential to differentiate between metastatic and non-metastatic disease to predict disease outcome and to determine treatment options. Furthermore, an accurate imaging method for determining the location, extent and biological potential of PC could improve patient outcome by directing therapy more accurately both in surgery and radiation therapy. Trans Rectal Ultrasound (TRUS) and conventional Magnetic Resonance Imaging (MRI) are rather effective for diagnosis of the primary tumor, but adequate detection of metastatic spread leaves room for further improvement. Positron Emission Tomography (PET) imaging is a widely used imaging modality to detect metastatic disease in several cancers. However, ^{18}F-FDG-PET is not suited for staging patients with PC, since sensitivity is low due to artifacts related to its renal excretion and due to the relatively low avidity of differentiated prostate cancer for ^{18}F-FDG [1, 2]. Several other radiotracers have been developed for imaging metastasized PC, but all of them have disadvantages, such as low sensitivity or practical considerations, such as the need for an on-site cyclotron for the ^{11}C-tracers. Antibody imaging in humans has been reported with several radiolabeled monoclonal antibodies, such as 7E11-C53 (Prostascint®, capromab pendetide) and J591 [2]. Due to the long circulatory half-lives of imaging agents based on intact antibody molecules, lesions can only be depicted several days after injection.

hRS7 is a humanized IgG1 monoclonal antibody directed against TROP-2, also known as EGP-1 (epithelial glycoprotein-1), GA733-1, gp50/T16, TACSTD2 (tumor-associated calcium signal transducer 2). TROP-2 is a 46 kDa transmembrane glycoprotein expressed in carcinomas of the lung, bladder, breast, cervix, ovary, stomach and prostate [3]. Most normal human tissues do not express TROP-2, but it is found at low levels in several normal glandular cells, including glands in the bronchus, breast, prostate and skin, and ducts and acini of the pancreas [4]. Given its expression in prostate cancer, we studied the potential targeting ability of hRS7 IgG in a nude mouse-human prostate cancer model [5], showing excellent in vivo targeting of PC3 xenografts with ^{89}Zr- and ^{111}In-hRS7 IgG within 3 days. The slow clearance from the circulation results in low tumor-to-background ratios at earlier time points after i.v. injection. For earlier imaging, we explored a pretargeting approach using the bispecific monoclonal antibody (bsAb) TF12, a trivalent bsAb that consists of two anti-TROP-2 Fab fragments and one anti-HSG (histamine-succinyl-glycine) Fab fragment [6]. In pretargeting, unlabeled TF12 is injected intravenously, and when it has cleared from the blood, an HSG-substituted

radiolabeled hapten-peptide is injected. This hapten-peptide will be trapped in the tumor by the anti-HSG arm of the bsAb or is rapidly cleared from the body.
In this study, the characteristics and the potential for pretargeted radioimmunoimaging and radioimmunotherapy with TF12 and the radiolabeled di-HSG peptide, IMP288, in mice with human PC xenografts were investigated.

Materials and methods

The anti-TROP-2 x anti-HSG bsAb TF12 was produced using the Dock-and-Lock technology (DNL®) as described previously [7]. The production and characterization of the anti-TROP-2 mAb hRS7 have been described previously [3].The DOTA-conjugated hapten-peptide IMP288 (DOTA-D-Tyr-D-Lys(HSG)-D-Glu-D-Lys(HSG)-NH_2) was prepared as described by McBride et al. [8].

Cell culture

The human prostate cancer cell line, PC3, is an androgen-independent cell line, originally derived from a PC bone metastasis. Cells were obtained from ATCC (CRL 1435; Manassas, VA) and were grown in RPMI 1640 medium (GIBCO®, Life Technologies Corporation, Carlsbad, CA, USA), supplemented with 10% FCS (fetal calf serum, Life Technologies, Grand Island, NY). Before subcutaneous inoculation of mice to induce PC3 xenografts, tumor cells were washed with 0.9% NaCl, disaggregated with trypsin and resuspended in 67% complete RPMI 1640 medium and 33% Matrigel (BD Biosciences, San Jose, CA) to the appropriate concentration (3 x 10^6 cells/200 µL).

Mouse model

All experiments were approved by the institutional Animal Welfare Committee of the Radboud University Medical Center (Nijmegen, The Netherlands), and were conducted in accordance with the principles set forth by the Revised Dutch Act on Animal Experimentation.
Male BALB/*c* nude mice (Janvier SAS, Le Genest Saint Isle, France), 8–9 weeks old, were adapted to laboratory conditions for at least one week before experimental use. They were housed under non-sterile standard conditions in filter-topped cages (5 mice per cage), with free access to animal chow (Sniff Voer®) and water.
The mice were inoculated s.c. in the flank with 200 µL of PC3 cell suspension (3 x 10^6 cells). The s.c. PC3 tumors grew to approximately 0.1 g in 10 days after tumor cell inoculation, as determined by caliper measurements in 3 dimensions using the formula $V = 4/3\pi$ (length/2 x width/2 x height/2), assuming that the density of tumor tissue is 1 g/cm^3. The radiolabeled preparations (0.2 mL) were injected intravenously.

Radiolabeling of IMP288 and hRS7

The DOTA-conjugated IMP288 was radiolabeled with ^{111}In (Covidien, Petten, The Netherlands), ^{177}Lu (IDB Holland BV, The Netherlands), or with ^{68}Ga from a TiO_2-based ^{68}Ge/^{68}Ga generator (Cyclotron Co, Ltd., Obninsk, Russian Federation). Radiolabeling was performed essentially as described previously by Schoffelen et al. [9]. For ^{68}Ga-labeling, 84 MBq of $^{68}GaCl_3$ was added to 1 µg of IMP288 in 1 M HEPES buffer (50 µL, 4-(2-hydroxyethyl)-1-piperazineethanesulfonic acid, Sigma-Aldrich, USA). After incubation at 95°C for 20 minutes, 50 mM ethylenediaminetetraacetic acid (EDTA, Sigma-Aldrich, St. Louis, MO, USA) was added to a final concentration of 1 µM. The ^{68}Ga-IMP288 preparation was purified on an Oasis® HLB cartridge (Waters, Milford, MA, USA) and eluted with 1 mL of 25% ethanol essentially as described previously [10]. Before i.v. injection, the preparation was diluted at least 2.5 times with 0.5% bovine serum albumin (BSA, Sigma-Aldrich) in PBS.

DTPA conjugation and subsequent labeling of hRS7 IgG with ^{177}Lu were performed essentially as described previously [3, 5]. The radiochemical purity of the labeled IMP288 preparations was determined using instant thin-layer chromatography (ITLC) and reversed-phase high-performance liquid chromatography (RP-HPLC), as described previously [9]. ITLC was performed to determine the fraction of unbound ^{111}In, ^{177}Lu, or ^{68}Ga (mobile phase 1:1 0.1 M ammonium acetate (Merck, Darmstadt, Germany) and 0.1 M EDTA), and the fraction of colloid (mobile phase 1:1 methanol (Merck) and 0.25 M ammonium acetate, pH 5.5).

For RP-HPLC, the C_{18} column (Zorbax Rx-C18; 5 µm, 4.6 × 250 mm; Agilent Technologies, Amstelveen, The Netherlands) was eluted with a mixture of 97% of a 0.1% trifluoroacetic acid in H_2O solution (TFA, Lab-scan, Analytical Sciences, Brussels, Belgium) with 3% of a 0.1% TFA in acetonitrile solution (Lab-scan, Analytical Sciences, Brussels, Belgium) with a linear gradient to 100% of the latter solution over 10 minutes at a flow rate of 1 mL/min. Radiochemical purity (RCP) of all labeled IMP288 preparations always exceeded 97%; the RCP of ^{177}Lu-hRS7 exceeded 98%.

Radiolabeling of TF12

The bsAb TF12 was radioiodinated with ^{125}I according to the iodogen method [11]. Twenty µg of TF12 and 3.7 MBq Na^{125}I (GE Healthcare Europe, Den Bosch, The Netherlands) in 50 mmol/L phosphate buffer, pH 7.4, were incubated in an Eppendorf vial coated with 50 µg of iodogen (1,3,4,6-tetrachloro-3,6-diphenylglycoluril; Pierce Biotechnology, Inc.) for 10 minutes at room temperature. ^{125}I-TF12 was purified on a PD-10 column (GE Healthcare, London, UK) eluted with PBS, 0.5% BSA.

Immunoreactivity

The anti-TROP-2 reactivity of radiolabeled TF12 and hRS7 was determined using freshly trypsinized PC3 cells, as described by Lindmo et al. [12] with minor modifications. The bispecific immunoreactivity of TF12 was demonstrated by incubating PC3 cells with TF12 (10 µg/mL) and subsequent incubation with ^{111}In-IMP288 (200 Bq/ml). After 1 h at 37°C, the total activity and activity in the cell pellet were determined in a γ-counter. More than 70% of the added hapten-peptide specifically bound to the PC3 cells.

Biodistribution studies

The effect of the TF12 dose on tumor uptake of a fixed amount (0.25 nmol = 400 ng) ^{111}In-labeled IMP288 in mice with s.c. PC3 tumors was determined by administering 1.25, 2.5, 5.0 or 12.5 nmol (231, 462, 924 or 2310 µg) of TF12 i.v., and then 16 hours later 0.4 MBq of ^{111}In-IMP288 was injected. Two hours later, mice were dissected and tissue uptake determined (5 mice/group).
Subsequently, the optimal amount of IMP288 that can be given after administering a fixed dose of TF12 (2.5 nmol = 462 µg) was determined. Four doses of IMP288 were examined: 25, 50, 100 and 200 nmol, each given 16 h after TF12. Two hours after injection of 0.4 MBq of ^{111}In-IMP288, mice were euthanized and necropsied (5 mice/group). The optimal interval between TF12 and ^{111}In-IMP288 injection was assessed at the pre-selected optimal TF12 (2.5 nmol) and IMP288 doses (0.1 nmol). The following intervals were tested: 12, 14, 18, 20, 24 and 36 h. Lastly, under optimized conditions (2.5 nmol TF12, 0.1 nmol IMP288, 16-h interval), the retention of ^{111}In-IMP288 in the tumor was monitored over the course of 3 days.

Pretargeted immunoPET

Groups of 5 mice with s.c. PC3 tumors were injected i.v. with 2.5 nmol of TF12 and 16 h later with 5 ± 2 MBq (0.1 nmol) of ^{68}Ga-IMP288. One hour after injection of ^{68}Ga-IMP288, mice were euthanized by O_2/CO_2 asphyxiation and PET/CT images were acquired with an Inveon® animal PET/CT scanner (Siemens Preclinical Solutions, Siemens Healthcare Molecular Imaging, Knoxville, TN, USA), having an intrinsic spatial resolution of 1.5 mm. The animals were placed in a prone position. PET emission scans were acquired for 20 min, preceded by CT scans for anatomic reference (spatial resolution, 113 µm; 80 kV; 500 µA; exposure time, 300 ms). Scans were reconstructed using Inveon Acquisition Workplace software (version 1.2; Siemens Preclinical Solutions), with an ordered set expectation maximization-3D/maximum a posteriori (OSEM3D/MAP) algorithm with the following parameters: matrix 256 x 256 x 159, pixel size 0.43 x 0.43 x 0.8 mm^3 and a beta-value of 0.1. After imaging,

tumors and organs were dissected, weighed and counted in a gamma counter to determine biodistribution of the radiolabel. The percent-injected dose per gram (% ID/g) tissue was calculated against an injection standard.

Pretargeted radioimmunotherapy

The potential of pretargeted radioimmunotherapy (PRIT) with TF12 and ^{177}Lu-IMP288 was assessed in a therapy experiment in mice with PC3 xenografts (10 mice/group). Mice were treated with TF12/^{177}Lu-IMP288 or ^{177}Lu-hRS7 IgG 9 days after PC3 cell inoculation, when tumors weighed approximately 0.1 g.
In the mice that were treated with PRIT, tumors were pretargeted with 2.5 nmol TF12 16 h before administration of the ^{177}Lu-IMP288. The next day, mice received the maximum ^{177}Lu activity dose that could be labeled to 0.1 nmol IMP288 (13.7 MBq). Another group was treated with the maximum tolerable dose of ^{177}Lu-hRS7 (11.1 MBq, 13.8 µg). One control group of PC3 tumor-bearing mice was injected i.v. with vehicle (200 µL PBS, 0.5% BSA) twice instead of TF12 and IMP288. The other control group received vehicle instead of TF12 and was injected 16 h later with 13.7 MBq of ^{177}Lu-IMP288. Tumor size was measured in three dimensions with a caliper and body weight was determined twice weekly starting 7 days after tumor cell inoculation. Blood samples of 0.1 mL of all mice were collected via submandibular bleeding before therapy, and 14, 21, 35, 42, 56, 70 and 88 days after administration of the agents to determine hemoglobin levels, and leukocyte and platelet counts. Blood creatinine and BUN levels were determined before and 4 and 7 weeks after start of the therapy. When the humane endpoint was reached (tumor size >2 cm^3 or animal discomfort level >3), mice were euthanized by O_2/CO_2-asphyxiation and dissected. At dissection, the tumor and kidneys were excised and weighed. The experiment was terminated 120 days after injection of the radiolabeled compounds and the remaining mice were euthanized and dissected.

Statistical analysis

Statistical analysis was performed using GraphPad Prism version 5.00 for Windows® Survival curves were compared using the log-rank test. The level of significance was set at a *P*-value of less than 0.05.

Results

Biodistribution studies

The optimal TF12 protein dose to pretarget the PC3 tumors was determined in a protein dose escalation study. Tumor uptake of ^{111}In-IMP288 (0.25 nmol) 2 h after injection increased with increasing bsAb TF12 protein doses, as summarized in Figure 1A. Highest uptake (7.5% ID/g) was obtained when the tumor was pretargeted by injection of 12.5 nmol of TF12. The optimal amount of TF12 was determined to be 2.5 nmol, since there was only minor improvement of tumor uptake (1.5-fold increase) at the highest bsAb dose (5-fold increase) .

Following injection of increasing amounts of IMP288 at a fixed TF12 dose of 2.5 nmol, tumor uptake clearly decreased (Figure 1B). Optimal uptake in the tumor (20-25% ID/g) was obtained at hapten-peptide doses ≤0.1 nmol IMP288. Based on these results, 0.1 nmol of IMP288 was used in further experiments, since this amount of IMP288 could be labeled with activity doses required for pretargeted immunoPET imaging (^{68}Ga) and for pretargeted radionuclide therapy (^{177}Lu).

Recently, in vitro experiments have shown that TF12 is slowly internalized by the tumor cell after binding to TROP-2 [6]. To estimate the kinetics of internalization of TF12 in vivo,

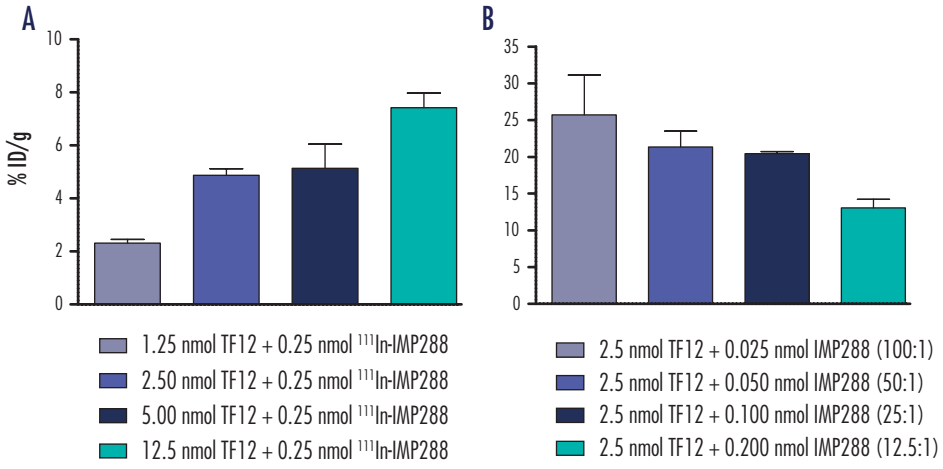

Figure 1A. Biodistribution of a fixed dose of ^{111}In-IMP288 (0.25 nmol, 0.4 MBq) injected intravenously 16 h after injection of escalating TF12 doses (1.25-12.5 nmol) in BALB/*c* nude mice with a subcutaneous PC3 xenograft at 2 h after injection (n=5).

Figure 1B. Biodistribution of escalating ^{111}In-IMP288 doses (0.025-0.2 nmol, 0.4 MBq) injected i.v. 16 h after a fixed dose of TF12 (2.5 nmol) in BALB/*c* nude mice with a subcutaneous PC3 xenograft at 2 h days after injection (n=5).

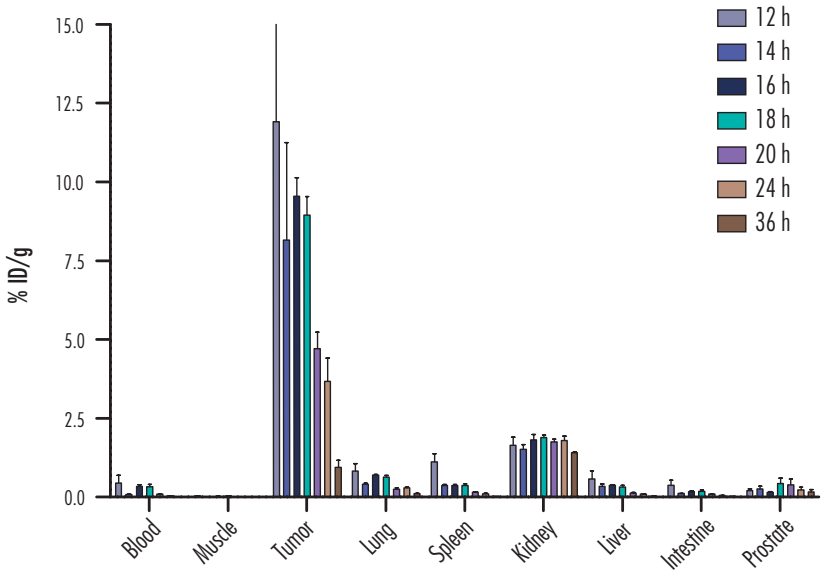

Figure 2. Biodistribution of ^{111}In-IMP288 (0.1 nmol, 0.4 MBq) in BALB/*c* nude mice with a subcutaneous PC3 xenograft measured 2 h after injection (n=3-5). Mice were pre-injected i.v. with 2.5 nmol of TF12 at increasing time interval before injection of ^{111}In-IMP288 (12, 14, 16, 18, 20, 24, and 36 h).

the biodistribution of bsAb TF12 labeled with ^{111}In and ^{125}I was studied in mice with s.c. PC3 tumors 16 h p.i. A clear and significant difference between uptake of ^{111}In-TF12 (4.9 ± 0.6% ID/g) and ^{125}I-TF12 (0.7 ± 0.2% ID/g, P<0.0001) in the tumor was observed 16 h after injection of the radiolabeled TF12, which could be explained by the internalizing characteristics of TF12. The biodistribution of the ^{111}In-labeled TF12 indicated that the bsAb accumulated preferentially in the tumor (4.9 ± 0.6% ID/g, 16 h p.i.), while the blood level at that time did not exceed 0.4 ± 0.1% ID/g. The optimal interval between injection of TF12 and ^{111}In-IMP288 was assessed by examining seven intervals: 12, 14, 16, 18, 20, 24 and 36 hours (3-5 mice/group, Figure 2). Extension of the time interval between injection of TF12 and injection of ^{111}In-IMP288 from 16 to 36 hours significantly decreased tumor uptake of the radiolabeled hapten, from 9.6 ± 1.3% ID/g to 1.0 ± 0.5% ID/g (P<0.0001). Shortening the interval from 16 to 14 or 12 h did not improve tumor uptake significantly (P=0.81 and P=0.14, respectively), while tumor-to-blood ratios where lower at the shorter intervals. Based on these observations an interval of 16 h between injection of TF12 and radiolabeled IMP288 was used.

Retention of radiolabeled IMP288 in the tumor over time is particularly important in pretargeted radioimmunotherapy. Retention was determined at the optimal TF12 and ^{111}In-IMP288 dose (16-h interval) during 3 days p.i. (5 mice/group). Figure 3

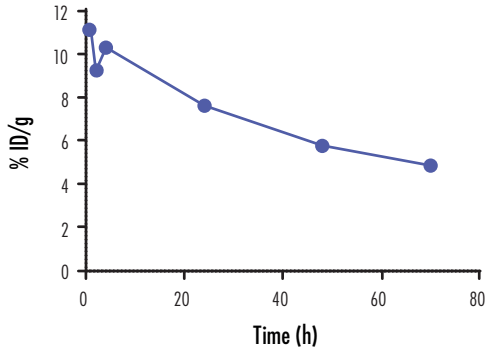

Figure 3. Tumor uptake at increasing time points (1, 2, 4, 24, 48, 70 h) after injection of TF12/^{111}In-IMP288 (2.5 nmol/0.1 nmol, 0.4 MBq, 16-h interval, n=5).

shows that >50% of the ^{111}In-label was still present in the tumor at 48 h after injection (5.8 ± 0.7% ID/g, t½ = 50 h).

At the optimized conditions determined in the experiments described above, ^{111}In-IMP288 showed a rapid and high uptake in the tumor (20.4 ± 0.6% ID/g, 2 h p.i.) while concentrations in blood (0.9 ± 0.2% ID/g) and normal tissues were low (Figure 4). ^{111}In-IMP288 cleared very rapidly from the blood via the kidneys. The kidneys were the normal organs with the highest uptake (2.2 ± 0.1% ID/g).

Pretargeted immunoPET

With the same dosing schedule, similar results were obtained with TF12 and ^{68}Ga-IMP288, with slightly lower tumor uptake (12.2 ± 2.3% ID/g). To determine the potential of pretargeted immunoPET to detect TROP-2-expressing tumors, microPET imaging of ^{68}Ga-IMP288 was performed in nude mice with s.c. PC3 tumors of

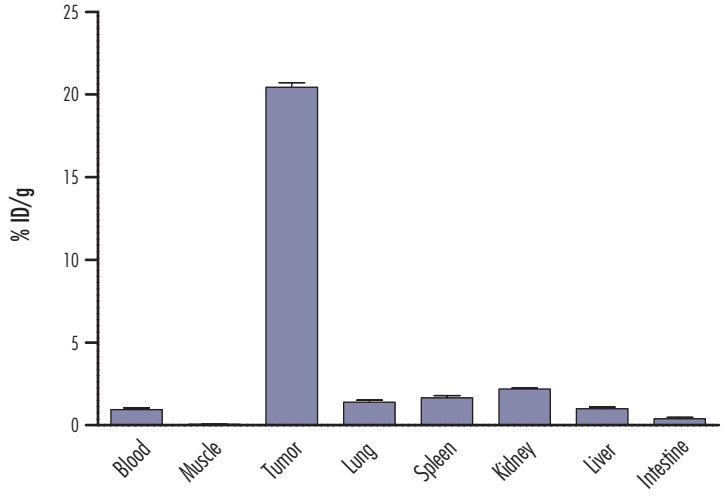

Figure 4. Biodistribution of ^{111}In-IMP288 (0.1 nmol, 0.4 MBq) injected i.v. 16 h after i.v. injection of TF12 (2.5 nmol) in BALB/*c* nude mice with a subcutaneous PC3 xenograft at 2 h after injection (n=5).

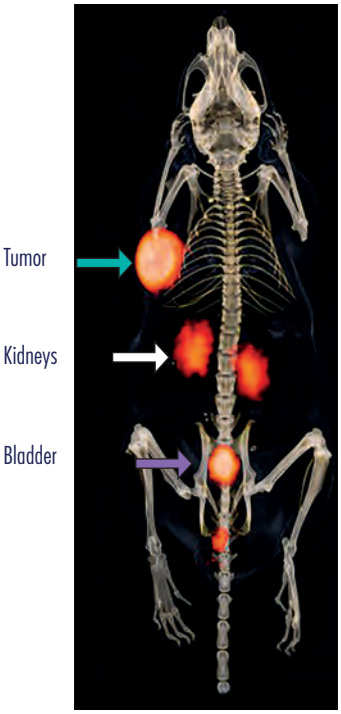

Figure 5. Anterior 3D volume-rendering projection of a microPET/CT scan of a BALB/*c* nude mouse with a subcutaneous PC3 tumor on the shoulder injected with TF12 and ^{68}Ga-IMP288 (0.1 nmol, 5 MBq) acquired 1 h after injection.

approximately 0.1 g. Images acquired as early as 1 h p.i. clearly showed the PC3 tumors (Figure 5). No accumulation of radioactivity in the other normal organs was observed, except for the kidneys and the bladder.

Pretargeted radioimmunotherapy

The potential of PRIT using the bsAb TF12 and ^{177}Lu-labeled IMP288 was determined in a therapy experiment and compared to RIT with ^{177}Lu-hRS7 (11.1 MBq, 13.8 µg). PRIT with 2.5 nmol TF12 and 13.7 MBq ^{177}Lu-IMP288 significantly improved the median survival of mice with s.c. PC3 tumors from 67 days to 90 days (P<0.0001, Figure 6). The control groups received either ^{177}Lu-IMP288 without TF12 or vehicle. Median survival of the mice in both control groups was similar, indicating that there is no effect of administration of a high activity dose of ^{177}Lu-IMP288 alone. At the end of the experiment (120 d), all mice treated with ^{177}Lu-hRS7 IgG were still alive.

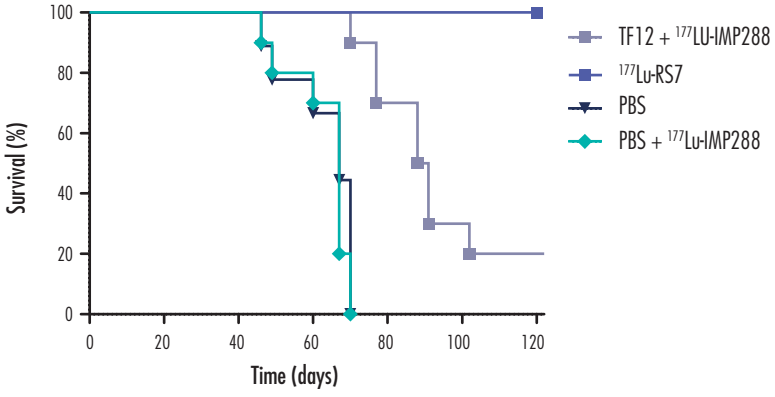

Figure 6. Survival of BALB/*c* nude mice with a subcutaneous PC3 xenograft treated with TF12/^{177}Lu-IMP288 (2.5 nmol/11.1 MBq, 0.1 nmol), ^{177}Lu-hRS7 (13.7 MBq, 30 µg), ^{177}Lu-IMP288 without pretargeting (11.1 MBq, 0.1 nmol) or vehicle (n=10).

However, this increase in survival (median survival >120 d) was accompanied by a significant decrease in platelets (from 1110 ± 230 x 10^9/L at t= -3 d to 430 ± 250 x 10^9/L at t= 14 d, *P*=0.0005) and leukocytes (from 3.2 ± 0.8 x 10^9/L at t= -3 d to 0.6 ± 0.3 x 10^9/L at t= 14 d, *P*<0.0001), which was not observed in the mice treated with PRIT. Thus, treatment with ^{177}Lu-hRS7 IgG appeared to be more effective, but also clearly more toxic.
In PRIT, the kidney could also be the organ at risk. Therefore, creatinine and urea levels were examined in the experimental groups and the kidneys were examined histologically after completion of the experiment (120 d). Creatinine and urea levels, and histologic analysis of the kidneys compared to age-matched control mice, did not show any indication of renal toxicity.

Discussion

The present study shows the potential of pretargeted immunoPET and PRIT of PC with the bsAb TF12 and the radiolabeled hapten peptide IMP288. The dose optimization studies in mice with s.c. PC3 tumors revealed that the highest uptake of the radiolabeled hapten peptide in the tumor was obtained at bsAb doses ≥2.5 nmol, and at lower IMP288 doses (≤0.1 nmol). The optimal time interval between injection of TF12 and ^{111}In-IMP288 was 16 h. Most importantly, these experiments showed that internalization does not disqualify bsAbs for pretargeting as long as the dosage interval is carefully tuned, as shown previously by Sharkey et al. [6]. Retention of the radiolabel in the tumor was high: more than 50% of the radiolabel that was present in the tumor at 1 h p.i. was still present after 48 h. In the TF2/IMP288 pretargeting system using the non-internalizing anti-CEA x anti-HSG bsAb in mice with LS174T tumors only 32% of the radiolabeled IMP288 was retained in the tumor [9], suggesting that the internalizing characteristics of TF12 could cause better retention of the radiolabel in the tumor due to internalization of the TF12-IMP288 complex by the tumor cells.
Retention in the tumor and rapid clearance from the blood enabled clear visualization of the tumor with PET as early as 1 h after injection. Some ^{68}Ga activity in the kidneys and bladder was observed, due to the renal clearance of IMP288. Renal clearance might be a disadvantage when imaging PC, since physiological uptake in the urinary tract might conceal pathological uptake in the lower abdomen. However, renal clearance of radiolabeled IMP288 is very efficient, which may enable the distinction between physiological and pathological uptake.

The pretargeted RIT experiment showed that TF12/^{177}Lu-IMP288 significantly improved the median survival of mice with s.c. PC3 tumors without significant hematological or renal toxicity. The improved median survival in the group of mice treated with ^{177}Lu-hRS7 IgG was achieved at the expense of severe hematological toxicity. In the

therapy experiments, the maximum activity dose of ^{177}Lu-IMP288 was used, which necessarily was below the maximum tolerated dose (MTD), due to the limited specific activity of the ^{177}Lu-chloride used for labeling of the peptide. Currently, carrier free ^{177}Lu-chloride has become available with improved specific activity. In future studies, we will determine the safety and efficacy of PRIT with higher activity doses of ^{177}Lu-IMP288 and of multiple cycles of TF12/^{177}Lu/^{90}Y-IMP288, as accomplished by Schoffelen et al with anti-CEA x anti-HSG bsAb TF2 [13].

Conclusion

The dosing of the pretargeting agents TF12 and IMP288 was optimized in mice with s.c. PC3 tumors. At optimized conditions, TROP-2-expressing PC3 tumors could be targeted efficiently and very rapidly with the radiolabeled hapten peptide IMP288. This pretargeting system allows rapid and sensitive PET imaging of PC using ^{68}Ga-labeled hapten peptide. TF12 in concert with ^{177}Lu-labeled IMP288 could also be a promising candidate for pretargeted radioimmunotherapy of TROP-2-expressing prostate tumors. Further PRIT studies at MTD with higher activity doses and/or multiple dosing are necessary to determine its application in the future.

Acknowledgements

We kindly thank Bianca Lemmers and Kitty Lemmens (Central Animal Facility, Radboud University Nijmegen Medical Centre, The Netherlands) for their excellent technical assistance in the animal experiments. The work was supported by the Dutch Cancer Society (KWF Kankerbestrijding, Grant KUN-2010-0480).

Disclaimer

David M. Goldenberg, William J. McBride, Robert M. Sharkey, and Edmund Rossi have financial interest as employment and/or stock interest in Immunomedics, Inc., or IBC Pharmaceuticals, Inc.

References

1. Beheshti M, Langsteger W, Fogelman I. Prostate Cancer: Role of SPECT and PET in Imaging Bone Metastases. Seminars in Nuclear Medicine 2009; 39(6):396-407.
2. Ravizzini G, Turkbey B, Kurdziel K, et al. New horizons in prostate cancer imaging. Eur J Radiol 2009; 70(2):212-226.
3. Basu A, Goldenberg DM, Stein R. The epithelial/carcinoma antigen EGP-1, recognized by monoclonal antibody RS7-3G11, is phosphorylated on serine 303. Int J Cancer 1995; 62(4):472-479.
4. Stein R, Basu A, Chen S, et al. Specificity and properties of MAb RS7-3G11 and the antigen defined by this pancarcinoma monoclonal antibody. Int J Cancer 1993; 55(6):938-946.
5. van Rij CM, Sharkey RM, Goldenberg DM et al. Imaging of prostate cancer with immunoPET and immunoSPECT using a radiolabeled anti-EGP-1 monoclonal antibody. J Nucl Med 2011; 52(10):1601-1607.
6. Sharkey RM, van Rij CM, Karacay H et al. A new tri-Fab bispecific antibody for pretargeting trop-2-expressing epithelial cancers. J Nucl Med 2012; 53(10):1625-1632.
7. Rossi EA, Goldenberg DM, Cardillo TM, et al. Stably tethered multifunctional structures of defined composition made by the dock and lock method for use in cancer targeting. Proc Natl Acad Sci USA 2006; 103(18):6841-6846.
8. McBride WJ, Zanzonico P, Sharkey RM et al. Bispecific Antibody Pretargeting PET (ImmunoPET) with an ^{124}I-Labeled Hapten-Peptide. J Nucl Med 2006; 47(10):1678-1688.
9. Schoffelen R, Sharkey RM, Goldenberg DM et al. Pretargeted immuno-positron emission tomography imaging of carcinoembryonic antigen-expressing tumors with a bispecific antibody and a ^{68}Ga- and ^{18}F-labeled hapten peptide in mice with human tumor xenografts. Mol Cancer Ther 2010; 9(4):1019-1027.
10. Brom M, Joosten L, Oyen WJG, et al. Improved labelling of DTPA- and DOTA-conjugated peptides and antibodies with ^{111}In in HEPES and MES buffer. EJNMMI Res 2012; 2:4.
11. Fraker PJ, Speck JC, Jr. Protein and cell membrane iodinations with a sparingly soluble chloroamide, 1,3,4,6-tetrachloro-3a,6a-diphrenylglycoluril. Biochem Biophys Res Commun 1978; 80(4):849-857.
12. Lindmo T, Boven E, Cuttitta F, et al. Determination of the immunoreactive fraction of radiolabeled monoclonal antibodies by linear extrapolation to binding at infinite antigen excess. J Immunol Methods 1984; 72(1):77-89.
13. Schoffelen R, van der Graaf WT, Franssen G et al. Pretargeted ^{177}Lu radioimmunotherapy of carcinoembryonic antigen-expressing human colonic tumors in mice. J Nucl Med 2010; 51(11):1780-1787.

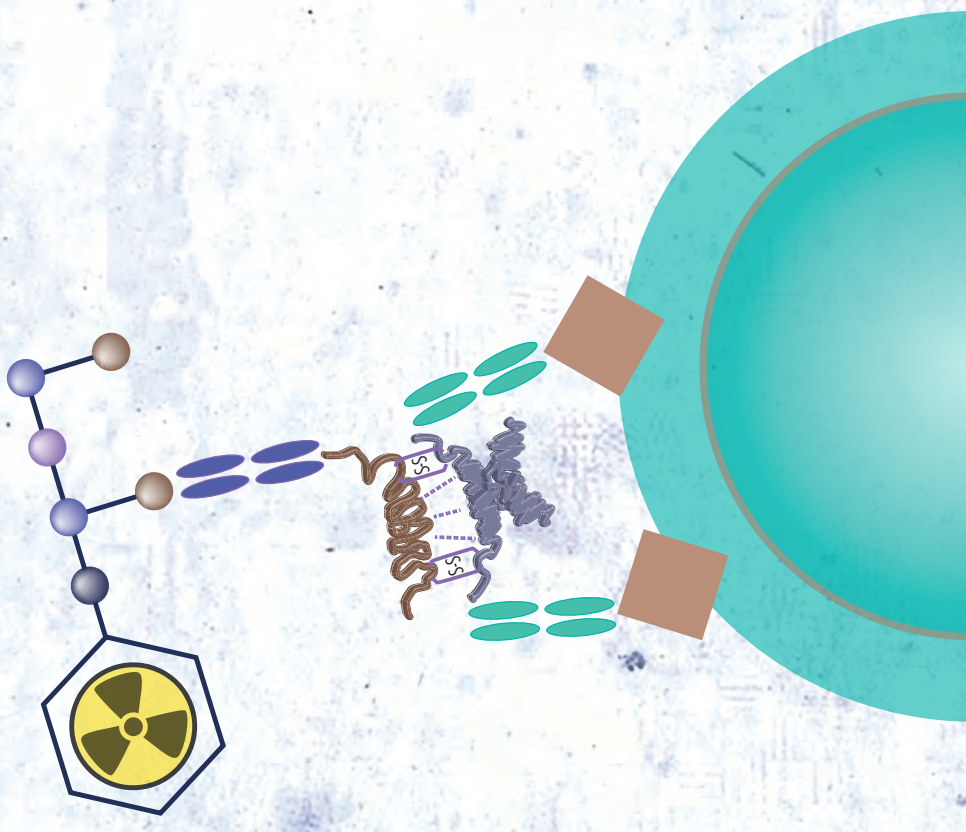

Pretargeted immunoPET of prostate cancer with an anti-TROP-2 x anti-HSG bispecific antibody in mice with PC3 xenografts

6

Catharina M. van Rij,
Cathelijne Frielink,
David M. Goldenberg,
Robert M. Sharkey,
Gerben M. Franssen,
Susanne Lütje,
William J. McBride,
Wim J.G. Oyen,
Otto C. Boerman

Mol Imaging Biol 2015; 17:94-101

Abstract

Purpose

Pretargeting with bispecific antibodies and radiolabeled hapten-peptides could be used to specifically target tumors with high target-to-background ratios. TF12 is a trivalent bispecific antibody that consists of two anti-TROP-2 Fab fragments and one anti-HSG (histamine-succinyl-glycine) Fab fragment. The TROP-2 antigen is expressed in many epithelial cancers, including prostate cancer (PC), and therefore this bispecific antibody can be used for pretargeting of PC. In this study, the potential for pretargeted radioimmunoPET with TF12 and the ^{68}Ga-labeled di-HSG peptide IMP288 in mice with human PC xenografts was investigated using 2-deoxy-2-^{18}F-fluorodeoxyglucose (^{18}F-FDG) as a reference.

Procedures

The potential of pretargeted immunoPET with TF12 and the ^{68}Ga-labeled di-HSG hapten peptide, IMP288, was studied in mice with subcutaneous PC3 tumors using ^{18}F-FDG as a reference. Furthermore, the use of this pretargeting system for imaging PC lesions was evaluated in mice with intraperitoneally growing tumors with ^{18}F-FDG as a reference.

Results

^{68}Ga-IMP288 showed rapid accumulation in the TF12 pretargeted subcutaneous tumor (7.2 ± 1.1% ID/g) with low uptake in the kidneys (1.8 ± 0.5% ID/g) and high tumor-to-blood ratios (17.4 ± 11.2) at 1 h p.i. Accumulation of ^{18}F-FDG in the s.c. tumors was significantly lower (3.4 ± 0.9% ID/g, P=0.008), with lower tumor-to-blood ratios (3.0 ± 1.9, P=0.011). ImmunoPET/CT images clearly visualized both subcutaneous and intraperitoneal tumors as small as 5 mm^3 with low blood levels and kidney uptake as early as 1 h p.i.

Conclusion

Pretargeted immunoPET with TF12 in combination with a ^{68}Ga-labeled hapten peptide is an efficient system for rapid, sensitive and specific imaging of prostate cancer.

Introduction

In most cancers, it is essential to differentiate between metastatic and non-metastatic disease to predict disease outcome and to determine treatment options. Especially in prostate cancer (PC), an accurate imaging method to determine the location, extent and biological potential of PC could improve patient outcome by fine-tuning the treatment based on the characteristics of the tumor both in surgery and during radiation therapy. Trans-rectal ultrasound (TRUS) and conventional magnetic resonance imaging (MRI) are effective for diagnosis of the primary tumor, but adequate detection of metastatic spread needs further improvement [1, 2, 3]. Positron emission tomography (PET) imaging is a widely used imaging modality to detect metastatic disease in several cancers. However, ^{18}F-FDG-PET is not suited for staging patients with PC, since sensitivity is low due to artifacts related to its renal excretion and due to the relatively low avidity of differentiated prostate cancer for 2-deoxy-2-^{18}F-fluorodeoxyglucose (^{18}F-FDG) [2, 4]. Several other radiotracers have been developed for imaging metastatic PC, such as radiolabeled bombesin-analogues (targeting the gastrin-releasing peptide receptor), ^{11}C- and ^{18}F-choline and ^{11}C-acetate, each with specific advantages and limitations [5]. A new class of promising tracers currently under clinical development are radiolabeled PSMA-ligands targeting prostate specific membrane antigen (PSMA) expressed on the vast majority of PC, such as ^{99m}Tc-MIP1404 [6] and ^{68}Ga-HBED-CC-PSMA [7]. The first clinical studies indicate that this tracer may have considerable advantages in detecting PC lesions, even in patients with low PSA levels.

Antibody imaging in humans has been reported with several radiolabeled monoclonal antibodies (mAbs), such as capromab pendetide (Prostascint®) and J591 [2]. Due to the long circulatory half-lives of imaging agents based on intact antibody molecules, lesions can only be depicted several days after injection.

For more rapid imaging, we developed a pretargeting approach using the bispecific monoclonal antibody (bsAb) TF12, a trivalent bsAb that consists of two anti-TROP-2 Fab fragments and one anti-HSG (histamine-succinyl-glycine) Fab fragment [8]. The target antigen TROP-2, also known as EGP-1 (epithelial glycoprotein-1), GA733-1, gp50/T16 and TACSTD2 (tumor-associated calcium signal transducer 2), is a 46 kDa transmembrane glycoprotein expressed in carcinomas of the lung, bladder, breast, cervix, ovary, stomach and prostate [9]. Most normal human tissues do not express TROP-2, although it is found at low levels in several normal glandular cells, including glands in the bronchus, breast, prostate and skin, and ducts and acini of the pancreas [10].

In pretargeting, unlabeled TF12 is injected intravenously, and when it has cleared from the blood, an HSG-substituted radiolabeled hapten-peptide is injected. This hapten-peptide will be trapped in the tumor by the anti-HSG arm of the bsAb or is rapidly cleared via the kidneys [8].

In this study, the potential of pretargeted radioimmunoimaging with TF12 and the radiolabeled di-HSG peptide IMP288 in mice with subcutaneous and intraperitoneal human PC xenografts was investigated.

Materials and methods

The anti-TROP-2 x anti-HSG bsAb TF12 (Mw 168 kDa) was produced using the Dock-and-Lock technology as described previously [11], and made available from IBC Pharmaceuticals, Inc., a subsidiary of Immunomedics, Inc. The DOTA-conjugated hapten-peptide IMP288 (DOTA-D-Tyr-D-Lys(HSG)-D-Glu-D-Lys(HSG)-NH_2) was prepared as described previously [12].

Cell culture

The human prostate cancer cell line, PC3, is an androgen-independent cell line, originally derived from a PC bone metastasis. Cells were obtained from ATCC (CRL 1435; Manassas, VA) and were grown in RPMI 1640 medium (GIBCO®, Life Technologies Corporation, Carlsbad, CA, USA), supplemented with 10% fetal calf serum (FCS, Life Technologies, Grand Island, NY) and 2 mM glutamine. For inoculation of the mice to induce growth of PC3 xenografts, tumor cells were washed with 0.9% NaCl, disaggregated with trypsin and resuspended in 67% complete RPMI 1640 medium and 33% Matrigel (BD Biosciences, San Jose, CA) to the appropriate concentration (3 x 10^6 cells/200 µL (s.c. model) and 2 x 10^6 cell/200 µL (i.p. model)).

Tumor models

All experiments were approved by the institutional Animal Welfare Committee of the Radboud University Medical Center (Nijmegen, The Netherlands), and were conducted in accordance with the principles set forth by the Revised Dutch Act on Animal Experimentation.
Male BALB/*c* nude mice (Janvier SAS, Le Genest Saint Isle, France), 8–9 weeks old, were adapted to laboratory conditions for at least one week before experimental use. They were housed under non-sterile standard conditions in individually ventilated cages (Tecniplast®, 5 mice per cage), with free access to animal chow (Sniff Voer®) and water. The mice were inoculated s.c. in the flank with 200 µL of PC3 cell suspension (3 x 10^6 cells). The s.c. PC3 tumors grew to approximately 0.1 g in 10 days after tumor cell inoculation, as determined by caliper measurements in 3 dimensions using the formula $V = 4/3\pi$ (length/2 x width/2 x height/2), assuming that the density of tumor tissue is 1 g/cm^3.
For the studies in mice with intraperitoneally-growing PC3 tumor lesions, male BALB/*c*

nude mice were also used. Using a 23-G needle and a 1 ml syringe, 5 x 200 µL of a cell suspension containing 2 × 10^6 PC3 cells in Matrigel was injected into the peritoneal cavity of the mice. After 7 days, palpable tumors developed intraperitoneally. All radiolabeled preparations (0.2 mL) were injected intravenously via the tail vein.

Radiolabeling of IMP288

The DOTA-conjugated IMP288 was radiolabeled with ^{68}Ga from a TiO_2-based IGG100 ^{68}Ge/^{68}Ga generator (Eckert & Ziegler, Berlin, Germany). Radiolabeling was performed essentially as described previously by Schoffelen et al. [13]. The generator was eluted with 0.1 M HCl and the pH of the ^{68}Ga-containing fraction was adjusted to 3.5 with 2.5 M HEPES (4-(2-hydroxyethyl)-1-piperazineethanesulfonic acid, Sigma-Aldrich, St. Louis, MO, USA). 148-185 MBq of ^{68}Ga-eluate was added to 1 µg of IMP288 in 2.5 M HEPES buffer (at a ratio HEPES buffer:eluate of 1:8). After incubation at 95°C for 20 minutes, 50 mM ethylenediaminetetraacetic acid (EDTA, Sigma-Aldrich,) was added to a final concentration of 1 mM. The ^{68}Ga-IMP288 preparation was loaded on an Oasis® HLB cartridge (Waters, Milford, MA, USA), that was activated with 1 ml 100% ethanol and washed with 1 ml water. The cartridge was subsequently washed with 2 ml water and then eluted with 0.2 ml 30% ethanol, essentially as described previously [14].
Before i.v. injection, the preparation was diluted at least 2.5 times in 0.5% bovine serum albumin (BSA, Sigma-Aldrich) in PBS. Radiochemical purity of the preparations was determined by ITLC and RP-HPLC. ITLC was performed to determine the fraction of unbound ^{68}Ga (mobile phase 0.1 M ammonium acetate and 0.1 M EDTA 1:1, pH 5.5), and the fraction of colloid (mobile phase DMF and 1.25 M ammonium acetate pH 5.5, 1:1). For RP-HPLC, the C_{18} column (Zorbax Rx-C18; 5 µm, 4.6 × 250 mm; Agilent Technologies, Amstelveen, The Netherlands) was eluted with 0.1% trifluoroacetic acid in water (TFA, Lab-scan, Analytical Sciences, Brussels, Belgium) and 0.1% TFA in acetonitrile solution (Lab-scan, Analytical Sciences, Brussels, Belgium) for 5 min with a linear gradient to 100% of the latter solution over 10 minutes at a flow rate of 1 mL/min. Radiochemical purity (RCP) of all labeled preparations used in these studies exceeded 97%, radiochemical yield always exceeded 95%.

Pretargeted ImmunoPET/CT

The potential of pretargeted immunoPET with TF12 and the ^{68}Ga-labeled di-HSG peptide IMP288 was studied in mice with subcutaneous PC3 tumors using ^{18}F-FDG as a reference. Each mouse was injected with both tracers (with a 48 h interval), enabling a direct comparison of the agents in the same mouse. One group of 5 mice with s.c. PC3 tumors was injected i.v. with 2.5 nmol (462 µg) of TF12 and 16 h later with 3.5-8 MBq (0.1 nmol) of ^{68}Ga-IMP288. One hour after injection of ^{68}Ga-IMP288, mice

were scanned in a small-animal PET/CT scanner, while warmed and anesthetized with a mixture of isoflurane and oxygen. After 48 h, the same mice were injected with ^{18}F-FDG, and microPET/CT images were acquired 45 min after injection. Mice were euthanized by O_2/CO_2 asphyxiation. After imaging, tumors and organs were dissected, weighed and counted in a gamma counter to determine biodistribution of the ^{18}F-FDG. Tissue uptake (% ID/g) was calculated against an injection standard. A second group of 5 mice received the same agents in reversed order, to be able to determine biodistribution of the ^{68}Ga-IMP288 after dissection. An additional control group of 5 mice received ^{68}Ga-IMP288 without pretargeting with TF12 to determine the nonspecific uptake of the radiolabeled hapten peptide without the bsAb.

To investigate the potential of pretargeted immunoPET for detecting i.p. lesions, a group of 7 mice with intraperitoneally-growing PC3 tumors was injected i.v. with 2.5 nmol of TF12 and 16 h later with 5 MBq (0.1 nmol) of ^{68}Ga-IMP288. A second group of 6 mice with intraperitoneal tumors was injected i.v. with 10 MBq of ^{18}F-FDG. A control group (n=4) had no intraperitoneal tumors and received the same agents as the first group, to determine the physiological uptake of ^{68}Ga-IMP288 in the abdomen. One hour after injection of ^{68}Ga-IMP288, or 45 min after injection of ^{18}F-FDG, mice were euthanized and PET/CT images were acquired. After imaging, mice were dissected, and tumors and normal tissues were weighed and counted in a gamma counter to determine the concentration of the radiolabel. The uptake of ^{68}Ga-IMP288 (% ID/g) was calculated against an injection standard.

MicroPET/CT imaging

PET/CT images were acquired with an Inveon® animal PET/CT scanner (Siemens Preclinical Solutions, Siemens Healthcare Molecular Imaging, Knoxville, TN), having an intrinsic spatial resolution of 1.5 mm. The animals were scanned in a prone (s.c. model) or a supine (i.p. model) position. PET emission scans were acquired for 20-30 min, preceded by CT scans for anatomic reference (spatial resolution, 113 µm; 80 kV; 500 µA; exposure time, 300 ms). Scans were reconstructed using Inveon Acquisition Workplace software (version 1.2; Siemens Preclinical Solutions), with an ordered set expectation maximization-3D/maximum a posteriori (OSEM3D/MAP) algorithm with the following parameters: matrix 256 x 256 x 159, pixel size 0.43 x 0.43 x 0.8 mm^3 and a beta-value of 0.1.

Statistical analysis

Statistical analysis was performed using GraphPad Prism version 5.00 for Windows®. Differences in uptake were tested for significance using the nonparametric Mann Whitney test for two groups. A *P*-value below 0.05 was considered significant.

Results

Pretargeted immunoPET in mice with s.c. tumors

The pretargeting system revealed high uptake of ^{68}Ga-IMP288 in all s.c. PC3 tumors (7.2 ± 1.1% ID/g) and rapid blood clearance, resulting in excellent tumor-to-blood ratios (17.4 ± 11.2) as early as 1 h after injection (Figure 1). The organ with the highest uptake was the kidney, with an uptake of 1.8 ± 0.5% ID/g at 1 h p.i. Tumor uptake of ^{18}F-FDG was significantly lower than that of ^{68}Ga-IMP288 (3.4 ± 0.9% *vs* 7.2 ± 1.1% ID/g, *P*=0.008), with much lower tumor-to-blood ratios (3.0 ± 1.9, *P*=0.011) and higher kidney uptake (5.9 ± 0.9% ID/g, *P*=0.004). ^{68}Ga-IMP288 not proceeded by injection of the bsAb showed virtually no tumor uptake (0.3 ± 0.1% ID/g, *P*=0.016), resulting in low tumor-to-blood ratios (2.4 ± 0.4, *P*=0.016). Kidney uptake of ^{68}Ga-IMP288 was not affected by the presence of TF12 (1.7 ± 0.3% ID/g *vs* 1.8 ± 0.5, *P*>0.99), indicating that renal uptake of the peptide was nonspecific. The blood level of ^{68}Ga-IMP288 in the mice that received TF12 (0.60 ± 0.39% ID/g) was significantly higher than blood level of ^{68}Ga-IMP288 in the mice that did not receive TF12 (0.13 ± 0.2% ID/g, *P*=0.016), indicating that some complexation of TF12 with IMP288 occurred in the circulation.

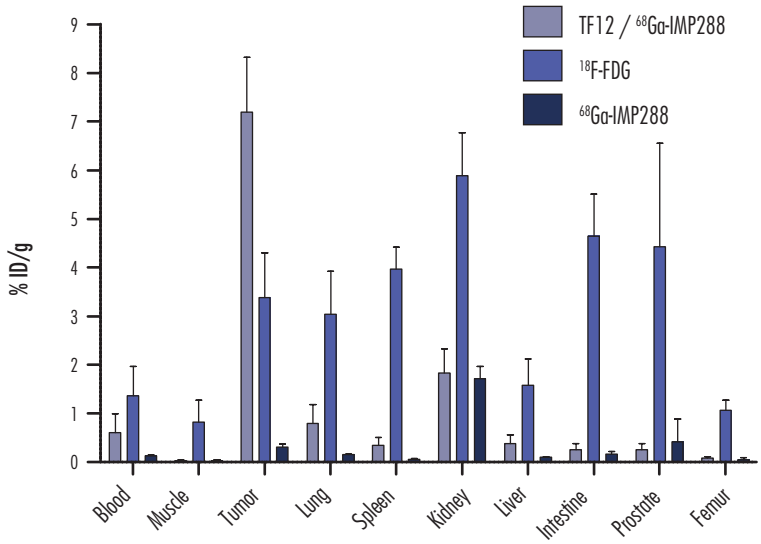

Figure 1. Biodistribution of ^{68}Ga-IMP288 (0.1 nmol, 5 MBq, injected intravenously 16 h after injection of TF12 (2.5 nmol)), ^{18}F-FDG (10 MBq) or ^{68}Ga-IMP288 without TF12 (0.1 nmol, 5 MBq) in BALB/*c* nude mice with a subcutaneous PC3 xenograft 45 min (^{18}F-FDG) or 1h (^{68}Ga-IMP288) after injection (n=5).

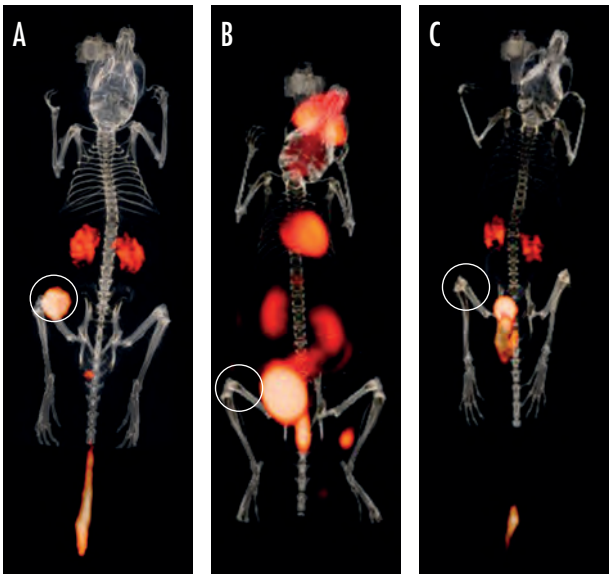

Figure 2. Anterior 3D volume-rendering projection of microPET/CT scan of a BALB/*c* nude mouse with a subcutaneous PC3 tumor on the flank injected with either TF12 and ^{68}Ga-IMP288 (0.1 nmol, 5 MBq, A) or ^{18}F-FDG (10 MBq, B, same mouse) or ^{68}Ga-IMP288 without TF12 (0.1 nmol, 5 MBq, C, different mouse) acquired 45 min ^{18}F-FDG) or 1 h ^{68}Ga-IMP288) after injection. The location of the s.c. tumor is indicated by the white circle.

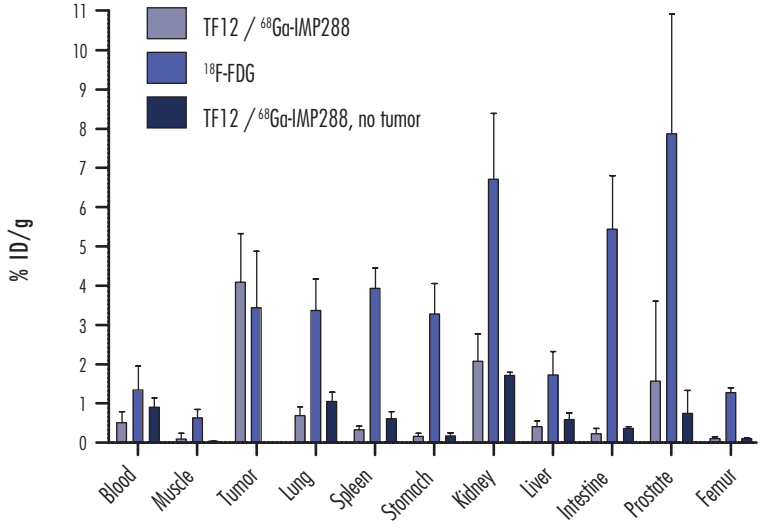

Figure 3. Biodistribution of ^{68}Ga-IMP288 (0.1 nmol, 5 MBq), injected intravenously 16 h after injection of TF12 (2.5 nmol) in BALB/*c* nude mice with intraperitoneal PC3 xenografts 1 h p.i. (n=7), ^{18}F-FDG (10 MBq, n=6) 45 min p.i. or TF12/^{68}Ga-IMP288 in tumorless mice (control group, 5 MBq, n=4) 1 h p.i.

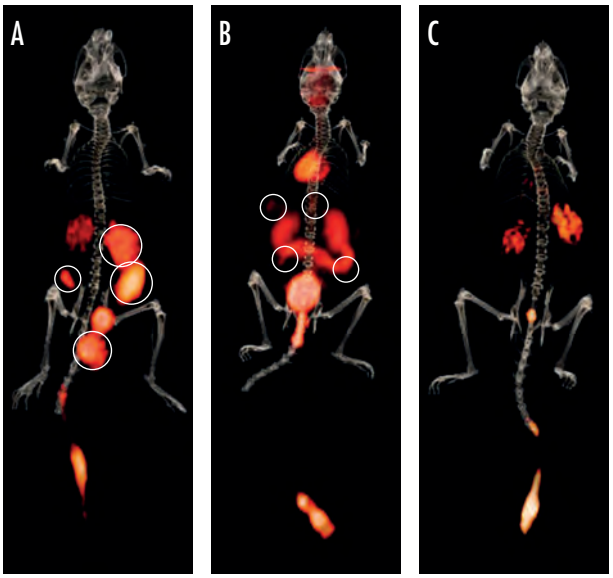

Figure 4. Anterior 3D volume-rendering projection of a microPET/CT scan of a BALB/*c* nude mouse with intraperitoneal PC3 tumors injected with either TF12 and ^{68}Ga-IMP288 (0.1 nmol, 5 MBq, A) at 1 h after injection or ^{18}F-FDG (10 MBq, B) at 45 min after injection and a control mouse (TF12 and ^{68}Ga-IMP288, no tumor, C), acquired 1 h after injection. The location of the i.p. tumors is indicated by the white circles.

Pretargeted immunoPET/CT images of ^{68}Ga-IMP288 clearly visualized the s.c. tumor with minimal activity in the kidneys (Figure 2A). The ^{18}F-FDG PET/CT images in the same mouse showed typical ^{18}F-FDG distribution with lower activity in the tumor and physiologic uptake in brain, heart and intestines (Figure 2B). Tumor-to-liver ratios were determined by ROI analysis and showed a significant difference between pretargeted ^{68}Ga-IMP288 (10.8 ± 4.8) and ^{18}F-FDG (3.4 ± 1.2, P<0.0001). Images acquired 1 h after injection of ^{68}Ga-IMP288 without prior administration of TF12 showed no tumor uptake, minimal activity in the kidneys, and excretion of the radiolabel via the urine (Figure 2C).

Pretargeted immunoPET in mice with i.p. tumors

To assess the potential of pretargeted immunoPET to image small PC lesions, the pretargeting approach was tested in mice with intraperitoneally-growing PC3 tumors. On average, in each mouse 5 lesions were found in the peritoneal cavity (range 3-7). Mice that received both TF12 and 16 h later ^{68}Ga-IMP288, showed specific uptake of the radiolabeled DOTA-conjugated di-HSG-peptide (4.1 ± 1.2% ID/g) in the intraperitoneal tumors (Figure 3). Uptake of the pretargeted ^{68}Ga-labeled di-HSG peptide in other tissues was comparable to that of the mice with s.c. tumors. Blood clearance was

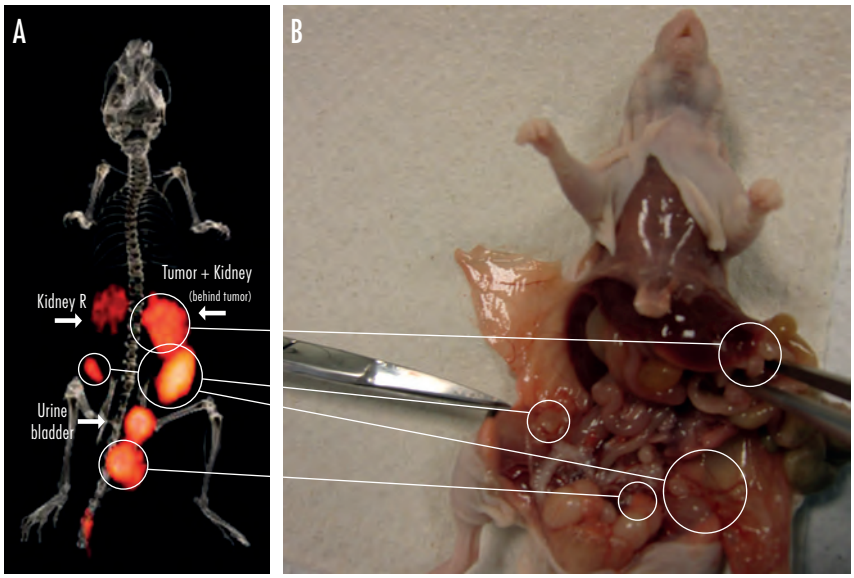

Figure 5. Anterior 3D volume-rendering projection of a microPET/CT scan of a BALB/*c* nude mouse with intraperitoneal PC3 tumors injected with TF12 and ^{68}Ga-IMP288 (0.1 nmol, 5 MBq), acquired 1 h after injection (A) and the same mouse at dissection (B). The location of the i.p. tumors is indicated by the white circles, arrows indicate kidneys and urine bladder.

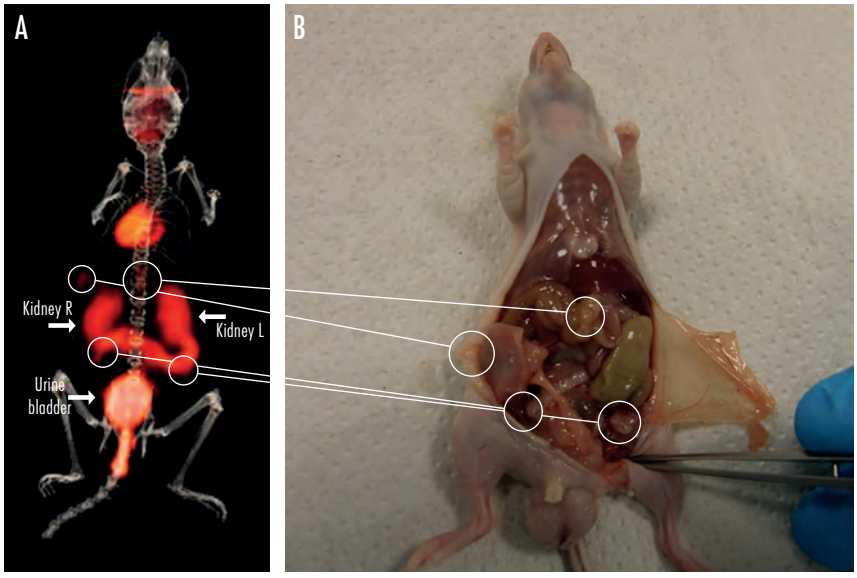

Figure 6. Anterior 3D volume-rendering projection of a microPET/CT scan of a BALB/*c* nude mouse with intraperitoneal PC3 tumors injected with ^{18}F-FDG (10 MBq), acquired 45 min after injection (A) and the same mouse at dissection (B). The location of the i.p. tumors is indicated by the white circles, arrows indicate kidneys and urine bladder.

rapid, resulting in high tumor-to-blood ratios (8.4 ± 3.8) as early as 1 h after injection. Tumor uptake of ^{18}F-FDG in this model was lower than that of the radiolabeled hapten-peptide (3.4 ± 1.5% ID/g, P=0.01), and tumor-to-blood ratios were significantly lower than that of ^{68}Ga-IMP288 (4.1 ± 3.4, P<0.0001).

Pretargeted immunoPET/CT images acquired 1 h after injection of ^{68}Ga-IMP288 clearly visualized the intraperitoneally-growing tumors in the mice with minimal activity in the kidneys and the bladder (Figure 4A). The conventional ^{18}F-FDG PET/CT images showed typical ^{18}F-FDG distribution with limited activity in the tumors (Figure 4B). Images of control mice without i.p. PC3 tumors injected with TF12/^{68}Ga-IMP288 showed some activity in the kidneys and excretion of the radiolabel via the urine (Figure 4C), but without any additional residual activity in the abdomen.

Figures 5 and 6 show the intraperitoneal tumors both on PET/CT images and at dissection. The smallest lesions clearly visualized with TF12/^{68}Ga-IMP288 were as small as 5 mm^3.

Discussion

The present study shows the potential of pretargeted immunoPET of PC with the bsAb TF12 and the ^{68}Ga-labeled di-HSG hapten peptide, IMP288. The studies in mice with s.c. PC3 tumors revealed high uptake of the radiolabeled hapten-peptide in the tumor together with low background levels shortly after injection (t = 1 h). Compared to TF12/^{68}Ga-IMP288, ^{18}F-FDG showed significantly lower tumor and higher kidney uptake. Tumor uptake was TF12-mediated, since tumor uptake was extremely low in mice that were not pretargeted and only received ^{68}Ga-IMP288. A significant difference between blood levels of pretargeted ^{68}Ga-IMP288 and ^{68}Ga-IMP288 without prior injection of TF12 was observed, indicating that circulating TF12 binds ^{68}Ga-IMP288, thereby elevating blood levels of the radiolabeled compound. Earlier studies have shown that increasing or decreasing the time interval between TF12 and IMP288 injection does not further improve tumor-to-blood ratios [8]. In the intraperitoneal model, tumor uptake of the radiolabeled hapten was lower, which might be due to the reduced vascularization of the small i.p. tumors. This is supported by earlier observations that tumor uptake in the intraperitoneal tumors was higher in mice imaged >7 days after tumor inoculation, and increased blood vessel formation in the i.p. tumors after 7 days. However, imaging of the mice >7 days after tumor cell inoculation was impossible due to the fast deterioration of the condition of the mice after 7 days. As a result, tumor-to-blood ratios (7.8 ± 4.1) in the i.p. model were lower than in the subcutaneous model (17.4 ± 11.2).

The pretargeting system of TF12 and ^{68}Ga-labeled IMP288 was able to clearly visualize s.c. or i.p. tumors, with only some background activity in the kidneys and the urinary bladder. In the i.p. model, tumors as small as 5 mm^3 were clearly visible on the

PET/CT images, indicating that pretargeted immunoPET with TF12 and ^{68}Ga-labeled IMP288 is a sensitive and rapid imaging method. These results suggest opportunities for clinical evaluation of this pretargeting approach in imaging of metastasized PC.
Currently, several radiotracers are used or developed for imaging of PC. ^{18}F-choline is clinically the most widely used imaging agent, with fair sensitivity (86%) and specificity (93%) for detection of lymph node metastases and recurrent disease in patients with PSA > 2ng/ml [5, 15]. ^{68}Ga- and ^{99m}Tc-PSMA ligands are promising new agents for imaging of advanced PC [6, 7, 16]; currenly, phase II trials with these agents are ongoing. Pretargeted immunoPET using TF12/^{68}Ga-IMP288, with its specific target on PC lesions and metastases may become a valuable addition to this imaging arsenal for metastatic PC.

Conclusion

Pretargeting with TF12 in combination with ^{68}Ga-labeled hapten peptides is a promising and efficient system for rapid, sensitive, and specific imaging of prostate cancer. Further studies are necessary to determine its application also in pretargeted immunotherapy.

Acknowledgements

We kindly thank Bianca Lemmers, Kitty Lemmens, Iris Lamers-Elemans and Henk Arnts (Central Animal Facility, Radboud University Nijmegen Medical Centre, The Netherlands) for their excellent technical assistance in the animal experiments. The reagents were generously provided by Dr. Chien-Hsing Chang and Dr. Edmund Rossi of IBC Pharmaceuticals, Inc. The work was supported by the Dutch Cancer Society (KWF Kankerbestrijding, Grant KUN-2010-0480).

Disclaimer

David M. Goldenberg, William J. McBride and Robert M. Sharkey have financial interest as employment and/or stock interest in Immunomedics, Inc.

References

1. Beheshti M, Langsteger W, Fogelman I. Prostate Cancer: Role of SPECT and PET in Imaging Bone Metastases. Semin Nucl Med 2009; 39:396-407.
2. Ravizzini G, Turkbey B, Kurdziel K, et al. New horizons in prostate cancer imaging. Eur J Radiol 2009; 70:212-226.
3. Outwater EK, Montilla-Soler JL. Imaging of prostate carcinoma. Cancer Control 2013; 20:161-176.
4. Lütje S, Boerman OC, van Rij CM, et al. Prospects in radionuclide imaging of prostate cancer. Prostate 2012: 72:1262-1272.
5. Jadvar H. Molecular imaging of prostate cancer with PET. J Nucl Med 2013: 54:1685-1688.
6. Hillier SM, Maresca KP, Lu G, et al. ^{99m}Tc-labeled small-molecule inhibitors of prostate specific membrane antigen for molecular imaging of prostate cancer. J Nucl Med 2013; 54:1369-1376.
7. Afshar-Oromieh A, Malcher A, Eder M, et al. PET imaging with a ^{68}Ga-labelled PSMA ligand for the diagnosis of prostate cancer: biodistribution in humans and first evaluation of tumour lesions. Eur J Nucl Med Mol Imaging 2013; 40:486-495.
8. van Rij CM, Lütje S, Frielink C, et al. Pretargeted immunoPET and radioimmunotherapy of prostate cancer with an anti-TROP-2 x anti-HSG bispecific antibody. Eur J Nucl Med Mol Imaging 2013; 40:1377-1383.
9. Basu A, Goldenberg DM, Stein R. The epithelial/carcinoma antigen EGP-1, recognized by monoclonal antibody RS7-3G11, is phosphorylated on serine 303. Int J Cancer 1995; 62:472-479.
10. Stein R, Basu A, Chen S, et al. Specificity and properties of MAb RS7-3G11 and the antigen defined by this pancarcinoma monoclonal antibody. Int J Cancer 1993; 55:938-946.
11. Rossi EA, Goldenberg DM, Cardillo TM, et al. Stably tethered multifunctional structures of defined composition made by the dock and lock method for use in cancer targeting. Proc Natl Acad Sci USA 2006; 103:6841-6846.
12. McBride WJ, Zanzonico P, Sharkey RM, et al. Bispecific Antibody Pretargeting PET (ImmunoPET) with an ^{124}I-Labeled Hapten-Peptide. J Nucl Med 2006; 47:1678-1688.
13. Schoffelen R, Sharkey RM, Goldenberg DM, et al. Pretargeted immuno-positron emission tomography imaging of carcinoembryonic antigen-expressing tumors with a bispecific antibody and a ^{68}Ga- and ^{18}F-labeled hapten peptide in mice with human tumor xenografts. Mol Cancer Ther 2010; 9:1019-1027.
14. Brom M, Joosten L, Oyen WJ, et al. Improved labelling of DTPA- and DOTA-conjugated peptides and antibodies with ^{111}In in HEPES and MES buffer. Eur J Nucl Med Mol Imaging Res 2012; 2:4.
15. Kitajima K, Murphy RC, Nathan, MA. Choline PET/CT for imaging prostate cancer: an update. Ann Nucl Med 2013; 27:581-591.
16. Ristau BT, O'Keefe DS, Bacich DJ. The prostate-specific membrane antigen: Lessons and current clinical implications from 20 years of research. Urol Oncol 2014; 323:272-279.

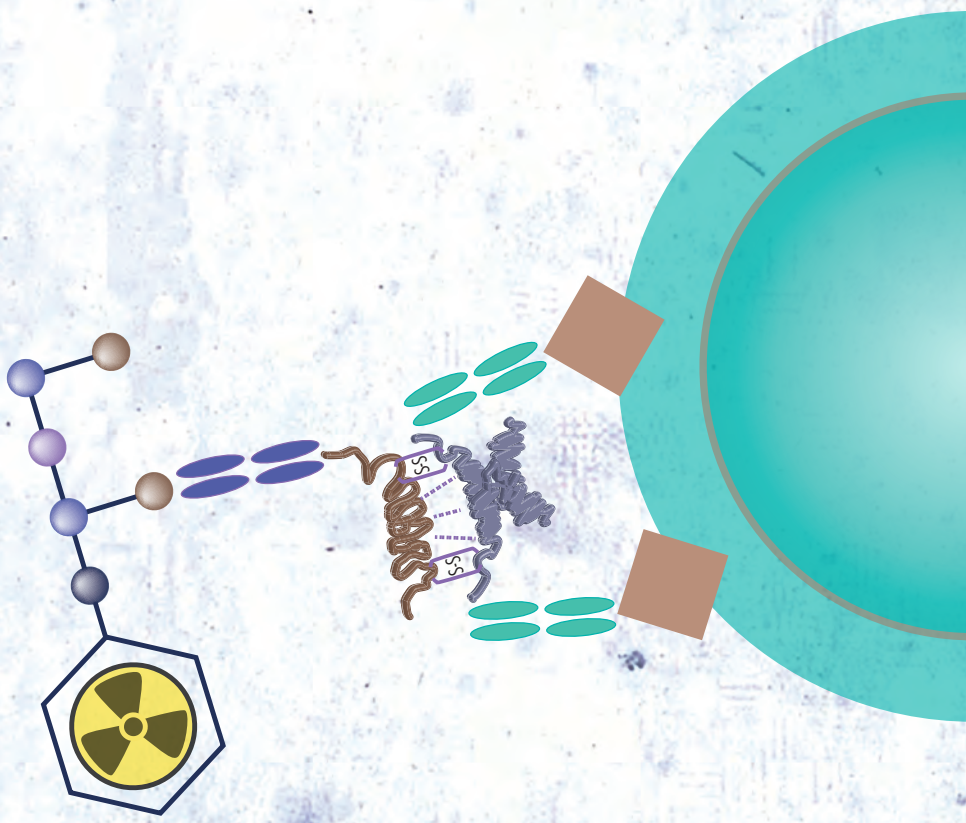

7

Pretargeted radioimmunotherapy of prostate cancer with an anti-TROP-2 x anti-HSG bispecific antibody and a ^{177}Lu-labeled peptide

Catharina M. van Rij,
Cathelijne Frielink,
David M. Goldenberg,
Robert M. Sharkey,
Susanne Lütje,
William J. McBride,
Wim J.G. Oyen,
Otto C. Boerman

Cancer Biother Radiopharm 2014; 29(8):323-9.

Abstract

TROP-2 is a pancarcinoma marker that is expressed at high levels in many epithelial cancers, including prostate cancer (PC). The trivalent bispecific antibody TF12 (anti-TROP-2 x anti-HSG (histamine-succinyl-glycine)) has shown to effectively target PC. In this study, the efficacy of pretargeted radioimmunotherapy (PRIT) with multiple cycles of TF12 and ^{177}Lu-labeled di-HSG-peptide (IMP288) in mice with s.c. PC3 tumors was investigated and compared to that of conventional RIT with ^{177}Lu-labeled anti-TROP-2 mAb hRS7.

Methods

The potential of one, two and three cycles of PRIT using the TF12 pretargeted ^{177}Lu-IMP288 (41 MBq per cycle) was determined in mice with s.c. PC3 tumors, and compared to the efficacy and toxicity of RIT with ^{177}Lu-hRS7 dosed at the maximum tolerated dose (11 MBq).

Results

PRIT with two and three cycles of PRIT showed significantly higher median survival (>150 days) compared to PRIT with one cycle of TF12 and ^{177}Lu-IMP288 (111 days, P<0.001) or the controls (76 days, P<0.0001). All mice treated with the mAb ^{177}Lu-hRS7 survived at the end of the experiment (150 days), compared to 80% in the mice that were treated with three cycles of PRIT and 70% in the group that received two cycles of PRIT. Clinically significant hematologic toxicity was found only in the groups that received either three cycles of PRIT (P<0.0009) or RIT (P<0.0001).

Conclusion

TROP-2-expressing prostate cancer can be targeted efficiently with TF12 and radiolabeled IMP288. ^{177}Lu-IMP288 accumulated rapidly in the tumors. Pretargeted radioimmunotherapy with multiple cycles of PRIT inhibited the growth of s.c. PC3 tumors. Clinically relevant hematological toxicity was observed in the group that received three cycles of PRIT, however, conventional RIT with the parent mAb ^{177}Lu-hRS7 was at least as effective with similar toxicity.

Introduction

Treatment options for metastatic castrate resistant prostate cancer (CRPC) are increasing. As current therapeutic agents have only limited efficacy, there remains a great need to develop effective treatments of PC, once it has advanced to the hormone-independent stage. Radioimmunotherapy (RIT) with the use of radiolabeled monoclonal antibodies in prostate cancer patients has been reported with the ^{177}Lu-labeled anti-PSMA antibody J591[1, 2]. However, due to the long circulatory half-life of agents based on intact antibody molecules, clinically relevant myelotoxicity limits the activity dose that can be safely administered. To avoid toxicity related to slow clearance of radiolabeled antibodies from the circulation, a pretargeting approach can be applied. In pretargeting, tumors are targeted by a non-radiolabeled bispecific antibody, allowing the unbound antibody to clear from the circulation, followed by injection of a radiolabeled small molecule that is recognized by the bispecific antibody. The unbound radiolabeled compound then rapidly accumulates in the tumor or clears quickly from the circulation [3]. A new and potent pretargeting strategy consists of administration of a trivalent bispecific monoclonal antibody followed by administration of a radiolabeled di-HSG hapten peptide. In a phase I/II clinical trial Schoffelen et al. have demonstrated the potential of such an approach to target colorectal carcinoma in patients [4].
For pretargeting of prostate cancer, the bispecific monoclonal antibody (bsAb) TF12 was developed, based on the monoclonal antibody hRS7 [5]. hRS7 is a humanized IgG1 monoclonal antibody directed against TROP-2, also known as EGP-1 (epithelial-glycoprotein-1), GA733-1, gp50/T16 and TACSTD2 (tumor-associated calcium signal transducer 2). TROP-2 is a 46 kDa transmembrane glycoprotein overexpressed in carcinomas of the lung, bladder, breast, cervix, ovary, stomach and prostate [6]. Most normal human tissues do not express TROP-2, but low levels are present in several normal glandular cells, including glands in the bronchus, breast, prostate and skin, and ducts and acini of the pancreas [7]. Given its overexpression in prostate cancer, we studied the potential targeting ability of hRS7 IgG in a nude mouse-human prostate cancer model [8], showing excellent in vivo targeting of PC3 xenografts with ^{89}Zr- and ^{111}In-hRS7 IgG within 3 days. The slow clearance from the circulation results in low tumor-to-background ratios, especially at earlier time points after i.v. injection.

The bsAb TF12, is a trivalent bsAb that consists of two anti-TROP-2 Fab fragments and one anti-HSG (histamine-succinyl-glycine) Fab fragment [9]. In this approach, unlabeled TF12 is injected intravenously, and when it has localized in the tumor and cleared from the blood, a di-HSG-substituted radiolabeled hapten-peptide is injected. This hapten-peptide will be trapped in the tumor by the anti-HSG arm of the bsAb or is rapidly cleared from the body. Previous feasibility studies have shown the potential of pretargeted radioimmunotherapy (PRIT) using TF12 and ^{177}Lu-IMP288 [5]. Due to the

unavailability of carrier-free $^{177}LuCl_3$, studies were performed with a ^{177}Lu-dose that was below MTD (Maximum Tolerated Dose). Since then, $^{177}LuCl_3$ with high specific activity (>3,000 GBq/mg) has become available, enabling labeling of the low peptide dose of IMP288 with a higher activity dose.
In this study, the potential of different regimens of pretargeted radioimmunotherapy with TF12 and the radiolabeled di-HSG peptide, IMP288, in mice with human PC xenografts was investigated.

Materials and methods

The anti-TROP-2 x anti-HSG bsAb TF12 was produced using the Dock-and-Lock technology (DNL®) as described by Rossi et al. [10], and made available from IBC Pharmaceuticals, Inc., a subsidiary of Immunomedics, Inc. The production and characterization of the anti-TROP-2 mAb hRS7 have been described previously [6]. The DOTA-conjugated hapten-peptide IMP288 (DOTA-D-Tyr-D-Lys(HSG)-D-Glu-D-Lys(HSG)-NH_2) was prepared as described by McBride et al. [11].

Cell culture

The human prostate cancer cell line, PC3, is an androgen-independent cell line, originally derived from a PC bone metastasis. Cells were obtained from ATCC (CRL 1435; Manassas, VA) and were grown in RPMI 1640 medium (GIBCO, Life Technologies Corporation, Carlsbad, CA, USA), supplemented with 10% FCS (fetal calf serum, Life Technologies, Grand Island, NY). For subcutaneous inoculation, PC3 cells were washed with 0.9% NaCl, disaggregated with trypsin and resuspended in 67% complete RPMI 1640 medium and 33% Matrigel (BD Biosciences, San Jose, CA) to the appropriate concentration (3 x 10^6 cells/200 µL).

Tumor model

All experiments were approved by the institutional Animal Welfare Committee of the Radboud University Medical Center (Nijmegen, Te Netherlands), and were conducted in accordance with the principles set forth by the Revised Dutch Act on Animal Experimentation.
Male BALB/*c* nude mice (Janvier SAS, Le Genest Saint Isle, France), 8–9 weeks old, were adapted to laboratory conditions for at least one week before experimental use. They were housed under non-sterile standard conditions in individually ventilated cages (Tecniplast, 5 mice per cage), with free access to animal chow (Sniff Voer®) and water. The mice were inoculated s.c. in the flank with 200 µL of PC3 cell suspension (3 x 10^6 cells in 67 % complete RPMI 1640 medium and 33 % Matrigel (BD Biosciences,

San Jose, CA, USA)). The s.c. PC3 tumors grew to approximately 0.1 g in 10 days after tumor cell inoculation, as determined by caliper measurements in 3 dimensions using the formula $V = 4/3\pi$ (length/2 x width/2 x height/2), assuming that the density of tumor tissue is 1 g/cm^3. The radiolabeled preparations (0.2 mL) were injected intravenously via the tail vein.

Radiolabeling of IMP288 and hRS7

The DOTA-conjugated IMP288 was radiolabeled with ^{177}Lu ($^{177}LuCl_3$, non-carrier added, ITG Isotopen Technologien Garching AG, Garching, Germany). Radiolabeling was performed essentially as described previously by Schoffelen et al. [12]. Prior to i.v. injection, the preparation was diluted at least 2.5 times with 0.5% bovine serum albumin (BSA, Sigma-Aldrich) in PBS.
DTPA conjugation and subsequent labeling of hRS7 IgG with ^{177}Lu were performed essentially as described previously [6, 8, 13]. The radiochemical purity of the labeled IMP288 and hRS7 preparations was determined using instant thin-layer chromatography (ITLC), and reversed-phase high-performance liquid chromatography for IMP288 as described previously [12]. ITLC using silicagel strips (Biodex, Shirley, NY, USA) was performed to determine the fraction of unbound ^{177}Lu (mobile phase: 0.1 M citrate pH 6.0 (Merck, Darmstadt, Germany).
For RP-HPLC, the C_{18} column (Zorbax Rx-C18; 5 µm, 4.6 × 250 mm; Agilent Technologies, Amstelveen, The Netherlands) was eluted with a mixture of 97% of a 0.1% trifluoroacetic acid in H_2O solution (TFA, Sigma-Aldrich) with 3% of a 0.1% TFA in acetonitrile solution (Lab-scan, Analytical Sciences, Brussels, Belgium) with a linear gradient to 100% of the latter solution over 10 minutes at a flow rate of 1 mL/min. Radiochemical purity (RCP) of all labeled IMP288 preparations always exceeded 97%; the RCP of ^{177}Lu-hRS7 exceeded 98%.

Immunoreactivity

The anti-TROP-2 reactivity of radiolabeled TF12 and hRS7 was determined using freshly trypsinized PC3 cells, as described by Lindmo et al. [14] with minor modifications. The bispecific immunoreactivity of TF12 was demonstrated by incubating PC3 cells with TF12 (10 µg/mL) during 30 min at 37°C, washing and subsequent incubation with ^{111}In-IMP288 (40,000 cpm). After 1 h at 37°C, the total activity and activity in the cell pellet was determined in a γ-counter. 88% of the added hapten-peptide specifically bound to the pretargeted PC3 cells.

Pretargeted radioimmunotherapy

The therapeutic effect of a single or multiple cycles of PRIT with TF12 and ^{177}Lu-IMP288 was assessed in mice with PC3 xenografts (10 mice/group) and compared to the efficacy of conventional RIT using the radiolabeled parent mAb, ^{177}Lu-hRS7. Mice were treated with the first cycle of TF12/^{177}Lu-IMP288 or ^{177}Lu-hRS7, 10 days after PC3 cell inoculation, when tumors weighed approximately 0.1 g.
In the mice that were treated with PRIT, tumors were pretargeted with 2.5 nmol TF12 (462 µg) 16 h before administration of the ^{177}Lu-IMP288 [5]. The next day, mice received the maximum activity dose of ^{177}Lu activity that could be labeled onto 0.1 nmol (160 ng) IMP288 (41 MBq, specific activity 410 MBq/nmol). Two additional groups of 10 mice received a second or a second and third cycle of TF12/^{177}Lu-IMP288, respectively. Time interval between cycles was 48 h, as determined in earlier experiments [5]. Another group was treated with one cycle of ^{177}Lu-hRS7 at the maximum tolerated dose (MTD, 11 MBq, 15 µg (0.1 nmol), specific activity 110 MBq/nmol).
One control group of PC3 tumor-bearing mice was injected i.v. with vehicle (200 µL PBS, 0.5% BSA) twice instead of TF12 and IMP288. The second control group received vehicle instead of TF12 and was injected 16 h later with 41 MBq of ^{177}Lu-IMP288. A third control group was neither inoculated with PC3 cells, nor received any radioimmunotherapy. The latter group was included to determine whether effects seen in the kidneys were attributable to the radioimmunotherapy, or to regular ageing processes.
Tumor size was measured in three dimensions with a caliper and body weight was determined twice weekly, starting 7 days after tumor cell inoculation. Blood samples of 0.1 mL of all mice were collected via submandibular bleeding before therapy, and 26, 33, 47 and 60 days after administration of the agents to determine hemoglobin levels, and leukocyte and platelet counts. When the humane endpoint was reached (tumor size >2 cm^3 or animal discomfort level >3 as judged by a blinded biotechnician), mice were euthanized by O_2/CO_2-asphyxiation and dissected. At dissection, the tumor and kidneys were excised, weighed, fixed in 4% formalin and processed for paraffin sectioning. The experiment was terminated 150 days after injection of the radiolabeled compounds and the remaining mice were euthanized and dissected. Sections of the kidneys were HE (Hematoxylin and Eosin) and PAS (Periodic Acid Schiff) stained and evaluated by a nephropathologist to determine potential (chronic) kidney damage caused by the (P)RIT.

Biodistribution studies

The effect of the multiple cycles of TF12 and ^{177}Lu-labeled IMP288 on tumor uptake in mice with s.c. PC3 tumors was determined by administering one, two or three cycles of TF12/^{177}Lu-IMP288 (0.4 MBq/cycle) to groups of 5 mice, as described above. Two hours later, mice were dissected and tissue uptake was determined in a

gamma counter. Biodistribution of the ^{177}Lu-hRS7 (0.4 MBq) 3 days after injection of the radiolabeled antibody was also determined in this mouse model. Tumor uptake, blood levels and uptake in relevant tissues (muscle tissue, lung, spleen, kidney, liver, intestine, prostate, femur and bone marrow) were determined. The uptake as percentage of injected dose per gram tissue (% ID/g) in each tissue sample was calculated.

SPECT/CT imaging

To visualize the in vivo distribution of the radiolabeled compounds, SPECT/CT scans were acquired 7 hours (TF12/^{177}Lu-IMP288) or 3 days (^{177}Lu-hRS7) after injection of the ^{177}Lu-labeled agent, respectively. Mice were scanned using a U-SPECT II microSPECT/CT scanner (Milabs, Utrecht, The Netherlands). Mice were anesthetized using isoflurane/O_2 (5% induction, 2.5% maintenance) and scanned for 30 min using the 1.0-mm diameter pinhole collimator tube. Scans were reconstructed with MILabs reconstruction software, which uses an ordered-subset expectation maximization algorithm, with a voxel size of 0.375 mm.

Statistical analysis

Statistical analysis was performed using GraphPad Prism version 5.0 for Windows®. Survival curves were compared using the log-rank test. The level of significance was set at a *P*-value of less than 0.05. Differences in uptake were tested for significance using the nonparametric Mann Whitney test, differences in survival were calculated using the Log-rank test.

Results

Biodistribution studies

The in vivo distribution of ^{177}Lu-IMP288 (0.1 nmol, 0.4 MBq) in mice that were pretargeted 16 h earlier with TF12 was determined 2 h after injection of the radiolabeled di-HSG peptide. Uptake of ^{177}Lu-IMP288 in the PC3 tumors after one (8.5 ± 1.4% ID/g), two (9.0 ± 2.2% ID/g) or three (8.2 ± 1.4% ID/g) cycles of PRIT showed no significant differences (P>0.9, Figure 1A). Two hours after injection, blood levels (<1% ID/g), and uptake in normal tissues were low in all groups. Organ distribution of the radiolabel did not show any significant differences among the three groups, nor obvious trends. ^{177}Lu-labeled parental mAb hRS7 showed high tumor uptake at 3 days after injection (62.0 ± 11.0% ID/g, Figure 1B), along with high blood levels (10.0 ± 1.6% ID/g).

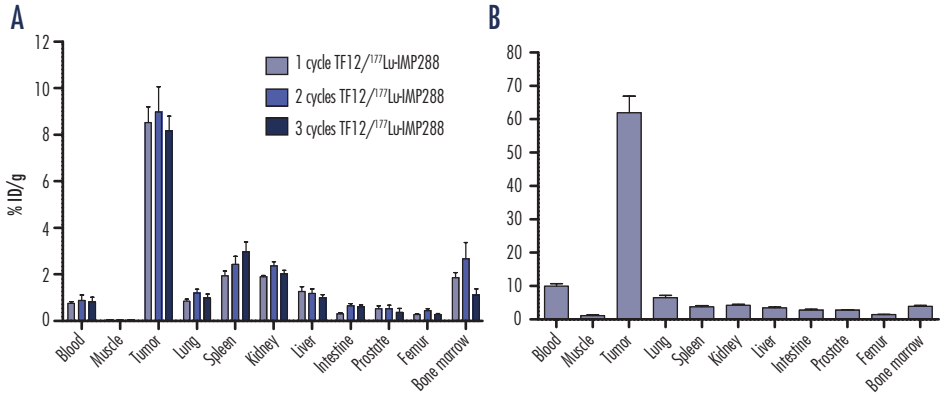

Figure 1A. Biodistribution of ^{177}Lu-IMP288 after one, two or three cycles of ^{177}Lu-IMP288 (0.1 nmol, 0.4 MBq) injected i.v. 16 h after the bsAb TF12 (2.5 nmol) in BALB/*c* nude mice with a subcutaneous PC3 xenograft at 2 h after injection (n=5).
Figure 1B. Biodistribution of ^{177}Lu-hRS7 (15 µg, 0.4 MBq) in BALB/*c* nude mice with a subcutaneous PC3 xenograft measured 3 d after injection (n=5).

Pretargeted radioimmunotherapy

The potential of multiple cycles of PRIT using the bsAb TF12 and ^{177}Lu-labeled IMP288 was determined in mice with s.c. PC3 tumors and was compared to that of RIT with ^{177}Lu-hRS7 (11 MBq, 15 µg). PRIT with 2.5 nmol TF12 and 41 MBq ^{177}Lu-IMP288 significantly improved the median survival of mice with s.c. PC3 tumors from 76 days to 111 days (P<0.0001, Figure 2). The median survival in the groups that received multiple cycles of PRIT or the group that was treated with ^{177}Lu-hRS7 (>150 days)

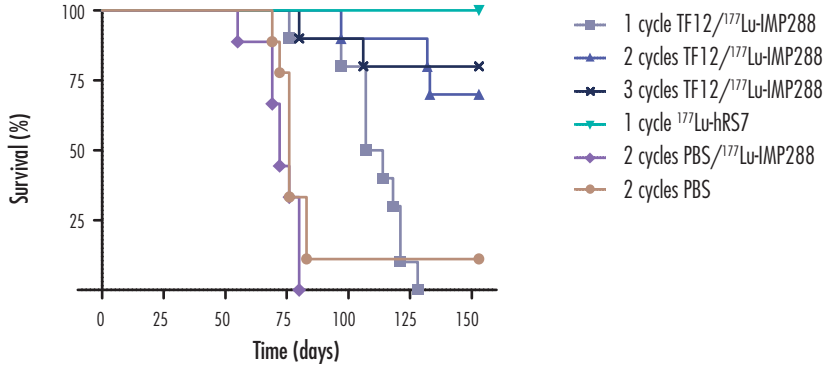

Figure 2. Survival of BALB/*c* nude mice with a subcutaneous PC3 xenograft treated with one, two or three cycles of TF12/^{177}Lu-IMP288 (2.5 nmol/0.1 nmol, 41 MBq per cycle), ^{177}Lu-hRS7 (15 µg, 11 MBq), ^{177}Lu-IMP288 without pretargeting (0.1 nmol, 41 MBq) or vehicle (PBS, n=10).

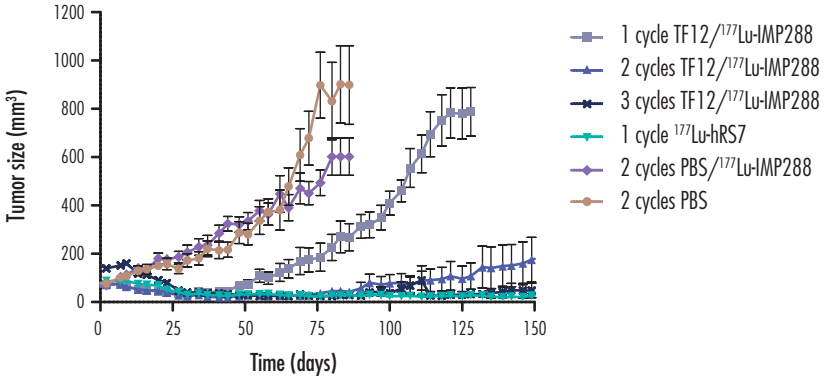

Figure 3. Tumor size of subcutaneous PC3 xenografts in BALB/*c* nude mice treated with one, two or three cycles of TF12/^{177}Lu-IMP288 (2.5 nmol/0.1 nmol, 41 MBq per cycle), ^{177}Lu-hRS7 (15 µg, 11 MBq), ^{177}Lu-IMP288 without pretargeting (0.1 nmol, 41 MBq) or vehicle (PBS, n=10).

was significantly higher (P<0.0001). The control groups received either ^{177}Lu-IMP288 without TF12 or vehicle. Median survival of mice in both control groups was similar (76 days *vs* 72 days), indicating that there was no effect of administration of a high activity dose of ^{177}Lu-IMP288 alone. At the end of the experiment (150 d), all mice treated with ^{177}Lu-hRS7 IgG were still alive. Of the groups that received either two or three cycles of TF12/^{177}Lu-IMP288, 70% and 80% of mice survived, respectively. The difference in survival between the groups that were treated with two or three cycles of TF12/^{177}Lu-IMP288 and the group that was treated with ^{177}Lu-hRS7 was not significant (P=0.067 and 0.146, respectively). At the end of the experiment, the average tumor size of the treated groups was significantly smaller than tumor size in the control groups (Figure 3). In the control groups and the group that received one cycle of PRIT, tumor (re)growth was seen, while the surviving mice in the other groups showed stabilization of tumor growth or a reduced tumor size.

There was no significant decrease in hemoglobin levels, platelets and body weight in either of the groups after treatment (Figure 4ABC). However, leukocyte counts decreased significantly (Figure 4D) in the groups that received either two (-39%, from 4.4 ± 1.5 x 10^9/L at t= -2 d to 2.7 ± 1.0 x 10^9/L at t= 26 d, P=0.01) or three cycles of PRIT (-66%, from 7.4 ± 2.0 x 10^9/L at t= -2 d to 2.5 ± 1.3 x 10^9/L at t= 26 d, P<0.0009) or RIT (-69%, from 4.5 ± 0.9 x 10^9/L at t= -2 d to 1.4 ± 0.6 x 10^9/L at t= 26 d, P<0.0001). Thus, treatment with two or three cycles of TF12/^{177}Lu-IMP288 or with ^{177}Lu-hRS7 IgG was more effective, but also more toxic.

In PRIT, the kidney could also be the organ at risk. Therefore, the kidneys of mice that were treated with PRIT were examined histologically after completion of the experiment (150 d). The kidneys of the treated mice were compared to the kidneys of the age-matched control mice: at this analysis no indication of renal toxicity was observed.

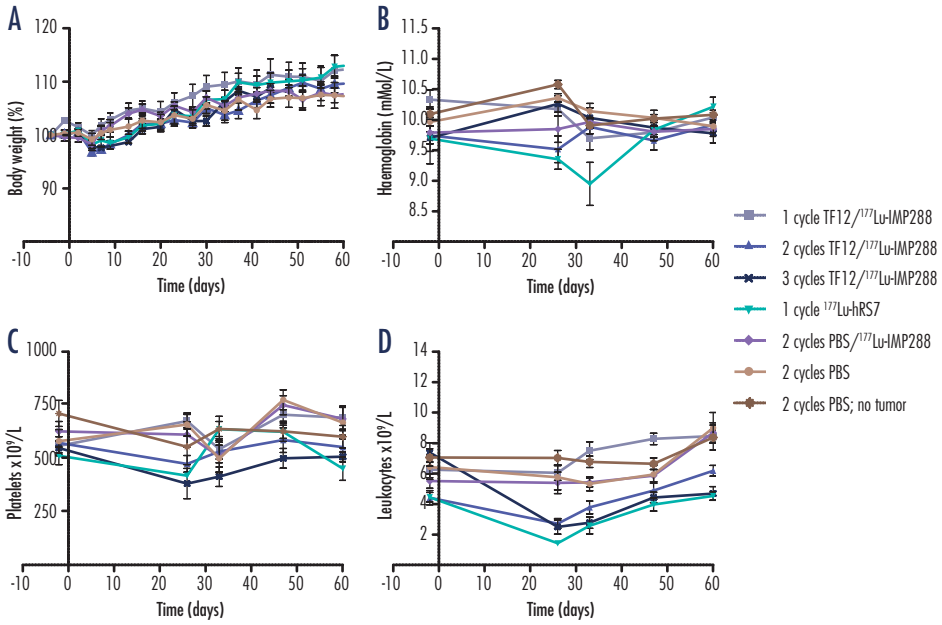

Figure 4. Body weight (A), Haemoglobin levels (B), Platelets (C) and Leukocyte counts (D) of BALB/*c* nude mice with a subcutaneous PC3 xenograft treated with one, two or three cycles of TF12/^{177}Lu-IMP288 (2.5 nmol/0.1 nmol, 41 MBq per cycle), ^{177}Lu-hRS7 (15 µg, 11 MBq), ^{177}Lu-IMP288 without pretargeting (0.1 nmol, 41 MBq) or vehicle (PBS, n=10).

Figure 5. Anterior projections of SPECT/CT scans of BALB/*c* nude mice with an s.c. PC3 tumor in the right flank injected with (A) TF12 (2.5 nmol) and ^{177}Lu-IMP288 (0.1 nmol, 41 MBq) or with (B) ^{177}Lu-hRS7 (15 µg, 11 MBq). Circles indicate tumor. Images were acquired 7 h (TF12/^{177}Lu-IMP288) or 3 days (^{177}Lu-hRS7) after injection of the radiolabel.

SPECT/CT imaging

To visualize distribution of the radiolabel in the tumor bearing mice, SPECT/CT images were acquired. In mice treated with TF12 and ^{177}Lu-IMP288, images acquired 7 h p.i. clearly showed uptake of ^{177}Lu-IMP288 in the PC3 tumors (Figure 5A), without retention of the radiolabeled hapten in other tissues. Due to its longer circulating half-life, images of ^{177}Lu-hRS7 distribution were acquired at 3 days p.i. (figure 5B). The images of the mice that received ^{177}Lu-hRS7 IgG showed the preferential uptake of the radiolabeled antibody in the tumor and low levels of the radiolabel in normal organs.

Discussion

In the present study the potential of multiple cycles of pretargeted radioimmunotherapy of PC with the bsAb TF12 and the ^{177}Lu-labeled hapten-peptide IMP288 was compared to that of conventional RIT with the parental mAb ^{177}Lu-hRS7. Biodistribution studies showed that tumor uptake of radiolabeled IMP288 was similar in the groups that received either one, two or three cycles of PRIT (8.2 - 9.0% ID/g), indicating tumors were targeted as efficiently with subsequent pretargeting cycles. Apparently, within 48 h sufficient TROP-2 epitopes in the tumor were available for another pretargeting cycle. Two hours after injection of the radiolabeled hapten-peptide, almost all activity had cleared form the blood via the kidneys (<1% ID/g). Tumor uptake of the ^{177}Lu-labeled parental mAb hRS7 was much higher (62.0 ± 11.0% ID/g), at the expense of higher blood levels (10.0 ± 1.6% ID/g), even at 3 days after injection of the radiolabel. Images of mice 7 h after PRIT and 3 d after RIT clearly showed uptake of the radiolabel in the PC3 tumor, with very low background activity levels.

The pretargeted RIT experiment showed that one cycle TF12/^{177}Lu-IMP288 significantly improved the median survival of mice with s.c. PC3 tumors without significant hematological or renal toxicity. However, a marked improvement of the median survival was observed in the groups that received multiple cycles of PRIT, or RIT. The improved median survival especially in the groups of mice that received RIT or three cycles of PRIT was achieved at the expense of hematological toxicity, resulting in significant decrease of leukocyte levels after treatment. Two cycles of PRIT showed less hematological toxicity, but was also less effective. At the end of the experiment, 70% of animals in the group with two PRIT cycles was still alive, *vs* 80% in the three cycle PRIT group and 100% of animals in the conventional RIT group, although these differences were not significant. This indicates that RIT with one dose of ^{177}Lu-hRS7 is at least as effective as three cycles of TF12/^{177}Lu-IMP288, with similar toxicity despite lower tumor/blood ratios of the ^{177}Lu-hRS7 as compared to TF12/^{177}Lu-IMP288. Furthermore, tumor growth curves

show regrowth of tumors after PRIT and stabilization of tumor size after RIT, underlining the long term effectiveness of RIT compared to multiple cycles of PRIT. Most likely this is due to the much higher tumor uptake of the ^{177}Lu-hRS7 (62.0% ID/g) compared to the tumor uptake of TF12/^{177}Lu-IMP288 (8.0-9.2% ID/g). These results are not in line with earlier studies comparing PRIT and RIT [15], and with an earlier study with comparable bsAb-hapten combinations by Frampas et al. [16], that showed higher efficacy and similar toxicity of PRIT compared to RIT. However, in this study the tumor uptake of the direct labeled mAb was much lower (20.4% ID/g in s.c. tumors) than that of the radiolabeled hRS7, whilst tumor uptake of the bsAb TF2 was comparable to that of TF12 (9.1% ID/g *vs* 8.5% ID/g).

In the present study, it is shown that additional therapy cycles improve the therapeutic efficacy of PRIT, but also increase hematological toxicity. In future studies, other therapeutic regimens should be investigated. Whilst a dose of 3 times 41 MBq is the MTD for 3 cycles of PRIT, a higher activity dose in one cycle might improve therapeutic efficacy of PRIT. However, higher radioactivity dose can only be achieved by increasing the amount of peptide (due to the maximum specific activity of 0.4 GBq/nmol that can be reached), resulting in decreased tumor uptake [5]. Perhaps a hapten-peptide with multiple DOTA moieties could be developed to further enhance the specific activity of the hapten-peptide. Also repetition of two cycles of PRIT two months after the initial therapy might increase survival, especially since tumor size has decreased dramatically which could enable improved access of the therapeutic agent to the deeper layers of the tumor.

Conclusion

PRIT could be particularly suited to treat PC in an adjuvant setting, either after prostatectomy or in case of biochemical recurrence as indicated by a rising PSA.
The pretargeting system consisting of the bsAb TF12 and the radiolabeled hapten-peptide IMP288 showed efficient and very rapid targeting of TROP-2-expressing PC3 tumors in mice. Pretargeted radioimmunotherapy with multiple cycles of PRIT showed improved median survival, accompanied by hematological toxicity in the groups that received two or three cycles of PRIT. However, conventional RIT with the parent mAb ^{177}Lu-hRS7 resulted in at least as effective treatment of the PC3 tumors, with similar toxicity.

Acknowledgements

We kindly thank Bianca Lemmers, Kitty Lemmens, Iris Lamers-Elemans and Henk Arnts (Central Animal Facility, Radboud University Medical Center) for their excellent technical assistance in the animal experiments and Eric Steenbergen (Department of Pathology, Radboud University Medical Center) for reviewing the kidney samples. The reagents were generously provided by Drs. Chien-Hsing Chang and Edmund Rossi of IBC Pharmaceuticals, Inc. The work was supported by the Dutch Cancer Society (KWF Kankerbestrijding, Grant KUN-2010-0480).

Disclaimer

David M. Goldenberg, William J. McBride, Robert M. Sharkey, and Edmund Rossi have financial interest as employment and/or stock interest in Immunomedics, Inc.

Reference List

1. Tagawa ST, Beltran H, Vallabhajosula S, et al. Anti-prostate-specific membrane antigen-based radioimmunotherapy for prostate cancer. Cancer 2010; 116(4 Suppl):1075-1083.
2. Tagawa ST, Milowsky MI, Morris M, et al. Phase II study of Lutetium-177-labeled anti-prostate-specific membrane antigen monoclonal antibody J591 for metastatic castration-resistant prostate cancer. Clin Cancer Res 2013; 19(18):5182-5191.
3. Frampas E, Rousseau C, Bodet-Milin C, et al. Improvement of radioimmunotherapy using pretargeting. Front Oncol 2013; 3:159.
4. Schoffelen R, Boerman OC, Goldenberg DM, et al. Development of an imaging-guided CEA-pretargeted radionuclide treatment of advanced colorectal cancer: first clinical results. Br J Cancer 2013; 109(4):934-942.
5. van Rij CM, Lütje S, Frielink C, et al. Pretargeted immuno-PET and radioimmunotherapy of prostate cancer with an anti-TROP-2 x anti-HSG bispecific antibody. Eur J Nucl Med Mol Imaging 2013; 40(9):1377-1383.
6. Basu A, Goldenberg DM, Stein R. The epithelial/carcinoma antigen EGP-1, recognized by monoclonal antibody RS7-3G11, is phosphorylated on serine 303. Int J Cancer 1995; 62(4):472-479.
7. Stein R, Basu A, Chen S, et al. Specificity and properties of MAb RS7-3G11 and the antigen defined by this pancarcinoma monoclonal antibody. Int J Cancer 1993; 55(6):938-946.
8. van Rij CM, Sharkey RM, Goldenberg DM, et al. Imaging of prostate cancer with immunoPET and immunoSPECT using a radiolabeled anti-EGP-1 monoclonal antibody. J Nucl Med 2011; 52(10):1601-1607.
9. Sharkey RM, van Rij CM, Karacay H, et al. A new tri-fab bispecific antibody for pretargeting TROP-2-expressing epithelial cancers. J Nucl Med.2012; 53(10):1625-1632.
10. Rossi EA, Goldenberg DM, Cardillo TM, et al. Stably tethered multifunctional structures of defined composition made by the dock and lock method for use in cancer targeting. Proc Natl Acad Sci USA 2006; 103(18):6841-6846.
11. McBride WJ, Zanzonico P, Sharkey RM, et al. Bispecific Antibody Pretargeting PET (ImmunoPET) with an ^{124}I-Labeled Hapten-Peptide. J Nucl Med 2006; 47(10):1678-1688.
12. Schoffelen R, Sharkey RM, Goldenberg DM, et al. Pretargeted immuno-positron emission tomography imaging of carcinoembryonic antigen-expressing tumors with a bispecific antibody and a ^{68}Ga- and ^{18}F-labeled hapten peptide in mice with human tumor xenografts. Mol Cancer Ther 2010; 9(4):1019-1027.
13. Brouwers AH, van Eerd EF, Frielink C, et al. Optimization of radioimmunotherapy of renal cancer: labeling of monoclonal antibody with ^{131}I, ^{90}Y, ^{177}Lu or ^{186}Re. J Nucl Med 2004; 45(2):327-37
14. Lindmo T, Boven E, Cuttitta F, et al. Determination of the immunoreactive fraction of radiolabeled monoclonal antibodies by linear extrapolation to binding at infinite antigen excess. J Immunol Methods 1984; 72(1):77-89.
15. Sharkey RM, Chang CH, Rossi EA, et al. Pretargeting: taking an alternate route for localizing radionuclides. Tumour Biol 2012; 33(3):591-600.

16. Frampas E, Maurel C, Remaud-Le SP, et al. Pretargeted radioimmunotherapy of colorectal cancer metastases: models and pharmacokinetics predict influence of the physical and radiochemical properties of the radionuclide. Eur J Nucl Med Mol Imaging 2011; 38(12):2153-2164.

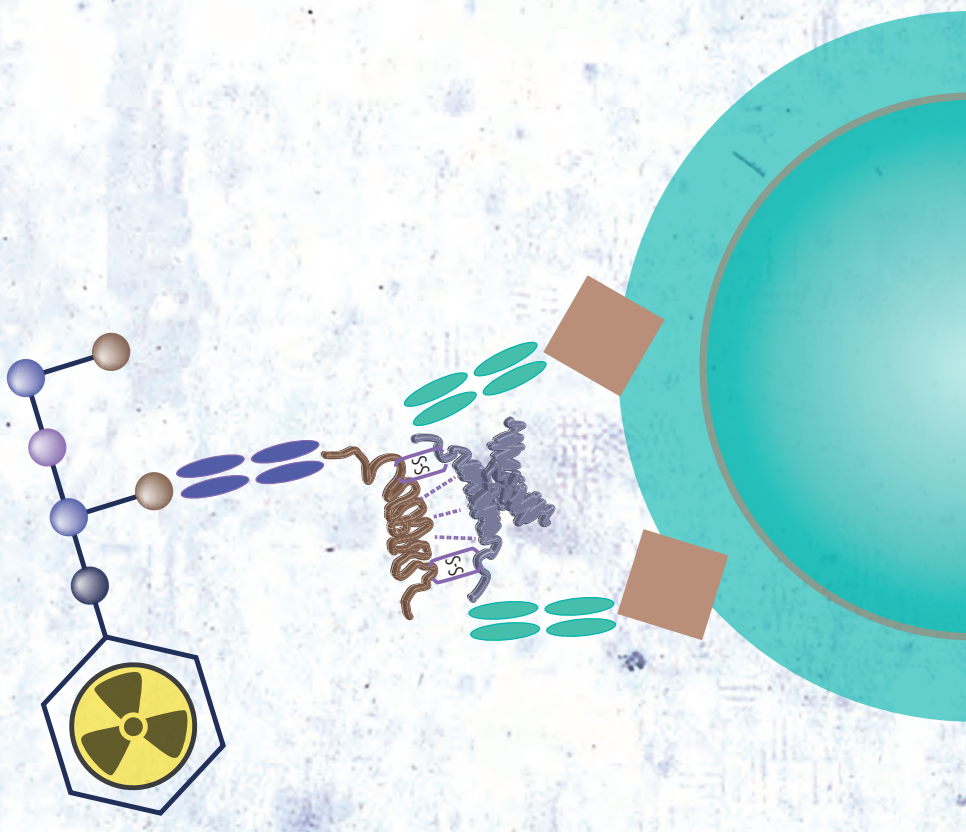

General discussion and future prospects

8

General discussion

In this thesis, the potential of (pre)targeted radioimmunoimaging and radioimmunotherapy of prostate cancer with a radiolabeled humanized anti-TROP-2 monoclonal antibody (hRS7) and an anti-TROP-2 x anti-HSG bispecific monoclonal antibody (TF12) in combination with a radiolabeled hapten peptide (IMP288) was investigated.

Despite effective diagnostic and treatment options for primary prostate cancer (PC), treatment options for advanced, hormone independent disease are limited. Once the cancer has spread beyond the prostate gland, survival rates drop dramatically [1]. At present, extensive research is aimed at the development of new molecular imaging techniques to improve detection and staging of PC, together with the development of new therapeutic options.

For both applications, radiolabeled monoclonal antibodies (mAbs) are of interest. The advantage of these pharmaceuticals is their potential for specific in vivo targeting. Radiolabeled mAbs that target prostate cancer-associated cell surface antigens, are of particular interest in PC. Promising developments are seen with J591, that is directed against the extracellular domain of the PSMA receptor. This monoclonal antibody has been labeled with ^{111}In and ^{89}Zr for immunoSPECT/PET [2], or with ^{177}Lu and ^{90}Y for radioimmunotherapy [3].

Another potential target for PC is TROP-2, a transmembrane glycoprotein that is overexpressed in several adenocarcinomas. We evaluated the characteristics of the anti-TROP-2 mAb humanized RS7 (hRS7) in a subcutaneous and in an orthotopic PC3 mouse model. Our studies revealed excellent immunoPET (using ^{89}Zr-hRS7) and immunoSPECT (using ^{111}In-hRS7) images of PC3 xenografts in mice, indicating that hRS7 has potential as a prostate cancer imaging agent.

However, there are several drawbacks to the use of mAbs in radioimmunoimaging and -therapy. Due to the long circulatory half-life of intact antibodies (IgG), lesions can only be depicted several days after injection when the antibody has cleared from the background. This is inconvenient for patients and for clinical practice. Besides this, sensitivity of mAb-based imaging may be hampered due to nonspecific accumulation in (inflamed) tissues caused by the enhanced permeability and retention (EPR) effect [4]. Furthermore, in radioimmunotherapy, the long circulatory half-life of mAbs causes relatively high radiation doses to well-perfused tissues, such as the (radiosensitive) bone marrow. The long exposure to the therapeutic radionuclide results in clinically relevant myelotoxicity limiting the activity dose that can be administered safely. To avoid toxicity related to slow clearance of radiolabeled antibodies from the circulation, various approaches can be applied. One of these approaches consists of the use of antibody fragments. However, due to their rapid clearance, tumor uptake of antibody fragments is lower and kidney uptake is higher.

An alternative strategy to exploit the excellent in vivo targeting capabilities of mAbs and to circumvent their disadvantages in imaging and RIT is pretargeting with bispecific anti-tumor x anti-hapten antibodies. In pretargeting, tumors are pretargeted by a non-radiolabeled bispecific antibody (bsAb). When the bsAb has cleared from the circulation, a radiolabeled small molecule (hapten-peptide) with affinity for the other binding arm of the bsAb is injected. The radiolabeled hapten-peptide rapidly accumulates in the tumor or clears quickly from the circulation. The potential of pretargeted imaging and radioimmunotherapy (PRIT) to target CEA-expressing colorectal carcinoma (CRC) has been demonstrated by Schoffelen et al. in a phase I/II clinical trial. The results showed rapid and specific tumor targeting of the ^{111}In- or ^{177}Lu-labeled hapten-peptide IMP288 after pretargeting with the anti-CEA x anti-hapten bispecific monoclonal antibody TF2. The study demonstrated that specific targeting in CEA expressing CRC is feasible and safe [5].

We investigated the potential of pretargeting of prostate cancer using the anti-TROP-2 x anti-HSG bsAb TF12 as targeting agent, together with the radiolabeled di-HSG-hapten-peptide IMP288. As opposed to TF2, TF12 has internalizing properties. Theoretically, internalization of a bsAb might limit subsequent binding of the radiolabeled hapten-peptide to the bsAb, since the bsAb would be no longer available on the cell surface to trap the di-HSG-peptide IMP288. We showed that TF12 indeed is slowly internalized by the target cell after binding to the TROP-2 antigen, while a substantial fraction (60%) remained accessible on the tumor cell surface to capture the hapten peptide after 24 h. We optimized the TF12 dose, the dose of the radiolabeled hapten-peptide and the interval between injection of the bsAb and IMP288 and determined the in vivo targeting characteristics of TF12/^{111}In-IMP288 in mice with subcutaneous PC3 tumors. Under these optimized conditions, immunoPET using TF12/^{68}Ga-IMP288 was performed. Retention in the tumor and rapid clearance from the blood enabled clear visualization of the tumor with PET as early as 1 h after injection. Tumor uptake was TF12-mediated, since tumor uptake was extremely low in mice that were not pretargeted and only received ^{68}Ga-IMP288. The pretargeting system of TF12 and ^{68}Ga-labeled IMP288 clearly visualized intraperitoneal tumors as small as 5 mm^3 within 1 h after injection of the radiolabeled peptide, indicating that immunoPET with TF12 and ^{68}Ga-labeled IMP288 is a sensitive and rapid imaging method.

Next to its potential as imaging approach, we investigated the potential of pretargeted radioimmunotherapy of PC with the bsAb TF12 and the ^{177}Lu-labeled hapten-peptide IMP288, and compared the efficacy to that of conventional RIT with the parental mAb hRS7 directly labeled with ^{177}Lu. In pretargeting, the amount of the radiolabeled peptide that can be targeted to the tumor cells is limited. In mice with PC3 tumors the maximum dose of IMP288 that results in optimal tumor uptake is 0.1 nmol. Therefore, the amount of ^{177}Lu activity that can be administrated is limited by the maximum specific activity of ^{177}Lu-IMP288 (14 MBq/0.1 nmol). After the introduction of carrier-free ^{177}Lu to the

market, it was possible to label 0.1 nmol of IMP288 with higher doses of ^{177}Lu, up to 41 MBq. However, mice tolerated even higher doses of ^{177}Lu-IMP288. To determine the maximum therapeutic effect of the PRIT in mice with PC3 tumors, multiple cycles of TF12/^{177}Lu-IMP288 were administered. The results of these PRIT studies showed that the growth of PC3 tumors could be inhibited significantly by repetitive cycles of PRIT.
In our studies we demonstrated the feasibility of pretargeting of prostate cancer using the radiolabeled humanized anti-TROP-2 monoclonal antibody (hRS7) or an anti-TROP-2 bispecific monoclonal antibody (TF12) in combination with a radiolabeled hapten peptide (IMP288).

Future prospects

Schoffelen et al. demonstrated fast clearance of the bsAb TF2 from serum in a phase I clinical trial [5]. Of the injected bsAb, 86% was cleared within 6 h after injection, and 99% within 24 h. This clearance rate is much higher than expected for such a large (168 kDa) protein. This may be caused by the lack of an Fc-part that is recognized by the neonatal Fc receptor (FcRn) , thus excluding the unique recirculation process for intact mAbs, responsible for the long circulation half life of IgG mAbs. Alternatively, the unexpectedly rapid clearance could be due to the limited stability of bsAbs in vivo: bsAbs manufactured by means of the Dock-and-Lock (DNL) method are based on disulfide bridges between the Fab fragments, that are prone to oxidation in vivo. However, Fab fragments have not been detected in blood samples after injection of bsAbs, although this could be due to the rapid clearance of the Fab fragments.
Furthermore, retention of the TF12/IMP288 complex in the tumor is limited: in mice of the radiolabeled IMP288 in the tumor is cleared from the tumor within 2 days. To optimize the efficacy of PRIT tumor retention of IMP288 should be further improved. Recently, Rossin et al. developed a novel method of pretargeting, making use of bioorthogonal chemistry revealing a covalent binding of the radiolabeled agent to the (TCO-modified) anti-tumor antibody [6]. Due to the covalent nature of the interaction between Ab and radiolabeled agent, tumor retention may be improved. Another possibility to enhance the efficacy of PRIT is the use of α-emitting radionuclides such as Astatine-211 (^{211}At) and Bismuth-213 (^{213}Bi), with high linear energy transfer (LET), allowing for effective delivery of radiation within short distance of the targeted lesions, preserving non-targeted tissues. The relatively short half-lives of these α-emitters (7.2 h and 45 min, respectively), matches with the tumor targeting kinetics of radiolabeled hapten-peptide [7].
Currently, several radiotracers based on PSMA are under clinical development. Due to its excellent expression in PC, that increases with increasing Gleason scores, PSMA is a very promising target for both PC imaging and treatment. In view of this, developing a

bsAb against PSMA would have clinical potential. Furthermore, dual modality imaging in combination with an IRDye, as demonstrated by Lütje et al. [8], may be of particular interest. While radionuclide imaging may allow pre-operative detection and intra-operative localization of tumor lesions, near infrared fluorescense (NIRF) imaging would enable real time intra-operative visualization of tumor lesions.

References

1. NIH. SEER Stat Fact Sheets: Prostate Cancer. Surveillance, Epidemiology and End Results program. http://seer.cancer.gov/statfacts/html/prost.html. Accessed 03-20, 2015.
2. Pandit-Taskar N, O'Donoghue JA, Beylergil V, et al. ^{89}Zr-huJ591 immunoPET imaging in patients with advanced metastatic prostate cancer. Eur J Nucl Med Mol Imaging 2014; 41(11):2093-2105.
3. Tagawa ST, Milowsky MI, Morris M, et al. Phase II study of Lutetium-177-labeled anti-prostate-specific membrane antigen monoclonal antibody J591 for metastatic castration-resistant prostate cancer. Clin Cancer Res 2013; 19(18):5182-5191.
4. Heskamp S, van Laarhoven HW, van der Graaf WT, et al. Radionuclide imaging of drug delivery for patient selection in targeted therapy. Expert Opin Drug Deliv 2014; 11(2):175-185.
5. Schoffelen R, Boerman OC, Goldenberg DM, et al. Development of an imaging-guided CEA-pretargeted radionuclide treatment of advanced colorectal cancer: first clinical results. Br J Cancer 2013; 109(4):934-942.
6. Rossin R, Robillard MS. Pretargeted imaging using bioorthogonal chemistry in mice. Curr Opin Chem Biol 2014; 21:161-169.
7. Kraeber-Bodere F, Rousseau C, Bodet-Milin C, et al. Tumor immunotargeting using innovative radionuclides. Int J Mol Sci 2015; 16(2):3932-3954.
8. Lütje S, Rijpkema M, Goldenberg DM, et al. Pretargeted dual-modality immunoSPECT and near-infrared fluorescence imaging for image-guided surgery of prostate cancer. Cancer Res 2014; 74(21):6216-6223.

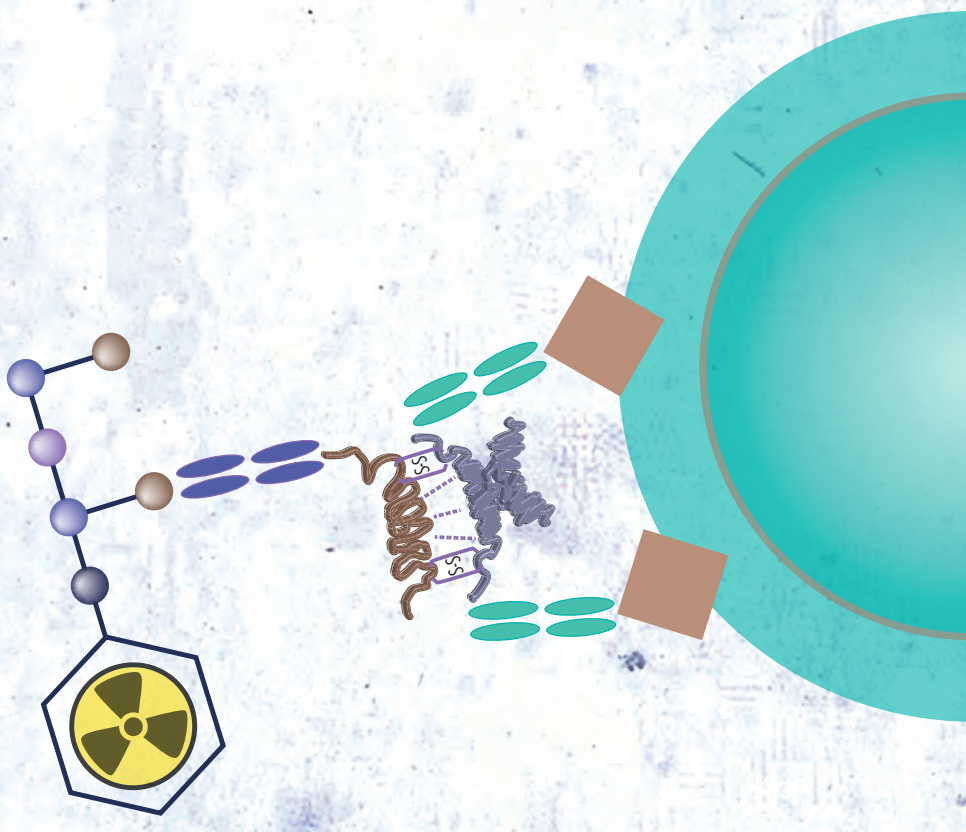
S-S
S-S

Summary

The aim of the studies described in this thesis was to investigate the potential of (pre) targeted radioimmunoimaging and radioimmunotherapy of prostate cancer with a humanized anti-TROP-2 monoclonal antibody (hRS7) and an anti-TROP-2 x anti-HSG bispecific monoclonal antibody (TF12).

Chapter 1 gives an overview of current diagnostic and treatment options in patients with prostate cancer (PC), and explores the advantages and disadvantages of radionuclide imaging and therapeutic techniques that are currently developed. Different novel radionuclide imaging techniques, using radiolabeled metabolic tracers (^{11}C/^{18}F-fluorocholine, ^{11}C-acetate), receptor-binding ligands (PSMA ligands, gastrin releasing peptide receptor ligands) and antibodies are reviewed.

In **Chapter 2** a review of the literature on conventional (US, CT, MRI) and radionuclide imaging (PET, SPECT) techniques of prostate cancer is presented. Sensitivity of ^{18}F-FDG-PET for imaging PC is limited, presumably due to low FDG avidity of most PC lesions. In addition, ^{18}F-FDG is excreted mainly via the urinary tract, obscuring the prostate gland, and restricting the identification of lymph node metastases. Thus, ^{18}F-FDG uptake in PC cells is insufficient to enable clear visualization of PC lesions, leaving room for other radiotracers to be developed for staging and follow up of PC.

The monoclonal antibody hRS7, a humanized antibody against TROP-2, an epithelial glycoprotein expressed in PC, was investigated. The studies described in **Chapter 3** show abundant expression of TROP-2 in human PC tumors and metastases, and in human PC3 tumors in mice. High and specific uptake of radiolabeled hRS7 in PC3 tumors was demonstrated in subcutaneous and intraprostatic mouse tumor models. Tumor-to-blood ratios increased with time, due to continuous accumulation of the radiolabeled hRS7 in the tumor and clearance of the agent from the blood. PET imaging with ^{89}Zr-labeled hRS7 clearly visualized the PC3 tumors in the mice with low background activity, especially at later time points (3-7 days after injection). The results of these studies indicated that hRS7 is a promising candidate for imaging of TROP-2 expressing tumors, and led to the development of a bispecific monoclonal antibody aimed at TROP-2 for pretargeted radionuclide imaging of PC.

TF12 is a trivalent bispecific monoclonal antibody (bsAb) composed of the anti-TROP-2 Fab-fragments and one anti-histidinesuccinylglycine (HSG) hapten Fab-fragment, covalently linked via the Dock-and-Lock (DNL) technology. TF12 was developed to overcome the disadvantages associated with the use of radiolabeled mAbs, mainly related to their relatively long circulatory half-life. In pretargeting, a bispecific mAb (bsAb) aimed at both an epitope typically overexpressed on prostate cancer cells and a hapten peptide that does not naturally occur is injected intravenously. After several hours/days, when the unlabeled bsAb has accumulated in the tumor (and has cleared from the blood), the radiolabeled hapten peptide is injected. The radiolabeled

hapten peptide is bound by the bsAb in the tumor or is rapidly cleared from the circulation. In **Chapter 4**, the possible internalizing properties of the bsAb TF12 were investigated in vitro and in vivo, to determine whether its internalizing properties would limit its application in pretargeting. In theory internalization of a bsAb might hamper subsequent binding of the radiolabeled hapten peptide to the bsAb, since it is no longer available on the cell surface to trap the di-HSG substituted peptide IMP288. We showed that TF12 indeed was slowly internalized by the target cell after binding to the TROP-2 antigen, but a substantial fraction remained accessible on the tumor cell surface. Approximately 60% of the TF12 remained available at the cell membrane after 24 h, leaving sufficient amounts of TF12 available to capture the hapten peptide. In vivo studies showed excellent tumor uptake of the ^{111}In-labeled hapten peptide IMP288. In the studies described in **Chapter 5**, the dose of the pretargeting agent TF12 and the hapten peptide IMP288 were optimized in a nude mouse human tumor model. In addition, the effect of the length of the time interval between administration of the two agents on tumor targeting was studied in detail. The optimal interval between TF12 and IMP288 was determined to be 16 h, while the optimal dose of TF12 was 2.5 nmol (462 µg) and 0.1 mmol (160 ng) for IMP288. Under these optimized conditions, the characteristics of TF12 in combination with radiolabeled IMP288 and its potential for pretargeted radioimmunoimaging and radioimmunotherapy were assessed. After pretargeting with TF12, ^{111}In-IMP288 showed high accumulation in s.c. PC3 tumors (20.4 ± 0.6% ID/g) as early as 2 h after injection, with low activity in normal organs. The organs with the highest uptake of ^{111}In-IMP288 were the kidneys (2.2 ± 0.1% ID/g), due to the renal excretion of the radiolabeled peptide. Blood levels were low (0.9 ± 0.2% ID/g), indicating rapid clearance of the unbound hapten peptide from the blood. Pretargeted immunoPET with TF12 and ^{68}Ga-labeled IMP288 rapidly visualized the PC3 tumors in the same mouse model, indicating this may be an efficient imaging method for PC. Pretargeted radioimmunotherapy (PRIT) with TF12 and ^{177}Lu-IMP288 showed a significant increase in survival, when compared to groups of mice that were injected with either PBS or ^{177}Lu-IMP288 without TF12. Mice that were treated with conventional radioimmunotherapy (RIT) with ^{177}Lu-hRS7 showed a significantly better survival, although these mice showed more hematological toxicity. Because PRIT was not given at the maximum tolerated dose and hematological and renal toxicity were absent, there was room for improvement of this therapy by further increasing the radioactivity dose.

The potential for imaging small metastatic prostate cancer lesions with pretargeted immunoPET was assessed in **Chapter 6**. In mice with intraperitoneally-growing PC3 tumors, pretargeted immunoPET was performed with TF12 and ^{68}Ga-IMP288, using ^{18}F-FDG PET as a reference. Tumors as small as 5 mm^3 could be clearly visualized after pretargeting with high tumor-to-blood ratios of ^{68}Ga-IMP288 (8.4 ± 3.8). Tumor-to-blood ratios for ^{18}F-FDG were significantly lower (4.1 ± 3.4), together with decreased tumor visualization due to physiologic ^{18}F-FDG uptake in the intestines.

In **Chapter 7**, the potential of PRIT for the treatment of prostate cancer was further explored in mice with s.c. PC3 tumors. PRIT with one, two or three cycles of TF12/^{177}Lu-IMP288, using a high activity dose (41 MBq/mouse/cycle), was compared to RIT with directly labeled ^{177}Lu-hRS7 (11 MBq). Three cycles of PRIT significantly improved survival compared to one or two cycles of PRIT, but was accompanied with significantly more hematological toxicity. This toxicity was similar to the hematological toxicity seen in RIT with ^{177}Lu-hRS7; RIT was at least as effective as 3 cycles of PRIT.

The studies described in this thesis show potential for the use of pretargeting for imaging and therapy of prostate cancer. Clinical studies are indicated to determine the value of pretargeted immunoPET of prostate cancer in patients.

Samenvatting

In dit proefschrift worden studies beschreven waarin de mogelijkheden worden onderzocht van (pre)targeted radioimmunoimaging en radioimmunotherapie van prostaatkanker, met behulp van een anti-TROP-2 monoklonaal antilichaam, hRS7, en een anti-TROP-2 x anti-HSG bispecifiek monoclonaal antilichaam, TF12.

In **Hoofdstuk 1** wordt een overzicht gegeven van de huidige diagnostiek en behandeling van patiënten met prostaatkanker. Daarnaast worden de mogelijkheden, voordelen en nadelen van imaging en therapie met behulp van nieuw ontwikkelde, radioactieve tracers behandeld. Verschillende radiofarmaca die in klinisch onderzoek en in de klinische praktijk worden toegepast, zoals radioactieve metabole tracers (^{11}C/^{18}F-fluorocholine, ^{11}C-acetaat), receptor bindende liganden (PSMA liganden, bombesine-analoga) en antilichamen worden besproken.

Hoofdstuk 2 bevat een overzicht van de literatuur van conventionele imaging technieken bij prostaatkanker (echografie, CT, MRI) en imaging met behulp van radiotracers (PET, SPECT). De sensitiviteit van ^{18}F-FDG-PET, een veelgebruikte techniek in de oncologische diagnostiek, in patiënten met prostaatkanker is beperkt. Dit wordt veroorzaakt doordat de meeste prostaattumoren en met name lymfekliermetastasen slechts een geringe ^{18}F-FDG-opname vertonen. Daarnaast wordt ^{18}F-FDG voornamelijk uitgescheiden via de nieren, waardoor tumoren in de urogenitale zone minder goed afgebeeld worden. Daarom is er een grote behoefte aan betere radiofarmaca voor met name stadiëring en follow-up van patiënten met prostaatkanker.

In **Hoofdstuk 3** wordt het gehumaniseerde monoklonale antilichaam hRS7 onderzocht, dat gericht is tegen TROP-2, een geglycosyleerd transmembraan eiwit. De studies beschreven in dit hoofdstuk tonen een goede expressie van TROP-2 in zowel primaire humane prostaattumoren als in metastasen. TROP-2 komt ook tot expressie in de experimentele PC3 tumor die in naakte muizen getransplanteerd kan worden. Hoge en specifieke opname van radioactief gelabeld hRS7 in PC3 tumoren werd gevonden in zowel subcutane als orthotope PC3 tumoren in immunodeficiënte muizen. Doordat het gelabelde antilichaam efficiënt in de PC3 tumoren accumuleerde en langzaam klaarde uit het bloed en de normale weefsels, konden de tumoren na 3-7 dagen duidelijk worden afgebeeld met PET met ^{89}Zr-gelabeled hRS7 als tracer. De resultaten van deze studies laten zien dat radioactief gelabeld hRS7 een veelbelovende tracer is voor de imaging van tumoren die TROP-2 tot expressie brengen.

Echter, het gebruik van intacte monoklonale antilichamen voor imaging heeft een aantal nadelen, die voornamelijk worden veroorzaakt door de lange halfwaardetijd van IgG antilichamen in het bloed. Daarom is een bispecifiek antilichaam ontwikkeld dat eveneens gericht is tegen TROP-2, voor pretargeted imaging van prostaatkanker. Dit antilichaam, TF12, bestaat uit twee anti-TROP-2 Fab-fragmenten en één anti-histidinesuccinylglycine (HSG) hapteen Fab-fragment, die covalent aan elkaar gebonden

zijn middels de Dock-and-Lock (DNL) technologie. Bij pretargeting wordt eerst het bispecifieke antilichaam, gericht tegen zowel het target op de tumorcellen als tegen een hapteen-peptide , intraveneus geïnjecteerd. Nadat het niet-gelabelde bispecifieke antilichaam zich heeft opgehoopt in de tumor en het niet-gebonden deel uit het bloed is geklaard, wordt het bijbehorende, radioactief gelabelde hapteen-peptide (IMP288) intraveneus toegediend. Dit hapteen-peptide wordt vervolgens gebonden door het bispecifieke antilichaam op de tumorcellen, of snel uitgescheiden via de nieren.
In **Hoofdstuk 4** wordt de internalisatie van het bispecifieke antilichaam TF12 door prostaatkankercellen zowel in vitro als in vivo onderzocht, om te bepalen of deze eventuele internalisatie gebruik van TF12 bij pretargeting in de weg staat. In feite kan binding van het hapteen-peptide aan het bispecifieke antilichaam alleen plaatsvinden zolang het TF12 nog niet door de tumorcel is geïnternaliseerd. De internalisatie studies lieten zien dat TF12 inderdaad langzaam wordt geïnternaliseerd door de tumorcellen na binding aan TROP-2, maar dat een substantieel deel beschikbaar blijft op de celmembraan. Na 24 uur is nog ongeveer 60% van het TF12 beschikbaar op het celoppervlak, wat voldoende is voor binding van het hapteen-peptide. De in vivo studies lieten uitstekende accumulatie van het ^{111}In-gelabelde hapteen-peptide in de tumor zien, wat bevestigt dat het langzaam internaliserende TF12 gebruikt kan worden voor pretargeting van prostaatkankercellen.
In de studies die zijn beschreven in **Hoofdstuk 5**, werden de optimale doses van het bispecifieke antilichaam TF12 en het hapteen peptide IMP288 voor pretargeting in muizen met subcutane PC3 tumoren bepaald. Verder werd het effect van de tijd tussen toediening van TF12 en het IMP288 op de tumor targeting in detail bestudeerd. Het optimale interval tussen toediening van TF12 en het IMP288 bleek 16 uur, de optimale dosering was 2.5 nmol (462 µg) TF12 and 0.1 mmol (160 ng) IMP288. Onder deze optimale omstandigheden werd de pretargeted imaging van de PC3 tumoren in muizen met TF12 en gelabeld IMP288 uitgevoerd. Na pretargeting met 2.5 nmol TF12 werd 2 uur na intraveneuze injectie van ^{111}In-IMP288 een hoge concentratie in subcutane PC3 tumoren gemeten (20.4 ± 0.6% ID/g), met zeer lage achtergrondactiviteit in de normale organen: de activiteit in het bloed was laag (0.9 ± 0.2% ID/g) en de hoogste concentratie werd gemeten in de nieren (2.2 ± 0.1% ID/g). Met pretargeted immunoPET met TF12 en ^{68}Ga-gelabeld IMP288 kon de PC3 tumor duidelijk worden afgebeeld. Pretargeted radioimmunotherapie (PRIT) met TF12 en ^{177}Lu-IMP288 bleek de groei van de PC3 tumoren significant te remmen. Bij muizen die werden behandeld met behulp van conventionele radioimmunotherapie (RIT) met ^{177}Lu-gelabeld hRS7 werd de groei van de tumoren ook significant geremd, maar dat ging gepaard met hematologische toxiciteit (daling van het aantal leukocyten in het bloed). In de muizen kon PRIT niet worden uitgevoerd op het maximale ^{177}Lu-IMP288 dosisniveau. Er werd nog geen hematologische en renale toxiciteit gezien, en dus was er ruimte om PRIT verder te verbeteren.

In **Hoofdstuk 6** is een studie beschreven waarin is onderzocht of kleine intraperitoneale prostaat tumoren met behulp van pretargeted immunoPET konden worden afgebeeld. In muizen met intraperitoneaal groeiende PC3 tumoren werd pretargeted immunoPET met TF12 en ^{68}Ga-IMP288 onderzocht, waarbij ^{18}F-FDG PET als referentie methode werd toegepast. Zeer kleine tumoren vanaf 5 mm^3 konden duidelijk afgebeeld worden met pretargeted immunoPET, met hoge tumor-bloed ratio's van het ^{68}Ga-IMP288 (8.4 ± 3.8). De tumor-bloed ratio's met ^{18}F-FDG PET waren significant lager (4.1 ± 3.4).
In **Hoofdstuk 7** wordt een studie beschreven waarin de mogelijkheden van PRIT voor de behandeling van prostaatkanker verder onderzocht zijn in muizen met een subcutane PC3 tumor. PRIT met één, twee of drie cycli TF12/^{177}Lu-IMP288 (41 MBq/muis/cyclus) werd vergeleken met RIT met direct gelabeld ^{177}Lu-hRS7. Drie cycli PRIT gaf een significant betere overleving dan één of twee cycli. Na drie cycli werd echter wel meer hematologische toxiciteit gezien. Deze toxiciteit was vergelijkbaar met die van ^{177}Lu-hRS7; één cyclus RIT was minstens zo effectief als drie cycli PRIT.

De studies beschreven in dit proefschrift tonen de mogelijkheden voor (pre)targeted imaging en therapie van prostaatkanker. Studies in patiënten zullen de waarde van pretargeted immunoPET moeten uitwijzen.

Dankwoord

Geachte prof. dr. Boerman, beste Otto, met wie zou ik dit dankwoord anders kunnen en willen starten dan met jou? Ik wil je danken voor al je steun; door je inspirerende begeleiding, hartelijkheid, humor en bijzonder indrukwekkende wetenschappelijke inbreng heb ik dit proefschrift kunnen volbrengen. En ik ken maar weinig mensen die in snelheid van beantwoorden van e-mails regelmatig de automatische beantwoording van Outlook verslaan… Daarnaast ben ik zeer onder de indruk van je vermogen om van "rol" te wisselen, van promotor naar collega en weer terug. Ik hoop nog lang met je te mogen samenwerken.

Geachte prof. dr. Oyen, beste Wim, dank voor je steun deze jaren, je suggesties, je fenomenale brede kennis en op zijn tijd een klein schouderklopje zijn me zeer tot steun geweest.

Beste Remco, aan jou ook een bijzonder woord van dank. Je onvoorwaardelijke geloof in de goede afloop van dit proefschrift en je volle vertrouwen zijn voor mij een belangrijke factor geweest voor de mogelijkheid dit proefschrift te schrijven en tevens voor het plezier dat ik heb in mijn 'gewone' werk. Daarnaast heb ik veel van je geleerd de afgelopen jaren, van je manier van out-of-the-box denken en van je visie op de farmaceutische zorg. Ik ben ervan overtuigd dat deze daadwerkelijk een verschil kan gaan maken voor de individuele patiënt.

Graag wil ik de leden van de manuscriptcommissie, prof. dr. Peter Mulders, prof. dr. Harry Hendrikse en prof. dr. Winald Gerritsen, bedanken voor het beoordelen van de wetenschappelijke waarde van dit proefschrift.

Mijn paranimfen, Cathelijne, Marieke en Tinka.
Cathelijne, lieve, betrouwbare, hardwerkende steun-en-toeverlaat, jij weet beter dan wie dan ook dat dit proefschrift zonder jou nooit tot stand was gekomen. Niets was je teveel om de studies tot een goed einde te helpen brengen, zelfs voor middernachtelijke activiteiten op het dierenlab draaide jij je hand niet om. En dan ben je daarnaast ook nog een ontzettend fijn mens! Met veel plezier en respect kijk ik terug op onze samenwerking, heel veel dank.
Tinka, lieve, eindeloos betrouwbare, intelligente, gezellige vriendin, wat heerlijk dat ik al zo lang zoveel met jou mag delen. Ik hoop nog lang regelmatig een glaasje bubbels met je te mogen heffen op alle goede dingen in het leven, te beginnen met het vervolmaken van dit proefschrift! Cheers!
Lieve Marieke, lieve Colleegaa ☺, wat heb ik toch een respect voor jou. Ik ken niemand die zo'n ongelofelijke doorzetter is als jij. Jij geeft nooit op, werkt harder dan

eigenlijk mogelijk is en probeert daarnaast ook nog anderen te steunen. Dank voor je interesse, ontelbare fijne telefoongesprekken en onvoorwaardelijke vriendschap. De Kwakel – Groningen is gelukkig helemaal niet zo ver!

Bianca, Henk, Iris en Kitty, heel veel dank voor jullie onmisbare hulp in PRIME! Dankzij jullie goede en professionele ondersteuning is het mogelijk geweest deze onderzoeken uit te voeren. Jullie zijn het levende bewijs dat diepe liefde voor dieren en dierexperimenteel onderzoek samen kunnen gaan, sterker nog, niet zonder elkaar kunnen. Een bijzonder woord van dank voor Bianca, ook jij was altijd bereid om op de meest onmogelijke tijdstippen naar PRIME te komen. Heel veel dank!

A special thanks to our colleagues from Immunomedics (New Jersey, USA), who provided the antibodies and peptide and therefore made this research possible.

Janine, lieve collega, wat leer ik toch veel van je! Je bent echt een kei in je vak en ook nog een enorm gezellig kamergenootje. Dank voor al die jaren delen van lief-en-leed, ik hoop nog lang met je te mogen samenwerken.

Jolande, voor jou uiteraard ook een bijzonder woord van dank. Al jaren werken we samen op het domein van de radiofarmacie en ik vind het geweldig om te zien hoe jij je hierin hebt ontwikkeld. Je enthousiasme is aanstekelijk en het is een fijn gevoel om met een gerust hart afwezig te kunnen zijn als jij er bent. Ik hoop ooit zo relaxed in het leven te kunnen staan als jij…

Lieve collega's van de Apotheek, Martijn, Marjolein, Nicole, Dirk, Karin, Monique, Anna, collega-(ziekenhuis)apothekers, collega's van het lab, collega's van bereidingen, collega's van de CTU, collega's van de Vakgroep, collega's van het secretariaat en van logistiek/magazijn… wat zijn we inmiddels groot geworden! Jullie maken het, naast uiteraard het uitdagende werk zelf, voor mij meer dan de moeite waard iedere keer naar Nijmegen te komen. Dank voor jullie collegialiteit!

Rian, Peter en Maichel, dank voor jullie eeuwige optimisme en de fijne samenwerking. Dankzij jullie inzet (en uiteraard die van ons hele team), is het mogelijk radiofarmaca die in ons eigen lab zijn ontwikkeld, geschikt te maken om toe te passen in klinisch onderzoek en in de klinische praktijk. From Mouse to Man. Fantastisch!

Michel, Sandra, Danny, Gerben, Janneke, Wim en Natascha, fijne collega's, jullie zijn de "stille kracht" op de afdeling. Jullie treden niet vaak op de voorgrond, maar zijn wel de basis van de activiteiten die we dagelijks uitvoeren. Dank voor de fijne samenwerking.

Alle collega's van Radiologie en Nucleaire Geneeskunde, laboranten, AIOS, nucleair geneeskundigen, onderzoekers, research analisten, secretariaat, dank voor de fijne samenwerking en jullie oprechte interesse in dit onderzoek.

Beste Eric Franssen, zonder jou zou ik wellicht nooit in de radiofarmacie zijn beland. Dankzij je aanstekelijke enthousiasme als opleider radiofarmacie ben ik me voor dit fantastische en uitdagende vakgebied gaan interesseren en zie waartoe dat heeft geleid!

Marinke, Vivienne, Tinka, Nanda, Willemijn, Daphne en Saskia, kortom: jaarclub Tiramisu. Sinds 1994 zijn we bij elkaar en hebben nog steeds zoveel pret samen! Op naar de volgende 20 jaar, en de daarop volgende, en de daarop volgende…

Lieve Mirella, wat hebben we al veel meegemaakt samen! Dank voor je vriendschap, en vooral ook voor je heerlijk relativerende gevoel voor humor!

Edward, Astrid, Dennis, Marc, Maykel, Ingrid, lieve vrienden, jullie zijn er altijd. Dat is makkelijk op te schrijven, maar betekent voor mij meer dan woorden kunnen uitdrukken. Jullie zijn geweldig, en zo gezellig, dank!

Lieve Hennie, voor jou ook graag een bijzonder woord van dank. Je hebt vast geen idee hoe inspirerend jouw levensvisie kan zijn voor anderen, graag maak ik van deze gelegenheid gebruik om je te laten weten hoeveel bewondering ik heb voor je benadering van het leven. Ik wens je alle goeds.

Lieve Martine, ook jij hebt zoveel geholpen de laatste jaren, zodat ik ruimte had om aan dit proefschrift te werken. Onze rots in de branding, dankjewel voor alles!

Lieve Oma, voor u uiteraard ook een bijzonder woord van dank. WOII heeft u veel kansen ontnomen, maar dit heeft u nooit uit het veld doen slaan. Integendeel, u heeft dit aangegrepen om mij en mijn broertje altijd van het belang van doorzetten te doordringen. Dank voor uw geloof en vertrouwen in ons.

Lieve schoonouders, Rick, Corinne, Yara en Finn. Wat heb ik het getroffen met zo'n fijne schoonfamilie! Veel dank ook voor alle steun bij de opvang van onze meisjes om tijd te kunnen maken voor dit proefschrift.

Lieve Mark, Nicole en Alexander, onze wereldreizigers. Schotland, Engeland en nu Australië… what's next? Uit het oog betekent zeker niet uit het hart, we komen graag langs!

Lieve pap en mam, wat een heerlijk gevoel te weten dat jullie altijd achter me staan en me altijd steunen. Het is fijn om jullie na een lange dag te kunnen spreken als ik weer eens in de auto zit en het is fantastisch om te zien wat een lieve opa en oma jullie zijn voor onze meisjes. Dank!

Lieve Marc, je bent er altijd voor me. Rotsvast, lief, sterk, humoristisch en een ongelofelijk lieve papa voor onze meisjes… wat hebben we het goed samen. Ons leven is één grote chaotische puzzel en toch weten we het elke keer weer samen te redden. Misschien komt er nu weer wat rust en wordt de puzzel eenvoudiger… of misschien ook niet ☺!

Lieve Dana, lieve Suus, mijn kleine vrolijke vrouwtjes, jullie maken elke dag mooier en elk moment intenser. Jullie zijn mijn alles.

Curriculum Vitae

Catharina Maria (Katja) van Rij werd 8 december 1976 geboren in het VUmc te Amsterdam. Gedurende haar jeugd woonde zij met haar ouders en jongere broer Mark in Mijdrecht. In 1994 heeft zij het VWO afgerond aan het Alkwin College te Uithoorn, waarna de studie Farmacie werd aangevangen aan de Faculteit Farmacie van de toenmalige Rijksuniversiteit Utrecht. In 1994 is zij lid geworden van studentenvereniging Unitas S.R. te Utrecht en van jaarclub Tiramisu. Tijdens haar studie heeft zij in het VUmc literatuuronderzoek uitgevoerd naar de rol van inflammatie bij Reflex Sympatische Dystrofie en heeft zij een HPLC methode opgezet voor het analyseren van midazolam glucuronides in bloed. In haar laatste studiejaar heeft zij via IPSF diverse stages gelopen in openbare en ziekenhuisapotheken in Zimbabwe.

Na het behalen van haar apothekersbul in 2000 heeft zij, na een half jaar werkzaam te zijn geweest als projectapotheker in het VUmc, de opleiding tot ziekenhuisapotheker aangevangen in hetzelfde ziekenhuis. Gedurende de opleiding heeft zij onderzoek gedaan naar populatie plasma farmacokinetiek van tracer hoeveelheden ^{11}C-flumazenil. Voor de voordracht van dit onderzoek heeft zij de Woldring Award 2004 van de Nederlandse Vereniging voor Nucleaire Geneeskunde ontvangen. Na afronding van de opleiding tot ziekenhuisapotheker in 2004 is zij gedurende twee jaar werkzaam geweest als ziekenhuisapotheker in het Groene Hart Ziekenhuis te Gouda, met als aandachtsgebieden het farmaceutisch laboratorium en radiofarmacie.

In 2006 heeft zij de overstap gemaakt naar het Radboudumc, alwaar zij werkzaam is als ziekenhuisapotheker radiofarmacie en Qualified Person.

Katja en haar partner Marc Hogenboom wonen met hun twee dochters Dana en Suus in De Kwakel. Haar hobby's zijn reizen, duiken, skiën en lezen.

List of publications

1. **van Rij CM**, Compas D, Swart EL, Goede PNFC de, Touw DJ. Reversed phase ion-pair HPLC method for the direct analysis of 1-OH-midazolam glucuronide. Ther Drug Monit 1999; 21:416-20.

2. **van Rij CM**, van Loenen AC, Boonstra A. Een geneesmiddel voor continue infusie: Epoprostenol bij pulmonale hypertensie. Pharm Weekbl 2002; 137:144-9.

3. **van Rij CM**, van Loenen AC, Wilhelm AJ. Herkenning en behandeling van hydroxy boterzuur intoxicaties. Ned Tijdschr Geneeskd 2004; 148:844-6.

4. **van Rij CM**, Huitema AD, Swart EL, Greuter HN, Lammertsma AA, van Loenen AC, Franssen EJF. Minder monsters mogelijk. Populatie farmacokinetiek van tracer hoeveelheden ^{11}C-flumazenil bij Positron Emissie Tomografie. Pharm Weekbl 2004; 139:1259-61.

5. **van Rij CM**, Wilhelm AJ, Sauerwein WA, van Loenen AC. Boron neutron capture therapy for glioblastoma multiforme. Pharm World Sci 2005; 27(2):92-5.

6. **van Rij CM**, Huitema AD, Swart EL, Greuter HN, Lammertsma AA, van Loenen AC, Franssen EJF. Population plasma pharmacokinetics of ^{11}C-flumazenil at tracer concentrations. Br J Clin Pharmacol 2005; 60(5):477-85.

7. **van Rij CM**, Sinjewel A, van Loenen AC, Sauerwein WA, Wittig A, Kriz O, Wilhelm AJ. Stability of ^{10}B-L-boronophenylalanine-fructose injection. Am J Health Syst Pharm 2005; 62(24):2608-10.

8. **van Rij CM**, Sturkenboom MGG, Luurtsema G, Franssen EJF. Productie en klinische toepassingen van [^{15}O]-gelabelde gassen. Pharm Weekbl WP 2008; 2:56-8.

9. **van Rij CM**, Sharkey RM, Goldenberg DM, Frielink C, Franssen GM, van Weerden WM, Oyen WJ, Boerman OC. Imaging of prostate cancer with immunoPET and immunoSPECT using a radiolabeled anti-EGP-1 monoclonal antibody. J Nucl Med 2011; 52(10):1601-7.

10. Lütje S, Boerman OC, **van Rij CM**, Sedelaar M, Helfrich W, Oyen WJ, Mulders PF. Prospects in radionuclide imaging of prostate cancer. Prostate 2012; 72(11):1262-72.

11. Sharkey RM, **van Rij CM**, Karacay H, Rossi EA, Frielink C, Regino C, Cardillo TM, McBride WJ, Chang CH, Boerman OC, Goldenberg DM. A new Tri-Fab bispecific antibody for pretargeting TROP-2 expressing epithelial cancers. J Nucl Med 2012; 53(10):1625-32.

12. **van Rij CM**, Lütje S, Frielink C, Sharkey RM, Goldenberg DM, Franssen GM, McBride WJ, Rossi EA, Oyen WJ, Boerman OC. Pretargeted immunoPET and radioimmunotherapy of prostate cancer using an anti-TROP-2 x anti-HSG bispecific antibody. Eur J Nucl Med Mol Imaging 2013; 40(9):137-83.

13. Lütje S, **van Rij CM**, Franssen GM, Fracasso G, Helfrich W, Eek A, Oyen WJ, Colombatti M, Boerman OC. Targeting human prostate cancer with ^{111}In-labeled D2B IgG, F(ab')2 and Fab fragments in nude mice with PSMA-expressing xenografts. Contrast Media Mol Imaging 2015; 10(1):28-36.

14. Lütje S, Rijpkema M, Goldenberg DM, **van Rij CM**, Sharkey RM, McBride WJ, Franssen GM, Frielink C, Helfrich W, Oyen WJ, Boerman OC. Pretargeted dual-modality immunoSPECT and near-infrared fluorescence imaging for image-guided surgery of prostate cancer. Cancer Res 2014; 74(21):6216-23.

15. **van Rij CM**, Frielink C, Goldenberg DM, Sharkey RM, Franssen GM, Lütje S, McBride WJ, Oyen WJ, Boerman OC. Pretargeted immunoPET of prostate cancer with an anti-TROP-2 x anti-HSG bispecific antibody in mice with PC3 xenografts. Mol Imaging Biol 2015; 17:94-101.

16. **van Rij CM**, Frielink C, Goldenberg DM, Sharkey RM, Lütje S, McBride WJ, Oyen WJ, Boerman OC. Pretargeted radioimmunotherapy of prostate cancer with an anti-TROP-2 x anti-HSG bispecific antibody and a ^{177}Lu-labeled peptide. Cancer Biother Radiopharm 2014; 29(8):323-9.

Book chapters

1. Requirements for Boron Neutron Capture Therapy (BNCT) at a nuclear Research Reactor. Editors: W.A.G. Sauerwein, R.L. Moss. Office for Official Publications of the European Communities 2009, chapter 4.3.2 Pharmaceutical issues (**van Rij CM**, Wilhelm AJ, Bet PM, pages 66-68), ISBN 978-92-79-12431-0.

2. Leerboek Nucleaire Geneeskunde. Editors: W.J.M van den Broek. Reed Business 2014, chapter 2 Radiofarmacie (**van Rij CM**, Franssen EJF, pages 32-92), ISBN 978-90-35-22968-6.